Intra-breath changes of respiratory mechanics in healthy infants by oscillometry: role of the upper airways

Bence L. Radics, MD

PhD Thesis

Szeged

2023

University of Szeged

Albert Szent-Györgyi Medical School

Doctoral School of Multidisciplinary Medical Sciences

Intra-breath changes of respiratory mechanics in healthy infants by oscillometry: role of the upper airways

PhD Thesis

Bence L. Radics, MD

Supervisor:

Zoltán Hantos, Ph.D., D.Sc.

Szeged

2023

List of papers underlying the PhD thesis:

I. **Radics, BL**., Makan, G., Coppens, T., André, N., Page, C., Dégrugilliers, L., Bayat, S., Gingl, Z., Gyurkovits, Z., M Tóth, T., Hantos, Z., & Bayat, S. (2020). Effect of nasal airway nonlinearities on oscillometric resistance measurements in infants. *J Appl Physiol* (1985), 129(3), 591-598. doi: 10.1152/japplphysiol.00128.2020.
IF: 3.531; SJR: Q1/Q2

II. **Radics BL**, Gyurkovits Z, Makan G, Gingl Z, Czövek D, Hantos Z. (2022) Respiratory oscillometry in newborn infants: conventional and intra-breath approaches. *Front Pediatr*. 4;10:867883. doi: 10.3389/fped.2022.867883.
IF: 2.6; SJR: Q1

List of papers related to the subject of the thesis

III. Hantos, Z., Czövek, D., Gyurkovits, Z., Szabó, H., Maár, B., **Radics, B**., Virág, K., Makan, G., Orvos, H., Gingl, Z., & Sly, P. (2015). Assessment of respiratory mechanics with forced oscillations in healthy newborns. *Pediatr Pulmonol*, 50(4), 344-52.

IV. Czovek, D., Shackleton, C., Hantos, Z., Taylor, K., Kumar, A., Chacko, A., Ware, R., Makan, G., **Radics, B**., Gingl, Z., & Sly, P. (2016). Tidal changes in respiratory resistance are sensitive indicators of airway obstruction in children. *Thorax*, 71(10), 907-915.

V. Lorx, A., Czovek, D., Gingl, Z., Makan, G., **Radics, B.**, Bartusek, D., Szigeti, S., Gal, J., Losonczy, G., Sly, P., & Hantos, Z. (2017). Airway dynamics in COPD patients by within-breath impedance tracking: effects of continuous positive airway pressure. *Eur Respir J*, 49(2): 1601270.

VI. Shackleton, C., Czovek, D., Grimwood, K., Ware, R., **Radics, B**., Hantos, Z., Sly, P. (2018). Defining 'healthy' in preschool-aged children for forced oscillation technique reference equations. *Respirology*, 23(4):406-13.

VII. Gray, D., Czovek, D., McMillan, L., Turkovic, L., Stadler, J., Vanker, A., **Radics, B**., Gingl, Z., Hall, G., Sly, P., Zar, H., & Hantos, Z. (2019). Intra-breath measures of respiratory mechanics in healthy African infants detect risk of respiratory illness in early life. *Eur Respir J*, 53(2): 1800998.

TABLE OF CONTENTS

ABBREVIATIONS

AX	area under reactance curve below the resonant frequency (absolute value)
BTPS	body temperature, atmospheric pressure and saturated
C	compliance
CT	computed tomography
fbr	breathing frequency (respiratory rate)
$FEV_{0.5}$	exhaled volume during the first half 0.5 second of forced expiration
FEV_1	exhaled volume during the first 1 second of forced expiration
FRC	functional residual capacity
f_{res}	resonant frequency
L	inertance
PFT	pulmonary function test
PTG	pneumotachograph
R	resistance
R_0	lowest oscillatory resistance
R_8, X_8	resistance and reactance measured at 8 Hz
R_{aw}	airway resistance
Re	Reynolds number
R_{eE}, X_{eE}	end-expiratory resistance and reactance
R_{eI}, X_{eI}	end-inspiratory resistance and reactance
R_n, X_n	nasal resistance and reactance
R_{ppE}, X_{ppE}	maximal expiratory peak-to-peak change in resistance and reactance
R_{ppI}, X_{ppI}	maximal inspiratory peak-to-peak change in resistance and reactance
Rrs, Xrs	respiratory system resistance and reactance
$R_{V'maxE}$, $X_{V'maxE}$	resistance and reactance measured at expiratory peak flow
$R_{V'maxI}$, $X_{V'maxI}$	resistance and reactance measured at inspiratory peak flow
RVRTC	raised volume rapid thoraco-abdominal pressure technique
sG_{aw}	specific airway conductance
SLP	structured light plethysmography
TBA	tidal breathing analysis
T_E/T_{Tot}	ratio of expiratory time and respiratory cycle time
TLC	total lung capacity
T_{PTEF}/T_E	ratio of time-to-peak expiratory flow and total expiratory time
V	volume
V’	volumetric flow
V'_{bp}	volumetric flow at the break point
V'_{maxE}, V'_{maxI}	expiratory and inspiratory peak flow
V”	volume acceleration
V''_{eE}, V''_{eI}	volume acceleration at end-expiration and end-inspiration
V_T	tidal volume
WBP	whole-body plethysmography
Zrs	mechanical impedance of the respiratory system
ΔR	difference between end-expiratory and end-inspiratory resistance
ΔV”	difference between end-expiratory and end-inspiratory volume acceleration
ΔX	difference between end-expiratory and end-inspiratory reactance

INTRODUCTION

The burdens of infant pulmonary function testing (PFT) imposed by the lack of active cooperation, the requirement for sleep, the obligatory nasal breathing, the high impedance of the respiratory system and several other factors have prevented the establishment of a gold standard in infant PFT. In addition, most data on lung function are derived from studies focusing on preterms or infants with current or previous respiratory diseases and data on healthy term newborns or infants are scarce. The use of numerous PFTs and the insufficient standardisation resulted in low level of comparability of the data on infant lung function.

Infant lung function tests are technically demanding

The ideal infant PFT should fulfil several requirements. It should not require the infant's active cooperation, thus forced spirometry - the most accepted PFT in pre-schoolers and adults - is not feasible in this age group. The raised volume rapid thoraco-abdominal pressure technique (RVRTC) was developed to imitate the forced expiratory manoeuver of adults. The infant's inspiration is augmented with positive airway pressure (typically ~30 hPa is used) and external thoracic compression is made with an inflatable jacket to achieve forced expiration. The main advantage of this technique is that the flow (V') – volume (V) curve is qualitatively similar to the curves achieved by conventional forced spirometry. As the expiration is quite short in infants, $FEV_{0.5}$ and not FEV_1 is typically measured. The success rate is relatively low without sedation and the inflation at the standardised pressure may not produce the same percentage of total lung capacity (TLC) in all infants [1]. The relatively high external pressure (~ 100 hPa) used in the vest often leads to artificial airway obstruction in healthy infants [2].

Sedation during the infant PFTs was acceptable in the early studies. Beside the ethical concerns related to sedation, triclofos sodium was found to change minute ventilation [3], chloral hydrate has highly variable pharmacokinetics with sleep induction time ranging from 15 min to 2 hours [4], and rarely unpredictable serious side effects (e.g. cardiac arrhythmia, apnea, oxygen desaturation, etc) happened [5]. Thus the ideal technique should be nonivasive and the infants should be measured unsedated. Tidal breathing analysis (TBA) is a simple and popular method for infant PFT and fulfils all criteria mentioned previously. The registration and analysis of spontaneous tidal V' is easy and has a high success rate making this technique popular in epidemiological studies (e.g. [6]). However, this method was found to be rather insensitive to detect airway obstruction ([6-10]).

Since newborns are obligate nasal breathers, the vast majority of infant PFTs use a face mask, attached to a bacterial filter and a V'-meter (typically a pneumotachograph (PTG)). The mechanical properties of the measurement setup (namely the resistive load and the dead space) were found to influence the tidal breathing pattern and thus the results of TBA [11-14]. The touch of the face mask acts as a tactile stimulus and can temporarily change the pattern of tidal breathing via a trigeminal reflex [13].

Structured light plethysmography (SLP) – a recently developed non-contact technique – is free from the confounding effects of equipment dead space and resistive load to the respiratory system. SLP was found to be a feasible technique to track the breathing pattern in infants [15]. However, problems in precise volume calibration may exist in SLP, as it was a serious problem in respiratory inductive plethysmography three decades before [16]. To our best knowledge, the outcomes derived from SLP measurements do not contain volumetric data [17]. Simultaneous measurements and comparison with classical PTG-derived outcomes are lacking.

Beside the instrumental problems detailed above, the other major source of bias of infant PFTs originates from the high natural variability of spontaneous tidal breathing and lung mechanics in newborns and infants.

Tidal breathing and lung mechanics are highly variable in infants

Almost every infant PFT exhibits great intra- and interindividual fluctuations of different measured variables. Unstable functional residual capacity (FRC) is a normal feature of the newborn lung. It originates from the imbalance of the low outward recoil of the soft chest wall and the high inward recoil of the immature lung. Newborns maintain their FRC with active respiratory control mechanisms, such as high respiratory rate, postinspiratory activity of the diaphragm, laryngeal breaking [18-21] and spontaneous sighs [22]. Whole-body plethysmography (WBP) is the standard method to measure FRC precisely in infants. Airway resistance (R_{aw}) and specific conductance (sG_{aw}) can be measured within the same session which is the main advantage of this method [23]. Nevertheless, infant WBP is technically demanding in many aspects. It requires a rebreathing bag attached to the face mask to minimize the confounding effect of thermal drift (since infants cannot perform the panting manoeuver like adults) [2]. The poor signal-to-noise ratio of measured box pressure, the difficulties of BTPS correction and the necessity of highly trained technicians are the main limiting factors that prevented the wide-spread use of WBP in the clinical practice [24].

While the changes in FRC were studied in details, the contribution of upper airways to the high variability of PFT results is less delineated.

Upper airway rheology - a neglected source of variability in the measurement of respiratory mechanics

The contribution of nasal resistance (R_n) to that of the respiratory system resistance (R_{rs}) in infants has been studied previously by posterior rhinomanometry. Using this technique, Polgar and Kong [25] estimated this contribution to be 26%, while Stocks and Godfrey [26] found a higher value of 49%. Using low-frequency oscillometry during apneic periods, Hall et al. [27] studied the impedance of the nasal pathways in infants, by measuring nasal pressure with a miniature catheter-tip transducer inserted through a nostril. They found a 45% contribution of the nasal impedance to R_{rs}.

Although some discrepancy in previous estimates of the contribution of R_n to R_{rs} may be attributed to differences in methodology and population, measurement and interpretation of R_n is profoundly complicated by the anatomical irregularity and complex flow rheology of the nasal passages. The nonlinear pressure (P) - flow (V') relationship in the upper airways contributes to the dynamic changes in R_{rs}, which has been well-documented with intra-breath oscillometry in adults [28-30], children [31] and infants [32]. Measurement of R_{rs} at points of zero V' (namely at end expiration and end inspiration, R_{eE} and R_{eI}, respectively) minimizes the nonlinear contribution of the nasal pathways and the consequent bias in the estimation of R of the lower respiratory tract. Intra-breath oscillometry is a unique lung function technique that is able to identify these zero-flow values of R_{rs}.

Oscillometry as a promising PFT in infants

Recent work has demonstrated its feasibility in normally breathing unsedated infants with a high success rate [33-36]. Additionally, a new tracking modality of oscillometry [37] has revealed disease-specific patterns of intra-breath changes in Zrs and has proven unique in predicting lower respiratory tract illness during infancy [32]. However, a comprehensive analysis is still needed to fully characterize the intra-breath dynamics of Zrs in infants, with special regard to the substantial contribution of the upper airways [25],[27],[37-39]. Confrontation of the novel intra-breath oscillometry with conventional spectral oscillometry is also lacking. While some data on the day-to-day Zrs changes in newborn infants are available [36, 40], the within-session reproducibility of oscillometry measures has not been studied.

AIMS

The current PhD work aimed to get a better insight in the confounding effects of upper airway rheology on the results of respiratory oscillometric measurements. Our basic assumption was that the V'-dependent nonlinear change in Zrs originates primarily from the upper airways. We conducted two studies utilizing the V'-dependent changes in Zrs to estimate the contribution of upper airways to total respiratory system mechanics.

Aims of Study 1

The aim of the first study was to use intra-breath oscillometry in anatomically faithful casts of the nasal pathways of infants from birth to 2 years, reconstructed from computed tomography (CT) images. We assessed the lowest oscillatory R without superimposed breathing (R_0), as well as the effect of varying V' on R_n by simulating breathing through the casts. We characterized the relationships of R_n to V' and volume acceleration (V"). Based on these relationships, we propose a graphical method to correct the error in intra-breath oscillometric R_{rs} measurements that results from V'-dependent nonlinearities. The relative contribution of these nonlinearities to R_{rs} was further assessed in a set of intra-breath oscillometric measurements in infants.

Aims of Study 2

The aims of the second study were a) to measure Zrs in healthy term newborns to characterize the physiological flow (V')- and volume (V)-dependent changes via intra-breath oscillometry, b) to examine the potentially confounding effects of intra-breath changes on average Zrs spectra obtained from conventional multi-frequency measurements and c) to determine the within-session variability of conventional and intra-breath oscillometry variables.

METHODS

Methods of Study 1

Study population

Data of head CT examinations of infants from birth to 24 months, available in the Department of Radiology of the Amiens University Hospital database, performed between October 2011 and August 2014, were collected for analysis. Requirement for written informed consent was waived for this retrospective study by the Internal Review Board of the Amiens University Hospital. Cases not including the entire nasal passages from the nares to the tip of the epiglottis, and those with craniofacial abnormalities or upper airway mass based on the radiologist's report, were excluded. Forty-six image sets met these criteria. Indication for head CT examination is summarized in the online supplement (Supplementary Table S4). Weight data were available in all cases from the electronic medical records. Height and gender data were recorded in 28 and 38 infants, respectively. A tidal volume (V_T) of 7 ml/kg was used to ventilate the casts, in one case based on ideal weight due to a lower than normal real weight.

Image analysis

All images were anonymized for analysis. Native Dicom images were converted to Nifti format. The nasal airway structures were segmented from the nares to the epiglottis, using an active contour algorithm in itk-SNAP software [41] (www.itksnap.org). A representative example is shown in Figure 1. The accuracy of the segmentation was visually examined and manually edited when necessary by an Ear-Nose-Throat specialist (NA). The resulting segmented image was converted to a mesh. A 3-dimensional model of the nasal airways was then produced with a 3D printer (Makerbot, Replicator2, New York, USA) with polylactide using Meshmixer software (www.meshmixer.com) with an accuracy of xy: 11 μm; *z*: 2.5 μm. The accuracy of the 3D-printed casts compared to the initial CT image was verified in one case by CT scanning the cast, followed by image segmentation [42]. Comparison to the initially segmented image, qualitatively by overlaying images showed a quasi-perfect match and a volume difference of 0.3 %.

The nasal airway passages were segmented and the volume, surface area, and various shape descriptors were measured with Imagej software (www.imagej.nih.gov), using the '3D Imagej Suite' plugins (https://github.com/mcib3d). *Sparseness* was defined as the ratio of the volume of a fitted ellipsoid to that of the 3D segmented image (Figure S1). *Flatness* was defined as

the ratio of the second axis to the third axis of the ellipsoid. *Elongation* was defined as the ratio of the first to the second axis of the ellipsoid. Sphericity was defined as:

$$\text{Sphericity} = \frac{\pi^{\frac{1}{3}}(6V_{aw})^{\frac{2}{3}}}{S_{aw}} \qquad \text{(Eq. 1)}$$

Where V_{aw} is the volume of the segmented upper airways and S_{aw} is the surface area. The theoretical background of these measures is given in: [43].

Estimating the effective cross sectional area of the nasal valve

The smallest cross sectional area (CSA) at the pyriform orifice region was selected manually from the 3D reconstructed stereolitography (*.stl) file in FreeCad software (version 0.15, Jürgen Riegel, Werner Mayer, Yorik van Havre) with the 'Clipping Plane' tool. The smallest area was determined on the frontal plane for the right and for the left nasal pathways separately. The selected cross sectional image of the nasal valve area was exported to bitmap (*.bmp) file. The CSA was measured with the manual polygonal line fit tool on the exported image in SightX Viewer software (version 2.0.2.748, JEOL Ltd.). The effective CSA (ECSA) was calculated as the sum of the CSAs of the right and left nasal valves, if the distal segments of the nasal cavity were open both sides. If total or near-total obstruction was revealed on one side of the nasal cavity, the occluded side was omitted from the calculation of ECSA. We diagnosed total occlusion if the nasal cavity contained total cross sectional interruption on the *stl. file. We defined near-toal occlusion if less or equal than one passage was open out of the three nasal meatus.

Experimental setup

Rheological measurements of the upper airway casts were performed with custom-made equipment (Figure 1).

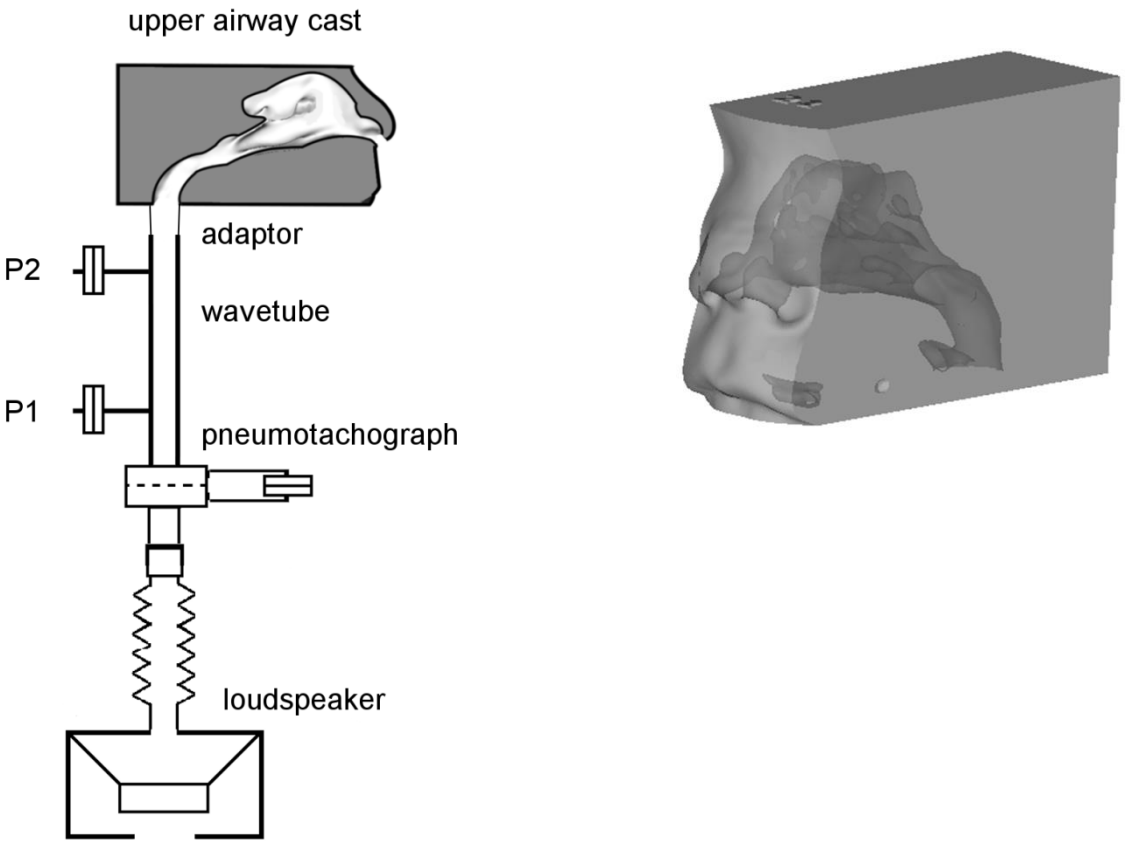

Figure 1. *Left: Schematic illlustration of the experimental setup. Right: Transparent three-dimensional (3D) reconstruction of the upper-airways, used as a sample for 3D-printing.*

Baseline measurements were recorded with the oscillatory signal only, without simulated breathing (R_0). Tidal excursions were generated by a 20-cm-diam. subwoofer loudspeaker (SRP 2030, Somogyi Audio Line, Budapest, Hungary) at three different respiratory rates (33, 45 and 57 cycles·min^{-1}). An estimated V_T (7 ml/kg) was applied at each rate. Measurements were repeated at half of the estimated V_T (Figure 2).

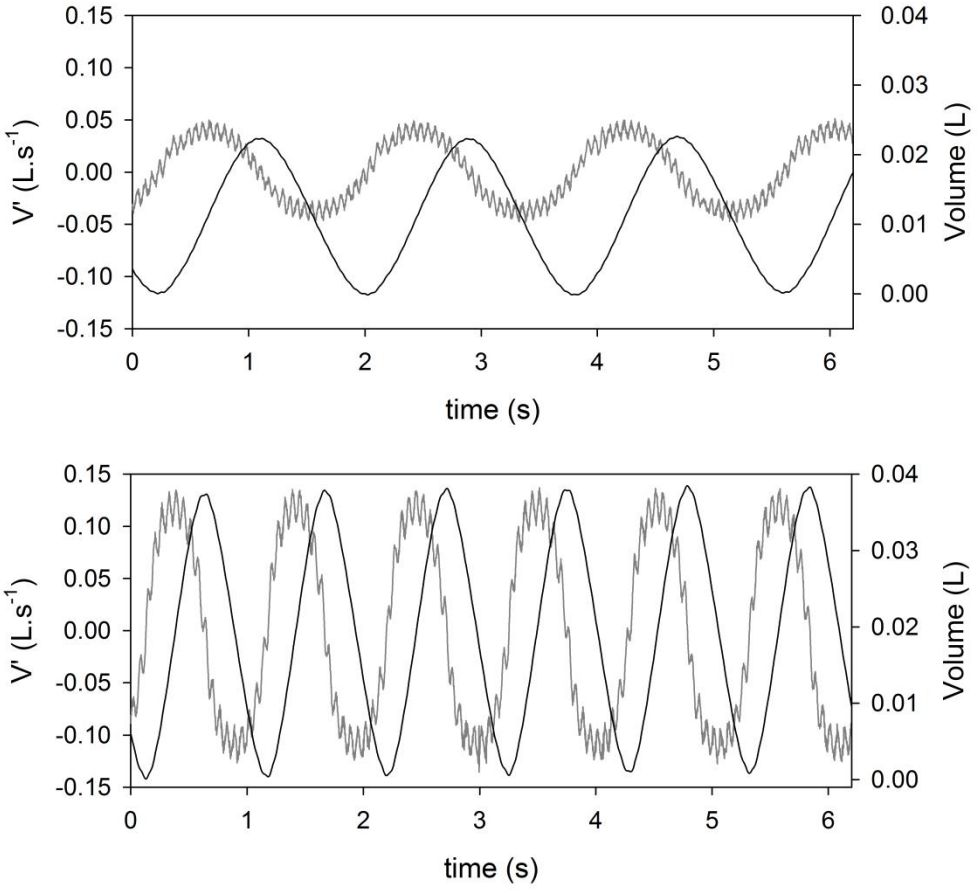

Figure 2. *Time-series of two representative measurement setting. Small-amplitude oscillatory signal (16 Hz) superimposed on the simulated tidal breathing. Top: 0.55 Hz breathing frequency with halved tidal volume ($V_T/2$). Bottom: 0.95 Hz respiratory rate with normal tidal volume (V_T). Black line: volume, gray line: flow (V').*

Small-amplitude (0.5 hPa) oscillations at 16 Hz and the superimposed simulated breathing pattern were generated by the loudspeaker. The combined V' signal was delivered to the pharyngeal opening of the cast via a custom-made pneumotachograph and a modification of the wave-tube oscillometer for infants [36] (length: 10 cm, internal diameter: 8 mm) measuring the input impedance of the naso-pharyngeal cast through a conic adaptor (length: 30 mm, average diameter: 10 mm). Leakage was prevented by a thin rim of silicone putty applied at the ends of the conic adaptor. Difference in the cross-sectional areas between the adaptor and the pharyngeal opening of the cast was negligible. The wave-tube and the pneumotachograph were equipped by identical pressure sensors (Honeywell model 26PCAFA6D, Golden Valley, MN, USA). The pressure and flow signals were low-pass filtered at 50 Hz and sampled at a rate of 512 s^{-1}.

Data analysis

Input impedance of the cast (Z_n) was calculated based on the auto- and cross-power spectra of the wave-tube's lateral pressures using the fast Fourier transform. The pressure signals were bandpass-filtered in the 16±2 Hz frequency range of the spectra. The Z_n values were computed for 4 oscillation cycles (0.0625 s each) and a moving average was calculated over the time span of 0.25 s. Z_n is expressed in terms of resistance (R_n) and reactance (X_n). Volume (V) was integrated from V' using the trapezoidal approach, while V" was calculated as the derivative of V' from individual datapoints, by simple one-sided difference quotients.

To characterize the relation between R_n and V', two separate linear equations were fitted below and above a characteristic breakpoint. For the segment below the breakpoint (1 $mL.s^{-1}$ $<V' \leq V'_{bp}$):

$$\ln R = k_1 \times \ln V' + k_0 \quad \text{(Eq. 2)}$$

For the segment above the breakpoint ($V' > V'_{bp}$):

$$\ln R = (k_1 + k_2) \times (\ln V' - \ln V'_{bp}) + \ln R_{bp} \quad \text{(Eq. 3)}$$

where R_{bp} is the breakpoint resistance at $V' = V'_{bp}$.

Estimation of Reynolds number (Re)

The airway volume (V) of each cast was divided by the characteristic pathway length (l) resulting in a rough estimate of average cross-sectional area (A) (Eq. 4). Volumetric flow rate at breakpoint or at peak V' was divided by A, to obtain linear velocity (u) (Eq. 5). *Re* was calculated with the equation for smooth cylindrical tubes, taking kinematic viscosity (ν) of air as $1.849 \cdot 10^{-5}$ $m^2 \cdot s^{-1}$ (at 25 °C) (Eq. 6).

$$A = \frac{V}{l} \quad \text{(Eq. 4.)}$$

$$u = \frac{V'}{A} \quad \text{(Eq. 5.)}$$

$$Re = \frac{u \times l}{\nu} \quad \text{(Eq. 6.)}$$

In vivo measurements

Oscillometric measurements of the respiratory system impedance (Z_{rs}) were performed in 15 healthy term newborns with a custom-made wave-tube setup, in a setting similar to described previously [32, 36]. These subjects formed a subgroup of the newborns whose study protocol is specified below (Study 2). A 16-Hz sine wave was applied as the oscillatory signal, and Z_{rs} was estimated with the same signal processing technique as that used in the casts (see above) and expressed as total respiratory resistance (R_{rs}) and reactance (X_{rs}). The measurements were performed before the 4th postpartum day, during quiet natural sleep. Exclusion criteria were: 1- poor cooperation; 2- lack of steady-state breathing; 3- nasal obstruction before or during measurement; 4- leakage around the face mask during measurement; 5- laryngeal breaking or inspiratory flow limitation detected during the measurements. A minimum of 5 steady-state, artefact-free breathing cycles was taken for analysis. A piecewise linear regression equation was fitted to the relationship between respiratory resistance (R_{rs}) and V', in the same manner as for the nasal airway casts.

Statistical analysis

Data are expressed as median (interquartile range) unless stated otherwise. Relationships between R_n and V'' and V' were examined by linear regression and piecewise linear regression, for expiratory and inspiratory data [44]. The relationship between structural and impedance data was assessed by Pearson's correlation coefficient. Statistical analysis was performed using the open-source R 3.5.1 software (R Foundation for Statistical Computing, Vienna, Austria, 2019), using the standard built-in and 'segmented' (1.0-0) packages. A p-value < 0.05 was considered as significant.

Methods of Study 2

The study protocol was approved by the Institutional Clinical Ethics Committee of the University of Szeged (91/2011, renewed in 2017). Written informed consent and assent were obtained from all mothers prior to the subject recruitment. The data collection period started in January 2017 and ended in May 2017. All measurements were performed in the Neonatal Unit, Department of Obstetrics and Gynaecology, University of Szeged.

Healthy term infants (>37th week of gestation, birthweight >2500 g, APGAR score at 5 minutes ≥8, uninterrupted early adaptation) were included in the study. Lung function was

measured between the 2nd-5th postpartum day on a single occasion, during natural sleep. Newborns were excluded from the study if steady-state breathing was not reached or leakage persisted around the face mask despite multiple trials.

Measurement setup

Oscillometric measurement of input Zrs was made with a custom-made wave-tube setup (length: 20 cm, internal diameter: 8 mm), in a setting similar to that described previously [32, 36]. Small-amplitude (0.5 hPa) oscillations were generated by the loudspeaker and superimposed on the breathing. Spectral oscillometric recordings were 30 s long, and five different pseudorandom signal specimens containing components at every 4 Hz between 8 and 48 Hz were applied. Intra-breath oscillometric recordings lasted for 90 s, and a single 16-Hz sinusoid was used. Multiple measurements were performed with both modalities in random order, without removing the face mask between recordings if the sleep stage was uninterrupted.

Airflow (V') was measured with a custom-made pneumotachograph. The wave-tube and the pneumotachograph were equipped with identical pressure sensors (Honeywell model 26PCAFA6D, Golden Valley, MN, USA). Single-use bacterial filter (Gibeck, Humid-Vent filter, small straight type, No. 19502 Teleflex Medical, Athlone, Ireland) and face mask (Hudson RCI, air-cushion mask with inflation valve, neonate size, No. 41277, Teleflex Medical) were attached to the setup. The equipment's dead space was flushed with medical air at a rate of 2 $L.min^{-1}$ to avoid hypercapnia.

Transcutaneous monitoring of peripheral haemoglobin oxygen-saturation was done (Edan M50, Bell Medical, Inc. St. Louis, MO, USA) during the recordings for safety reasons. No desaturation episode was detected during data collection. Oxygen saturation data were not stored for further analysis.

Signal processing

Pressure and V' signals were sampled at a rate of 512 s^{-1}, bandpass filtered in the 4-50 Hz range for spectral oscillometry and the 14-18 Hz range for the intra-breath measurements. Zrs was calculated based on the auto- and cross-correlation spectra of the wave-tube's lateral pressures using the fast Fourier transform, and expressed as resistance (Rrs) and reactance (Xrs). The intra-breath Zrs values were computed for each oscillation cycle (0.0625 s) and a

moving average was calculated over a time window of 0.25 s. The signals of V and V", respectively, were obtained by numerical integration and differentiation of V'.

Analysis of Zrs spectra

An average spectrum was calculated from a minimum of 3 recordings of lowest Rrs. Recordings or segments thereof containing artefacts, such as glottis closure, vocalisation, body movements and leaks around the mask were discarded. No criteria relating to tidal volume (V_T) were set and sighs *per se* were not considered as artefacts. A simple resistance (R) - compliance (C) - inertance (L) model was fit to the average Zrs data, as described in detail previously [36]. Conventional spectral oscillometry measures, such as the lowest-frequency (8-Hz) values of Zrs magnitude ($|Z_8|$), resonance frequency (f_{res}) and reactance area below f_{res} (Ax) were also calculated; the frequency dependence of Rrs was characterized by the difference in Rrs between 8 Hz and 32 Hz (R_{8-32}).

Intra-breath measures

All regular artefact-free breaths (see previous section) except sighs were included in the analysis. Specific points of the respiratory cycle were selected to characterize the intra-breath dynamics of Zrs (Fig. 1). Values of Rrs at end-expiration and end-inspiration (R_{eE} and R_{eI}, respectively) were calculated from the closest data points to zero V' obtained with linear interpolation. Tidal change in Rrs (ΔR) was determined as R_{eE}-R_{eI}. Peak-to-peak changes in Rrs during inspiration (R_{ppI}) and expiration (R_{ppE}) were determined. The corresponding parameters of Xrs (X_{eE}, X_{eI}, ΔX, X_{ppE} and X_{ppI}) and the average zero-flow impedance magnitude, $|Z_0|=|½(Z_{eE}+Z_{eI})|$ were also calculated.

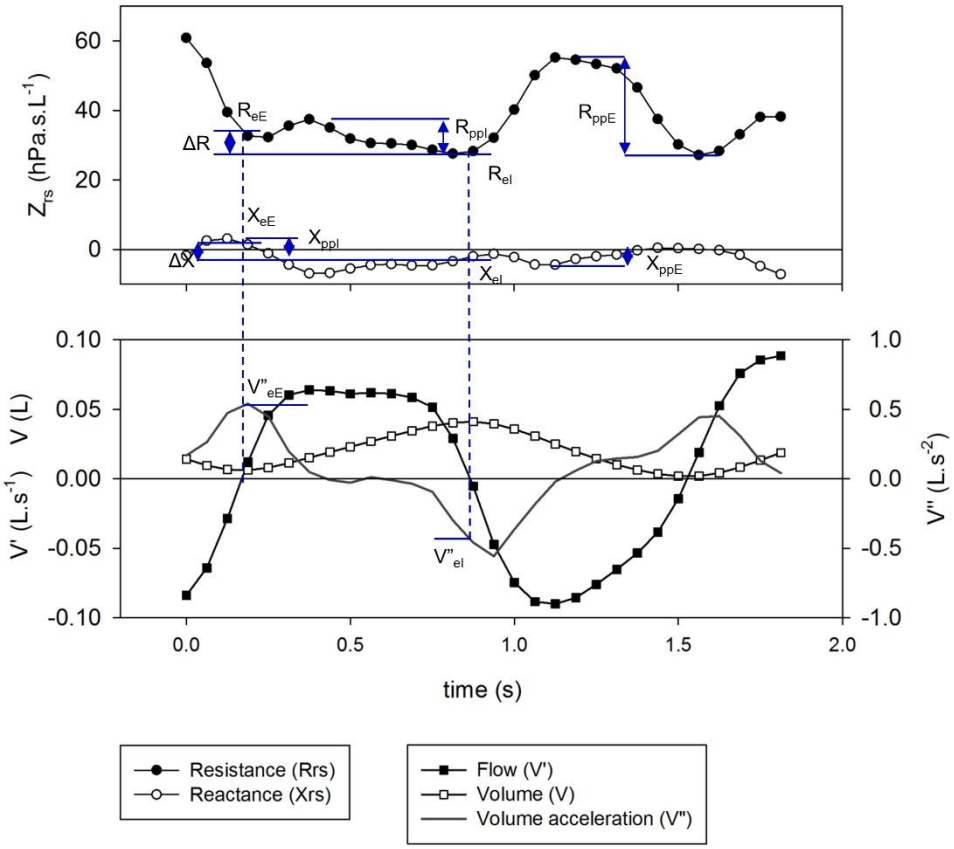

Figure 3*. Definition of specific intra-breath measures of resistance (Rrs) and reactance (Xrs). Shown are the time points of end inspiration (eI) and end expiration (eE) (indicated by dotted lines), their differences (Δ) and peak-to-peak changes in inspiration (ppI) and expiration (ppE).*

Tidal breathing parameters

Simple tidal breath descriptors, such as V_T, respiratory rate (f_{br}), ratio of expiratory time over cycle time (T_E/T_{tot}), and the ratio of time to peak expiratory flow (V'_{maxE}) and T_E (T_{PTEF}/T_E) were obtained from the spirogram. Volume acceleration at end-expiration and end-inspiration (V''_{eE} and V''_{eI}, respectively) were determined from pairs of V" data adjacent to the zero crossing.

Statistical analysis and graphics

Data are presented as mean ± standard deviation (SD). Two sample t-test, correlation analysis with Pearson's correlation coefficients were performed with the open-source RStudio software (https://www.rstudio.com) based on R language (R.4.1). Cluster analysis was also

performed in R using Euclidean distances and Ward's hierarchical method. Graphs were prepared with SigmaPlot 13.5 (Systat Software Inc., San José, CA, USA).

RESULTS

Results of Study 1

A total of 45 of the 46 casts were measured successfully. The study population characteristics are summarized in Table 1.

Table 1. *Upper airway model subject characterisitics*

	Median (Q1, Q3)	**Range**
Age (wk)	25.4 (9.3, 46.3)	(0.3 - 86.7)
Weight (kg)	6.5 (5.4, 8.9)	(2.3 - 12)
Height (cm)	59.4 (56.8, 62.1)	(49 - 80.5)
Sex (F/M)	0.81	

One cast was excluded because of apparent bilateral nasal obstruction, confirmed by re-assessment of the CT images, which resulted in extremely high R_n values.

Intra-breath changes in R_n and X_n as functions of V’ and V’’ are illustrated in Figure 4.

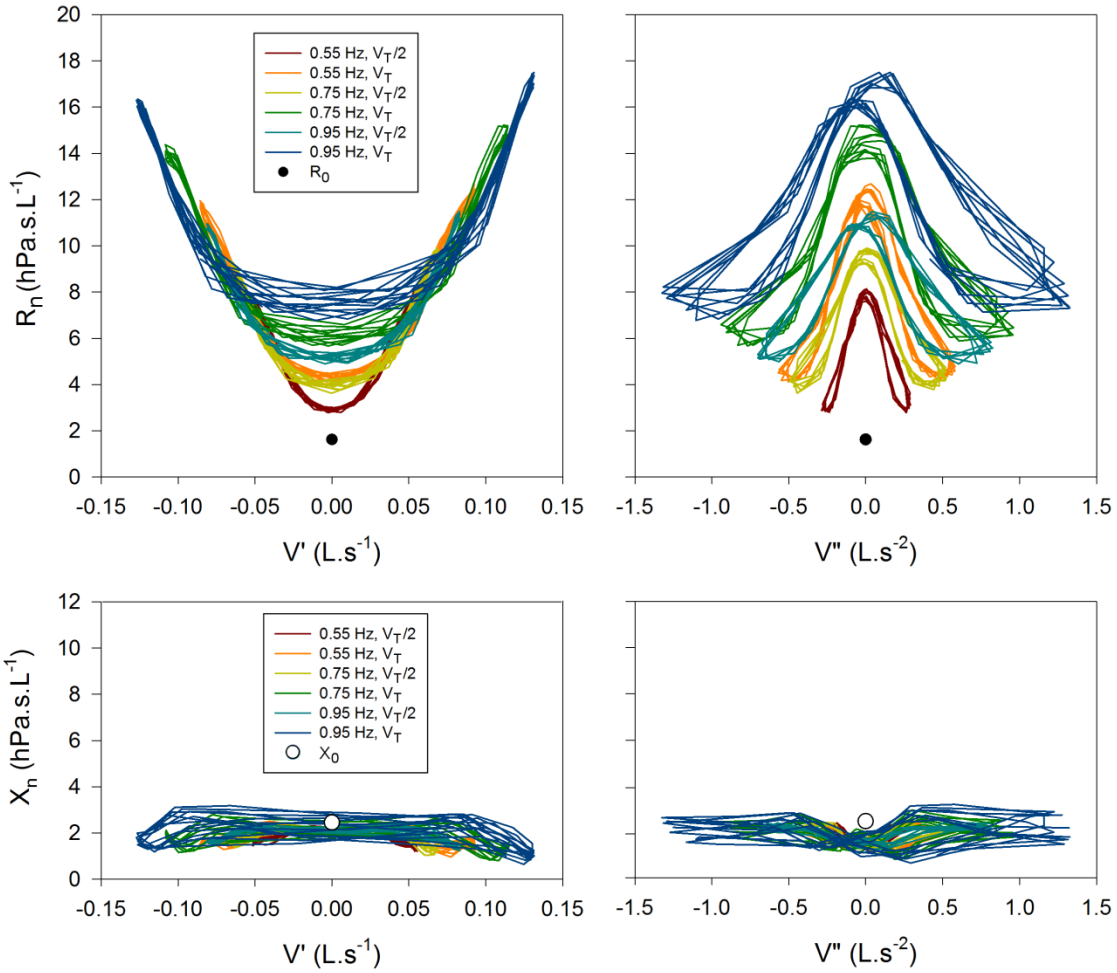

Figure 4. *Resistance (R_n) and reactance (X_n) plotted against flow (V') (left) and volume accelaration (V") (right) from a representative cast. Each set of coloured loops (see insets) corresponds to preset breathing frequencies (0.55, 0.75 and 0.95 Hz) and tidal volumes (V_T and $V_T/2$). Filled and empty circles indicate the lowest oscillatory R (R_0) and X (X_0), respectively, determined without tidal flow (V'=0).*

R_{eE} was shifted to higher values from R_0 even at the smallest V". The fluctuations of X_n were small and largely unaffected by changes in V' and V" (see also Supplement Figure S6). For all casts, a median value of shift in R_{eE} of 47% (range 41-52%) was observed at the lowest respiratory rate and V_T. A very strong linear relationship was observed between R_{eE} and $V"_{eE}$ in each set of cast measurements: r^2=0.994 (Q1 – Q3: 0.988 – 0.996, p<0.001) with considerable inter-individual variability in the coefficients of regression (Supplement Figure S2). The intercept of the linear regression was found to be a close estimate of R_0, characterized by a median of relative bias of -4.5% (-12 – 6%).

A characteristic nonlinear relationship was found between R_n and V', exhibiting segmental linearity and a prominent breakpoint after logarithmic transformation (Fig. 5).

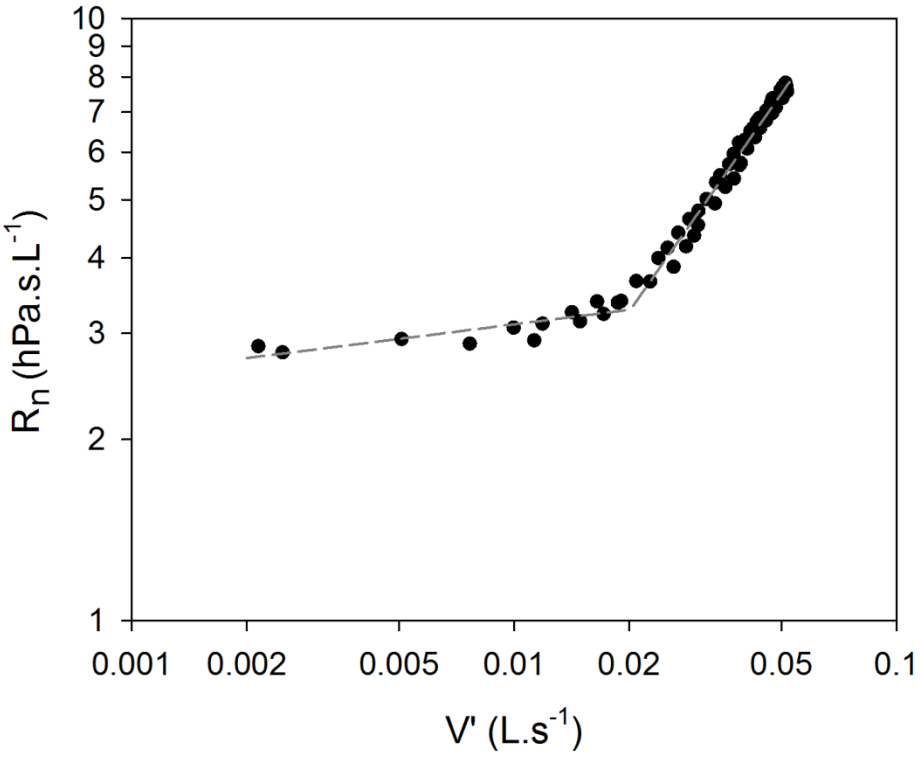

Figure 5. *Log-log plot of resistance (R_n) vs absolute value of flow (V') during expiration from a representative measurement (Setting: 0.55 Hz, halved tidal volume [V_T/2]). A segmented linear model with a breakpoint is fitted to the data, indicating power-law relationship with two exponents: a lower exponent for the first segment and a higher exponent for the second segment (below and above breakpoint, respectively).*

The adjusted r^2 values for the fitted piecewise linear model were 0.984 (0.974-0.989) and 0.984 (0.974-0.988) for the expiratory and inspiratory phase, respectively, with all frequencies and volumes included. V'_{bp} during the expiratory phase had a median value of 0.041 $L \cdot s^{-1}$ (0.028-0.058) for the entire dataset. The slope of the first segment (k1) was 0.0426 (0.0262-0.0649), while slope of the second segment (k1+k2) was steeper, with a median of 0.9572 (0.857-1.101). Similar piecewise linear R_{rs} *vs* V' relationships were observed in the *in vivo* measurements (Supplement Fig. S3).

V'_{bp} was found to be linearly related to V'' (r^2=0.96, p<0.001) with increasing residual errors at higher values (Fig. 6). The *in vivo* data exhibited a similar V'_{bp} *vs* V'' relationship at slightly lower values of V'_{bp}.

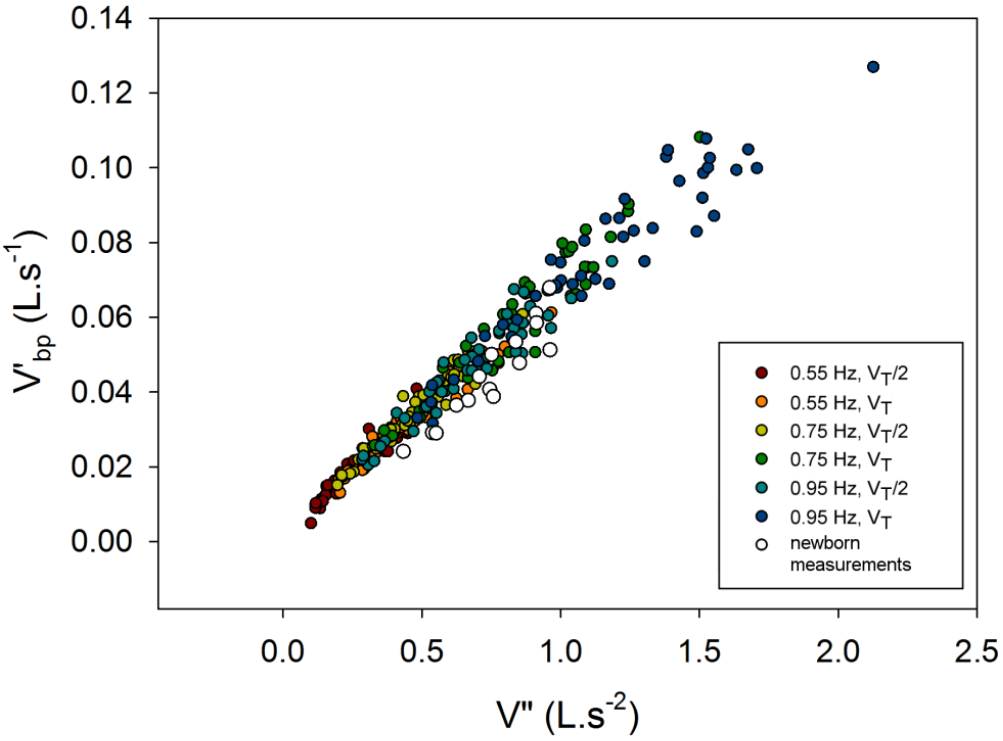

Figure 6. *Relationship between volume acceleration (V'') and flow at break point (V'$_{bp}$) estimated at different simulated breathing settings. Each colored circle represents a single measurement from all (n=45) casts. In vivo measurement from each newborn (n=15) recorded during the first 3 days of life are also shown (open circles).*

The estimated *Re* at maximal flow was 118.4 (91.3-154.9), while *Re* at V'$_{bp}$ at maximum respiratory rate (0.95 Hz) and full V_T was 60.8 (47.3-81.4). Figure 7 shows the relationships between the shape indices of the nasal airways and *Re*. The *Re* at V'$_{bp}$ (*Re*(V'$_{bp}$)) was found to be inversely proportional to the sparseness of the airway (r^2 = 0.43, $p<0.001$) and directly proportional to its flatness (r^2 = 0.31, $p<0.001$). Other structural descriptors (tortuosity, elongation or sphericity) had no connection with *Re*(V'$_{bp}$) ($p>0.10$). X_0 exhibited moderate correlation with sparseness and was found to be inversely proportional to flatness (r^2 = 0.24 and r^2 = 0.14, respectively, $p<0.05$). R_0 correlated weakly with sparseness (r^2=0.09, $p<0.05$) and had no correlation with flatness (r^2= 0.05, $p>0.10$).

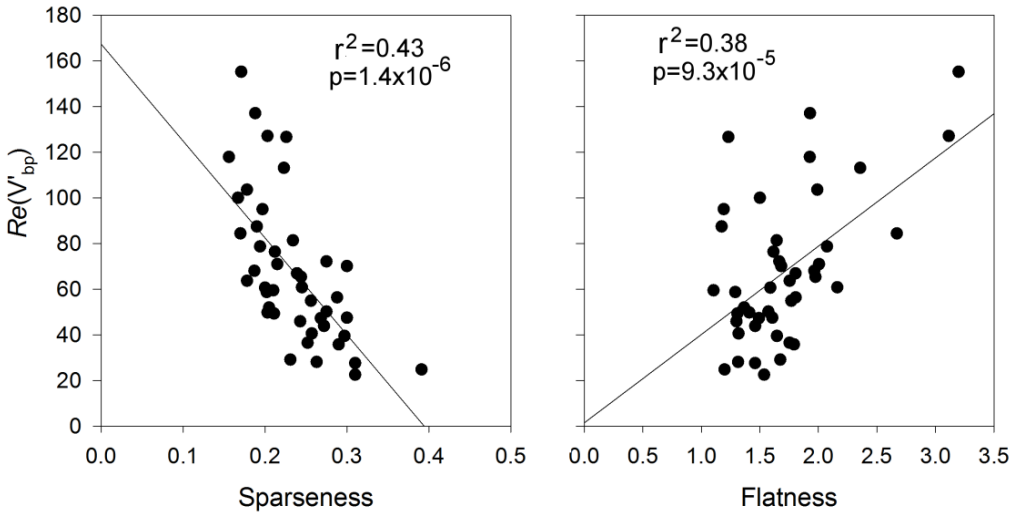

Figure 7. *Correlation between the Reynolds number at breakpoint flow Re(V'_{bp}) versus sparseness (left) and flatness (right) of the casts. High Re can be found for casts characterised by low sparseness and high flatness indicating that flow transition is delayed in narrow and flat upper airways (dominance of viscous forces). Each point corresponds to an individual cast (setting: 0.95 Hz, normal tidal volume).*

The nasal pathway was open both sides in 27 of the 45 casts. Unilateral total or near-total occlusion was present in 5 and 9 cases, respectively. Casts with bilateral near-total occlusion (n=4) were omitted from further analysis. A single case was found to have diffuse narrowing of the nasopharynx, resulting in extremely high R_0 and X_0 and was omitted from further analysis. The ECSA values of the nasal valve correlated significantly ($p<0.001$) and inversely with R_0 and X_0 (r= (-0.704) and (-0.709), respectively) (see Figure 8). The linearly approximated V'-dependent increase in R_n ($R_{V'maxE}$-$R_{eI}.V'^{-1}_{maxE}$ and $R_{V'maxI}$-$R_{eE}.V'^{-1}_{maxI}$) correlated moderately with ECSA (Figure 9).

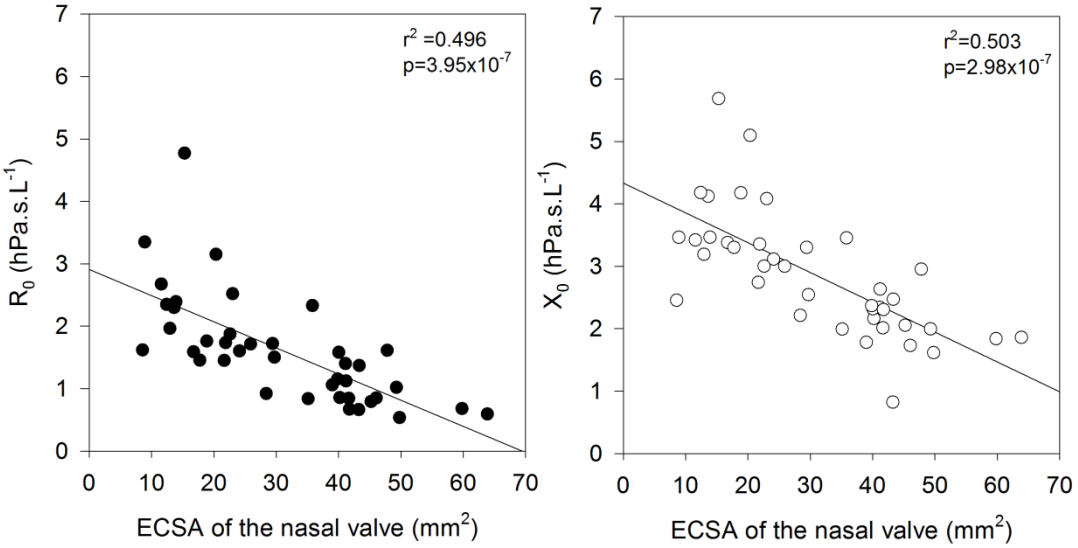

Figure 8. *Correlation between effective cross sectional area (ECSA) at nasal valve versus lowest oscillatory resistance (R_0) (left panel) and lowest oscillatory reactance (X_0) (right panel). Cases with bilateral critical narrowing (n=4) and nasopharyngeal obstruction (n=1) were not included in the final statistical analysis (n=40) (unpublished data).*

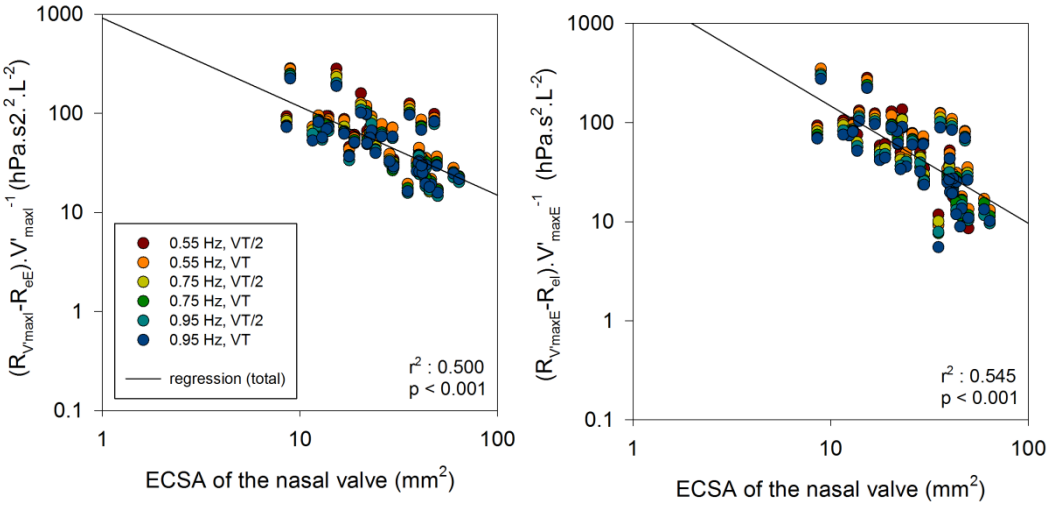

Figure 9. *Correlation between effective cross sectional area (ECSA) at nasal valve versus normalized flow-dependent increase in inspiratory (left) and expiratory resistance (right). Each symbol represents a cast (from n=40), measured at different respiratory rates at full or halved tidal volume (V_T). Unpublished data.*

To estimate R_0 based on the intra-breath R-V' loops (Fig. 10, top panel) the slope of the fitted line was determined between R_{eE} and R_n at maximum inspiratory flow (RV'_{maxI}). The slope of this linear fit remained constant across the different respiratory rates and V_T's. When this linearly approximated V'-dependent increase in R_n was compared to the V"-dependent shift in R_{eE} (Fig. 10, bottom panel) strong linear relationships were found. By utilizing this relationship, R_0 can be estimated from a single intra-breath impedance measurement:

$$R_0 = R_{eI} - V''_{eI} \times c \times \frac{R_{V'maxE} - R_{eI}}{V'_{maxE}} \qquad \text{(Eq. 7.)}$$

where *c* is a correction factor with a value of 0.0646 s^{-1}, the slope determined from the expiratory limb in Fig. 10, bottom panel. A strong relationship with a similar slope (0.0709 s-1, $p<0.001$) was also observed for the inspiratory limb (data not shown). This estimation of R_0 is hence independent of respiratory rate and tidal volume.

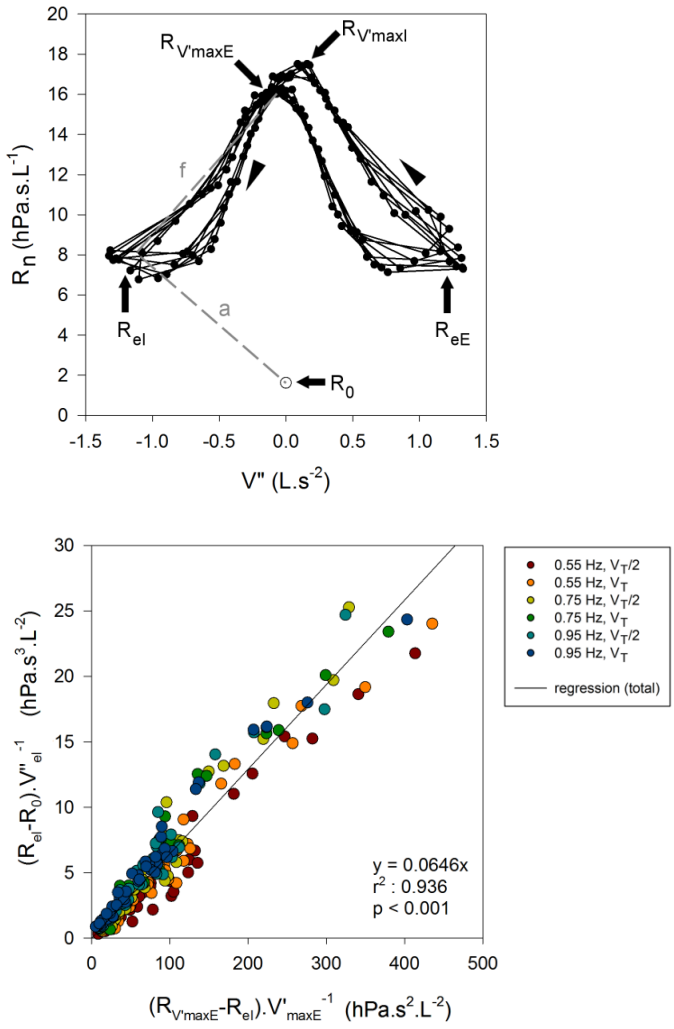

Figure 10. *Top: Resistance (R_n) vs. volume acceleration (V") plot from a representative cast. Lowest oscillatory R ($R_{0;}$ ○), and R_n measured with superimposed breathing at 0.95 Hz with full tidal volume (V_T) (black line and ●). Each data point is marked with a closed symbol. Dashed line marked with letter "f" shows the slope of V'-dependent increase in R; dashed line marked with the letter "a" represents the shift in the minimal resistance (R_0) due to V". Arrowheads indicate inspiratory limb of the loops. Highest resistances occur at peak inspiratory flow ($R_{V'maxI}$) and at peak expiratory flow ($R_{V'maxE}$). Bottom: V"- dependent shift in R_{eI} [$(R_{eI}-R_0).V"^{-1}_{eI}$], i.e. slope "a" at top, plotted against V'-dependent increase in R_n [$(R_{V'maxE}-R_{eI}.V'^{-1}_{maxE}$], slope "f", reflecting a strong linear relationship. Each symbol represents a cast, measured at different respiratory rates at full or halved tidal volume (V_T and $V_T/2$).*

The relative error of measured and corrected R_{eE} with respect to the R_0 at each setting of the respirator is shown in Fig. 11. Measured R_{eE} was significantly ($p<0.001$) higher than corrected R_{eE} at each setting with increasing differences at higher frequency and V_T.

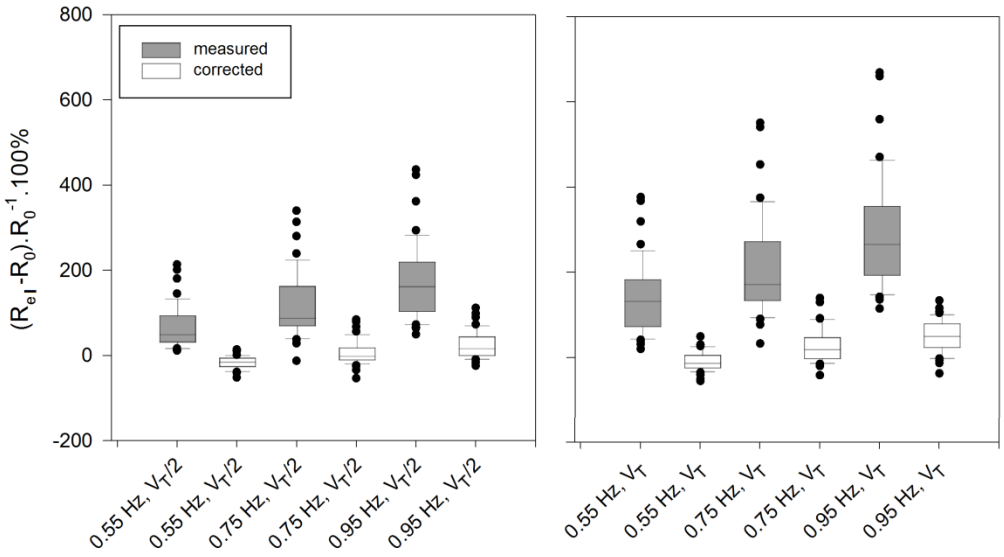

Figure 11. *Relative error of measured (gray box) and corrected (open box) lowest resistances (ReE) with respect to the oscillatory resistance without superimposed breathing (R_0) at each setting of the respirator. Respiratory rate varied from 0.55 Hz to 0.95 Hz, at full (V_T, right panel) and halved ($V_T/2$, left) tidal volume.*

After applying the mathematical correction in R_{eE} to the *in vivo* measurements, the end-inspiratory R (R_{eI}) decreased by 33% (9.5 - 70%, $p<0.001$), while R_{eE} dropped by 19% (1.6 - 33%, $p<0.001$) (Supplement Fig. S3).

X_0 had positive values in all casts, indicating the presence of inertance in the rigid upper airway casts. The overall shape of X_n-V' loops mirrored the pattern of R_n-V' loops (Supplement Fig. S6); however, the changes of X_n were smaller and not as regular as seen for R_n. X_n decreased significantly (Repeated measures ANOVA on Ranks, $p<0.001$) when simulated breathing was applied (Supplement Fig. S7). End-expiratory X_n (X_{eE}) was found to be somewhat lower than X_0, indicating the influence of V'' on X_n. However the V'' - X_{eE} relationship was not strictly monotonous like the V'' - R_{eE} . X_n was found to be V'-dependent: the lowest values of X_n were measured at peak inspiratory and expiratory flows ($X_{V'maxI}$ and $X_{V'maxE}$). However, the decrease was independent of the actual values of V'_{max}.

The ”mirroring” pattern of Xrs-V’ loops was visible in most of the *in vivo* measurements in healthy newborns (Supplement Fig. S8). However, in some newborns we also observed increases in Rrs accompanied with increasing (less negative) Xrs values at peak V’s – a phenomenon never encountered *in vitro*.

Results of Study 2

A total of 109 newborns were enrolled in the study. Six subjects were excluded due to technical reasons (see pre-defined exclusion criteria in the Methods section). Although the measurements were technically acceptable, 17 of the remaining 103 subjects were excluded on the basis of physiologically unrealistic values of Zrs parameters, such as negative L (n=4), low C (<0.5 $mL.hPa^{-1}$) (n=6) or high RL product (>10 $hPa^2.s^3.L^{-2}$) suggestive for nasal obstruction (n=7); in 4 of these 17 subjects, two exclusion criteria applied. Most of these subjects were also identified as outliers during regression diagnostics, and therefore they were omitted from further analysis. Statistical analysis was performed on the data of the remaining 86 newborns (41 females, 45 males; spontaneous delivery: 41, caesarean section: 45). The birth weight was (mean ± sd) 3269 ± 546 g, the body length was 49 ± 2.4 cm. The gestational age at birth was 38.7 ± 1.3 weeks.

The mean total recording time in the 103 subjects was 14 min (range: 8-21 min); the recordings were suspended for 3-10 min in 13 subjects, and the measurements were successful only on the following day in 3 neonates. On the average, 48 (range: 15-105) respiratory cycles were analysed from the intra-breath oscillometry in each newborn; these were collected as segments of steady-state breathing from a minimum of three 90-s recordings. The average values of spectral outcomes were calculated from 6 (3-11) recordings of a mean length of 26 s (12-30 s).

No significant (p= 0.20) difference were found with pairwise t-test when comparing mean Rrs (51.0 ± 14 and 52.4 ± 16.8 $hPa.s.L^{-1}$) measured with spectral and intra-breath oscillometry, respectively.

Overall, the intra-breath changes in Zrs, dominated by the V’ dependence, were remarkably large. R_{ppE} and R_{ppI} amounted to 91.4 ± 33.3 % and 55.9 ± 27.6 %, respectively, of the average zero-flow impedance magnitude, i.e. $Z_0=½(Z_{eE}+Z_{eI})$. The maximum Rrs was usually located near the peak V’, while the minimum was found around V’=0. The corresponding

changes in Xrs (X_{ppE} and X_{ppI}) were roughly half as large (44.9 ± 26.8 % and 32.7 ± 19.3 %, respectively, of Z_0). Tidal change in Rrs was on the average close to zero (ΔR= -0.4 ±6.5 hPa.s.L^{-1}), with negative values of ΔR observed in 51% of the subjects, whereas the decreases in Xrs between end expiration and end inspiration were more uniform (ΔX = 2.39 ± 3.44 hPa.s.L^{-1}).

Short-term changes in Zrs are illustrated with a few selected segments of intra-breath recordings (Fig. 12). These examples are not intended to be exhaustive; they only highlight epochs where *(i)* regular intra-breath fluctuations in Rrs and Xrs are observed despite a slightly irregular spirogram (panel A), *(ii)* a slow negative drift in Xrs occurs (panel B) or *(iii)* increasing fluctuations in both Rrs and Xrs take place at virtually even tidal volumes (panel C), and *(iv)* the large expiratory increases in Rrs and decreases in Xrs are reduced following a sigh (panel D).

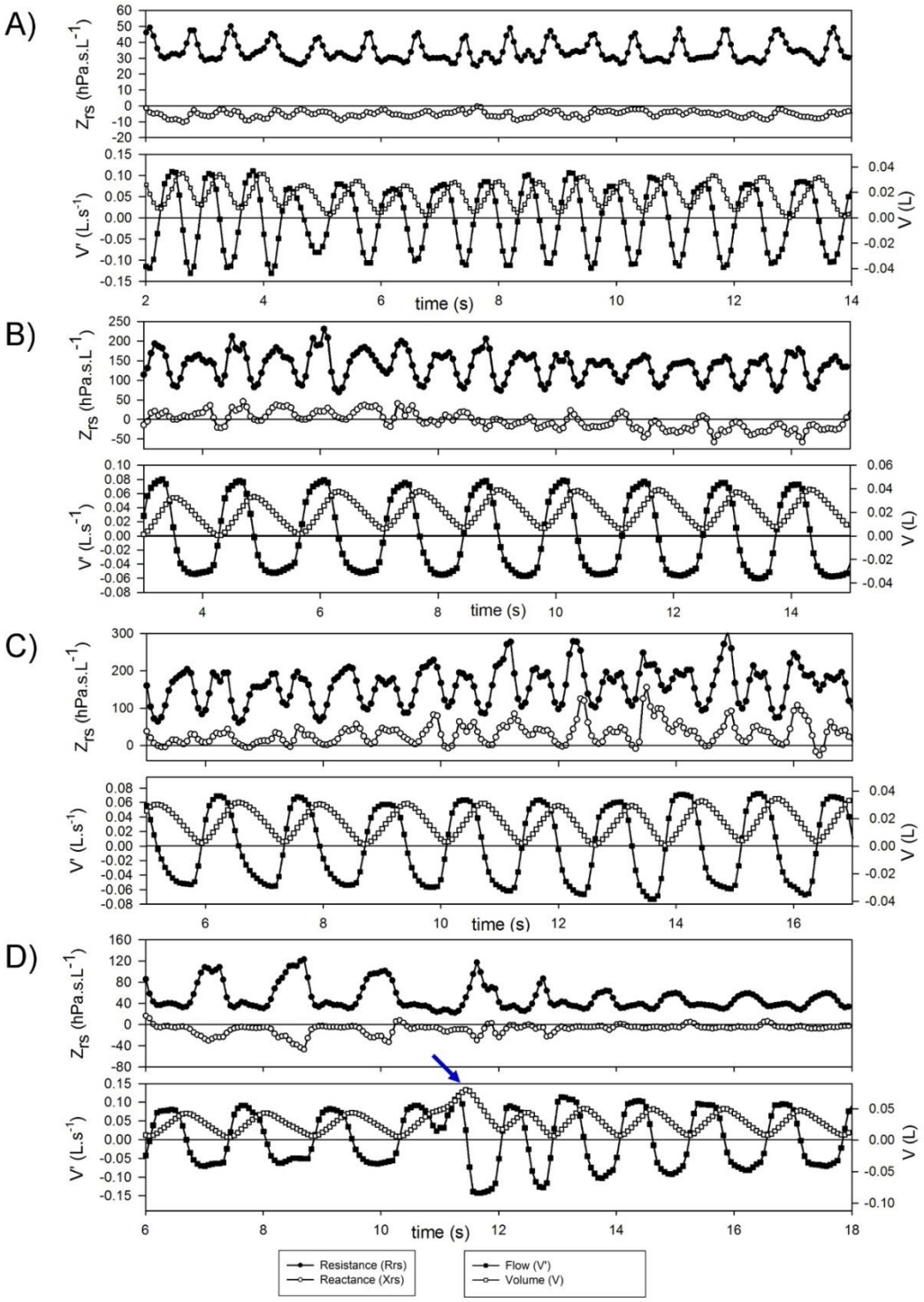

Figure 12. *Examples of short term changes in impedance (Zrs) and breathing pattern. Each graph represents a 12-s period. A: Slightly irregular tidal flow but stable and low Zrs. B: Slow downward drift in reactance (Xrs) during regular breathing. C: Increasing flow dependence of Zrs during steady-state breathing; this probably reflects spontaneous development of nasal obstruction. D: Transient decrease of expiratory flow limitation after a spontaneous sigh (arrow).*

Whereas Rrs exhibited positive V’ dependences during inspiration and expiration, the intra-breath changes in Xrs were more diverse. Four typical patterns were determined qualitatively and are exemplified in Fig. 13 where Rrs and Xrs are plotted against V and V’. These patterns are characterised as minimal dependence of Xrs on V’ (Pattern A), marked V’-dependent decrease in Xrs during expiration (Pattern B), marked V’-dependent decrease during inspiration (Pattern C) and marked V’-dependent increases in Xrs (Pattern D).

Each newborn was classified into one group according to the V’-dependence of Xrs by cluster analysis, presuming that four different patterns exist (Fig. 14).

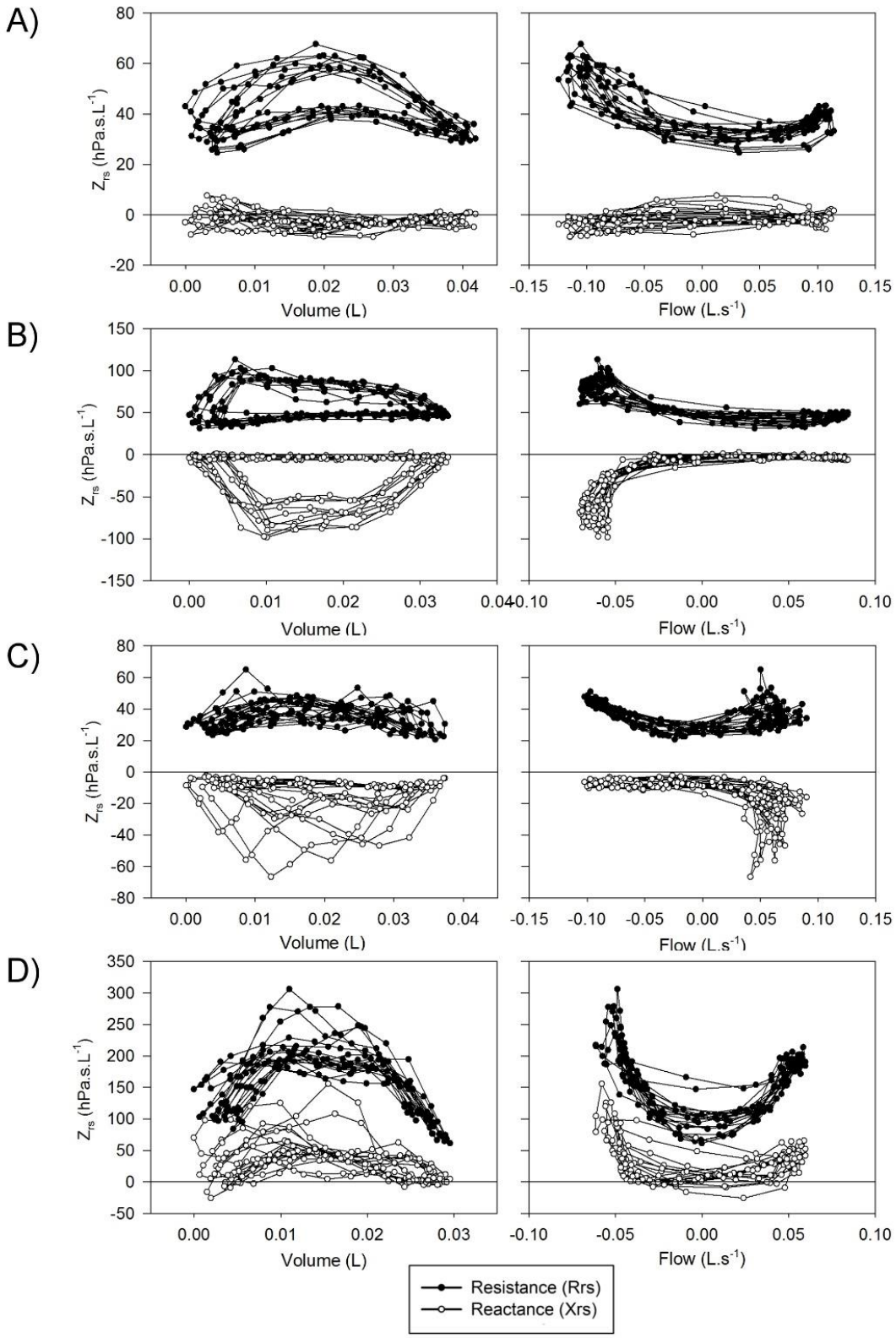

Figure 13. *Typical patterns of intra-breath changes in respiratory impedance (Zrs). A: insignificant changes in reactance (Xrs) and mild flow nonlinearity in resistance (Rrs); B: marked fall in Xrs and increase in Rrs during expiration; C: marked fall in Xrs in inspiration; D: increases in Xrs and Rrs with both inspiratory and expiratory flow.*

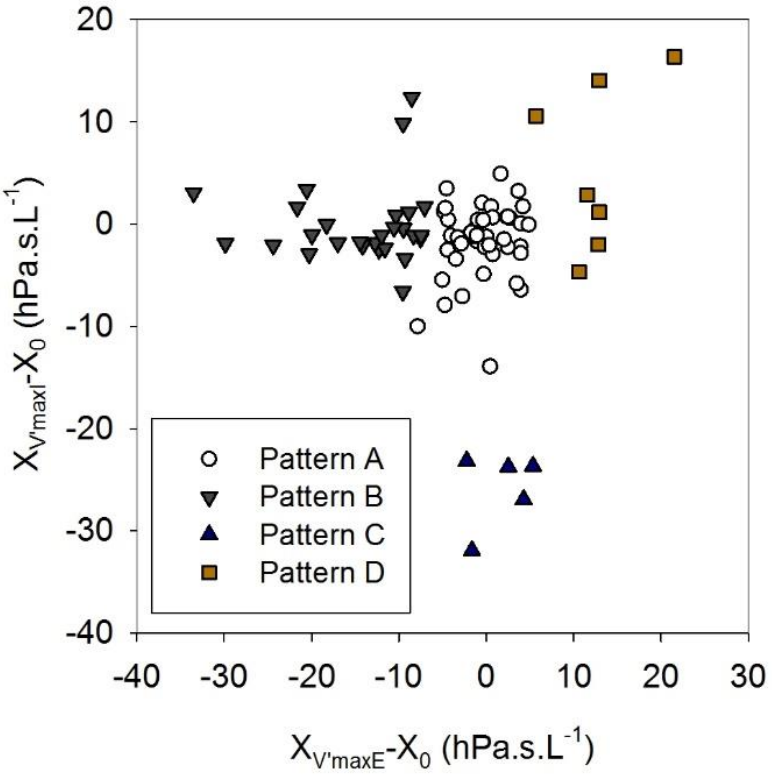

Figure 14. *Clusters established in the relationships between inspiratory and expiratory flow dependences of reactance. $X_{V'maxI}$ and $X_{V'maxE}$ are reactance values at peak inspiratory and expiratory flows, X_0 is the average zero-flow value of reactance. For definitions of Patterns A-D, see text or the legend to Table 2.*

Subjects with the lowest V'-dependence in Xrs (Pattern A) were considered the control group. Tables 2, 3 and 4, respectively, contain the anthropometrical and tidal breathing data, the spectral oscillometry measures and the intra-breath variables in the 4 clusters. Slightly lower body measures were found in the Pattern C and D groups and lower f_{br} values in Pattern B-D groups compared to the Pattern A data (Table 2).

Table 2. *Comparison of anthropometry and spirogram data between subject groups of different patterns of flow dependence of reactance. Mean ± SD values.*

	All (n=86)	**Pattern A (n=47)**	**Pattern B (n=27)**	**Pattern C (n=5)**	**Pattern D (n=7)**
GA (weeks)	38.7 ± 1.3	38.9 ± 1.2	38.6 ± 1.2	38.0 ± 2.1	38.3 ± 1.4
BL (cm)	49.5 ± 2.4	50.0±2.5	49.3 ± 2.3	48.0 ± 2.7	47.7 ± 1.5**
BW (g)	3269 ± 546	3365 ± 569	3293 ± 490	2694 ± 491*	2931 ± 210**
f_{br} (min^{-1})	62.0 ± 11.4	65.3 ± 12.2	58.2 ± 9.5**	57.9 ± 5.0*	57.5 ± 10.1
V_T (mL)	29.3 ± 5.5	29.3 ± 5.9	29.7 ± 4.6	26.2 ± 3.6	30.6 ± 6.5
V'_{maxE} ($mL.s^{-1}$)	90 ± 17	93 ± 17	81 ± 15**	77 ± 15	81 ± 16
T_E/T_{tot}	0.50 ± 0.03	0.50 ± 0.03	0.52 ± 0.03**	0.47 ± 0.03	0.51 ± 0.01
T_{PTEF}/T_E	0.47 ± 0.07	0.47 ± 0.07	0.45 ± 0.09	0.49 ± 0.07	0.49 ± 0.07
CoV[T_{tot}]	0.155 ± 0.058	0.155 ± 0.059	0.168 ± 0.055	0.132 ± 0.032	0.118 ± 0.058
CoV[V_T]	0.219 ± 0.092	0.231 ± 0.07	0.212 ± 0.069	0.162 ± 0.072	0.202 ± 0.097

Pattern A: minimal dependence of reactance (Xrs) on flow (V').

Pattern B: marked V'-dependent decrease in Xrs during expiration.

Pattern C: marked V'-dependent decrease during inspiration.

Pattern D: marked V'-dependent increases in Xrs.

GA: gestational age, BL: birth length, BW: birth weight, f_{br}: respiratory rate, V_T: tidal volume, V'_{maxE}: peak expiratory flow, T_E: expiratory time, T_{tot}: total respiratory cycle time, T_{PTEF}: time to peak tidal expiratory flow, CoV: coefficient of variation.

**p<0.05 vs Pattern A; **p<0.01 vs Pattern A*

Table 3. *Comparison of spectral oscillometry data between subject groups of different patterns of flow dependence of respiratory reactance. Mean ± SD values.*

	All (n=86)	**Pattern A (n=47)**	**Pattern B (n=27)**	**Pattern C (n=5)**	**Pattern D (n=7)**
R (hPa.s.L^{-1})	48.7 ± 12.9	46.0 ± 12.6	48.7 ± 11.5	59.9 ± 17.4	58.3 ± 9.4*
C (mL.hPa^{-1})	1.08 ± 0.30	1.13 ± 0. 32	1.01 ± 0. 29	1.05 ± 0.28	1.06 ± 0. 15
L (hPa.s^2.L^{-1})	0.068 ± 0.028	0.071 ± 0.027	0.057 ± 0.023*	0.047 ± 0.031	0.102 ± 0.020**
R_8 (hPa.s.L^{-1})	63.2 ± 16.8	59.6 ± 16.3	64.6 ± 16.4	77.3 ± 22.1	72.0 ± 11.2*
X_8 (hPa.s.L^{-1})	-14.9 ± 5.4	-13.9 ± 5.1	-16.7 ± 5.8*	-17.1 ± 5.8	-13.3 ± 4.2
R_{8-32} (hPa.s.L^{-1})	18.6 ± 7.3	16.9 ± 6.4	20.6 ± 8.5	24.7 ± 5.9*	17.6 ± 5.0
f_{res} (Hz)	21.4 ±5.9	20.1 ± 5.2	23.7 ± 4.7**	29.2 ± 11.9	16.3 ± 1.9**
Ax (hPa.L^{-1})	103.1 ± 59.6	90.7 ± 55.1	124.8 ± 58.5*	157.0 ± 80.3	64.0 ± 20.8*

For definitions of Patterns A-D, see text or the legend to Table 2. R: resistance (model fitting), C: compliance (model fitting), L: inertance (model fitting), R_8: resistance at 8 Hz; X_8: reactance at 8 Hz, R_{8-32}: resistance difference between 8 and 32 Hz, f_{res}: resonance frequency, Ax: reactance area below f_{res}.
**p<0.05 vs Pattern A; **p<0.01 vs Pattern A*

L was the highest while f_{res} and Ax were the lowest in the positive V' dependence (Pattern D) group (Table 3). L was significantly ($p<0.05$) lower and Ax was higher in subjects with negative expiratory swings in Xrs (Pattern B) compared to Pattern A. Unlike the values of X_8, parameter C was found to be not different between groups. The overall fitting error of the R-C-L model to the Zrs data was 7.4±2.8%; its components broken down to Rrs and Xrs were 6.3±2.7% and 3.7±1.6%, respectively.

Comparison of intra-breath measures (Table 4) revealed mild elevations in R_{eE} and R_{eI} in the C and D groups but no differences in ΔR between the different patterns. ΔX reached significantly higher values in the Pattern B group than in the rest of groups.

Table 4. *Comparison of intra-breath oscillometry data between subject groups of different patterns of flow dependence of respiratory reactance. Mean ± SD values.*

	All (n=86)	**Pattern A (n=47)**	**Pattern B (n=27)**	**Pattern C (n=5)**	**Pattern D (n=7)**
R_{eE} (hPa.s.L^{-1})	41.7 ± 11.3	38.7 ± 10.1	41.9 ± 9.0	53.3 ± 16.0	52.7 ± 13.2*
R_{eI} (hPa.s.L^{-1})	42.1 ± 13.5	38.5 ± 13.4	43.7 ± 11.7	51.3 ± 15.8	53.5 ± 11.2*
X_{eE} (hPa.s.L^{-1})	-1.35 ± 3.98	-1.55 ± 3.55	-1.516 ± 3.14	-6.74 ± 2.84*	4.53 ±3.86**
X_{eI} (hPa.s.L^{-1})	-3.73 ±4.21	-3.14 ± 3.54	-5.45 ± 3.69*	-8.05 ± 4.23	1.92 ± 3.92*
ΔR	-0.40 ± 6.48	0.23 ± 6.30	-1.83 ± 7.48	2.03 ± 2.43	-0.81 ± 5.16
ΔX	2.39 ± 3.44	1.58 ± 3.30	3.93 ± 3.72**	1.30 ± 1.74	2.62 ± 2.36
$R_{ppE}/\|Z_0\|$	0.91 ± 0.33	0.80 ± 0.26	1.08 ± 0.32**	0.67 ± 0.20	1.25 ± 0.43*
$R_{ppI}/\|Z_0\|$	0.56 ± 0.28	0.52 ± 0.24	0.50 ± 0.22	0.87 ± 0.21*	0.85 ± 0.46
$X_{ppE}/\|Z_0\|$	0.45 ± 0.27	0.32 ± 0.13	0.70 ± 0.31**	0.28 ± 0.08	0.50 ± 0.14**
$X_{ppI}/\|Z_0\|$	0.32 ± 0.19	0.30 ± 0.13	0.28 ± 0.09	0.90 ± 0.28**	0.33 ± 0.14

For definitions of Patterns A-D, see text or the legend to Table 2. R_{eE}: resistance at end expiration, R_{eI}: resistance at end inspiration, X_{eE}: reactance at end expiration, X_{eI}: reactance at end inspiration, ΔR: tidal change in resistance (R_{eE}-R_{eI}), ΔX: tidal change in reactance (X_{eE}-X_{eI}), R_{ppE}: peak-to-peak resistance difference in expiration, R_{ppI}: peak-to-peak resistance difference in inspiration, X_{ppE}: peak-to-peak resistance difference in expiration, X_{ppI}: peak-to-peak resistance difference in inspiration, $|Z_0|$: impedance magnitude at zero flow [½($|Z_{eE}|+|Z_{eI}|$)].

**p<0.05 vs Pattern A; **p<0.01 vs Pattern A*

Differences in the V' dependence of Rrs measures (R_{ppE} and R_{ppI}) were milder between groups than that of Xrs measures (X_{ppE} and X_{ppI}) as the latter are related to the clustering variables (Fig. 14).

Fig. 15 gives an overview on the correlations between selected indices of the spirogram, spectral oscillometry and intra-breath analysis. Among the between-category comparisons, high correlation coefficients were found between R and the intra-breath Rrs measures and between the spectral (L, f_{res} and Ax) and intra-breath Xrs measures, except C which was most correlated with Ax and X_8 but not with intra-breath Xrs data. A weak although statistically significant ($r=0.39$, $p<0.001$) linear correlation was found between ΔR and $|V''_{eE}/V''_{eI}|$.

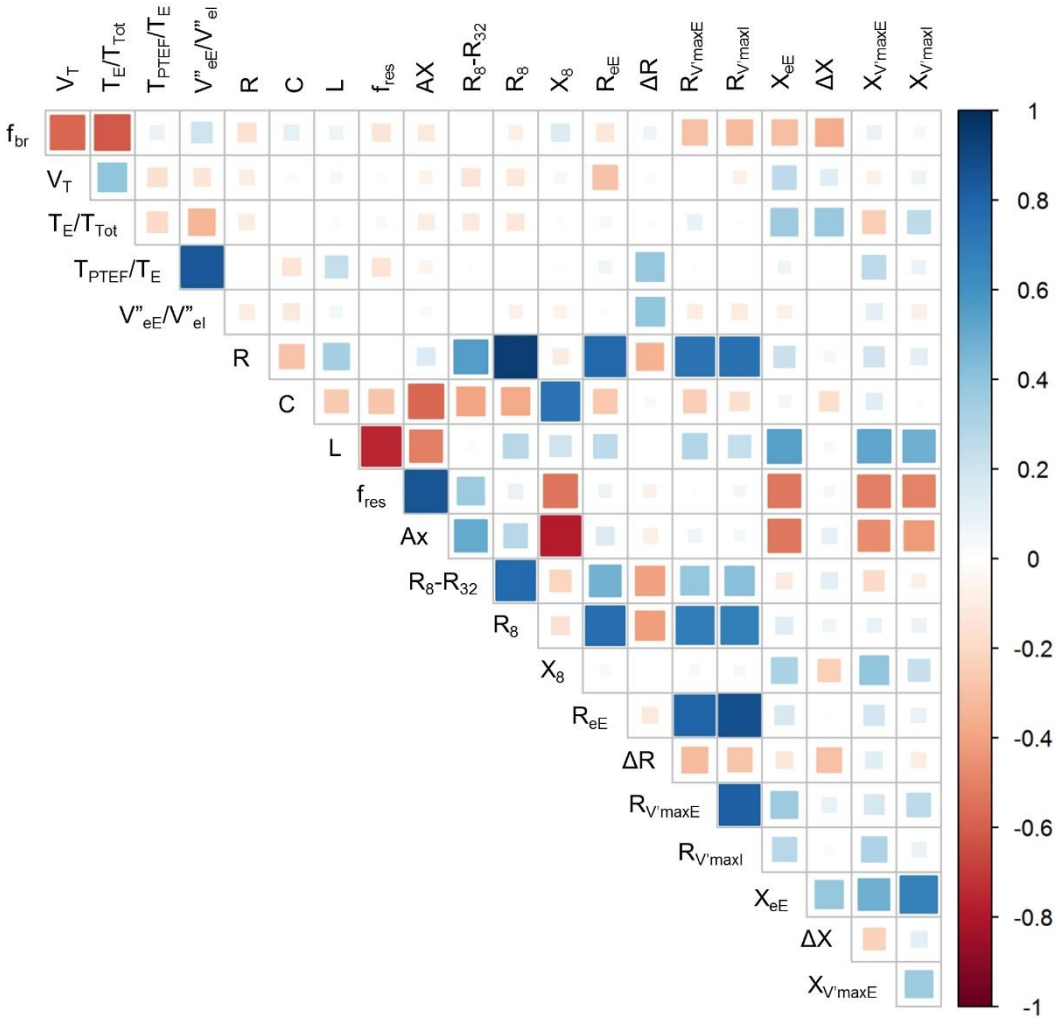

Figure 15. *Correlogram for selected measures of tidal breathing, spectral oscillometry and intra-breath oscillometry. For definition of variables, see legend to Table 5.*

T_{PTEF}/T_E was not correlated with any of the spectral and intra-breath Rrs or Xrs outcomes, but exhibited a very strong relationship ($r=0.84$, $p<0.001$) with $|V''_{eE}/V''_{eI}|$, apparently unrelated to the pattern of V' dependence of Xrs (Fig. 16).

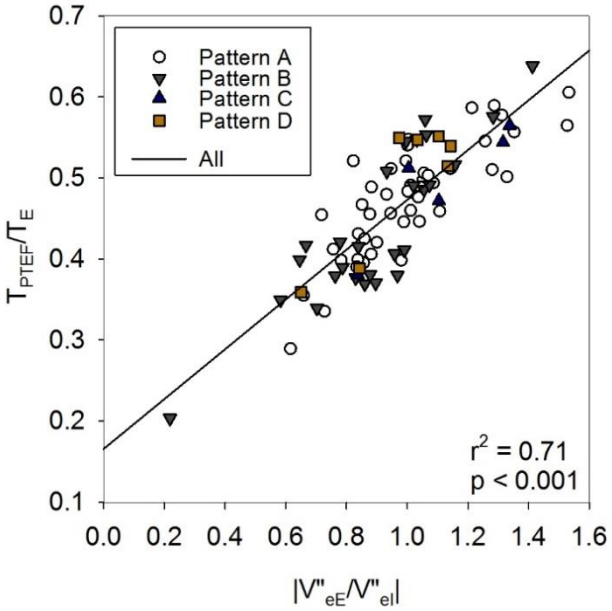

Figure 16. *Effect of asymmetry in volume acceleration (V''_{eE}/V''_{eI}) on T_{PTEF}/T_E.*
V''_{eE}: end-expiratory volume acceleration, V''_{eI}: end-inspiratory volume acceleration. T_{PTEF}: time to peak tidal expiratory flow; T_E: expiratory time. For definitions of Patterns A-D, see text or the legend to Table 2.

Table 5. *Within-session variability presented as coefficient of variation (in %) of tidal breathing, spectral oscillometry and intra-breath oscillometry indices. Mean (range) values.*

Variable	Mean (min - max)
f_{br}	14.0 (3.9 - 38.2)
V_T	21.9 (7.8 - 42.3)
T_E/T_{tot}	7.9 (3.3 - 13.8)
T_{PTEF}/T_E	19.6 (11.1 - 44.4)
R	10.3 (1.9 - 29.7)
C	20.3 (3.3 - 88.4)
L	26.6 (3.6 -154.0)
$\|Z_8\|$	13.6 (5.3 – 30.7)
R_{8-32}	26.5 (5.2 - 64.6)
f_{res}	15.7 (1.9 - 67.6)
Ax	37.9 (7.5 - 186.1)
$\|Z_{eE}\|$	19.6 (5.3 – 117.7)
$\|Z_{eI}\|$	23.1 (4.9 – 100.6)
$\|Z_{V'maxE}\|$	23.6 (4.3 – 71.0)
$\|Z_{V'maxI}\|$	22.2 (5.5 – 58.0)

f_{br}: respiratory rate, V_T: tidal volume, V'_{maxE}: peak expiratory flow, T_E: expiratory time, T_{tot}: total respiratory cycle time, T_{PTEF}: time to peak tidal expiratory flow, R: resistance (model fitting), C: compliance (model fitting), L: inertance (model fitting), $|Z_8|$: impedance magnitude at 8 Hz, R_{8-32}: resistance difference between 8 and 32 Hz, f_{res}: resonance frequency, Ax: reactance area below f_{res}., $|Z_{eE}|$: impedance magnitude at end expiration, $|Z_{eI}|$: impedance magnitude at end inspiration, $|Z_{V'maxE}|$: impedance magnitude at maximum expiratory flow, $|Z_{V'maxI}|$: impedance magnitude at maximum inspiratory flow.

DISCUSSION

Discussion of Study 1

The primary aim of this study was to examine the confounding effect of the nasal pathway during oscillometric assessment of lung mechanics. The contribution of R_n to R_{rs} (especially during tidal breathing) is a main problem in infant pulmonary function testing, but examining this effect is difficult with non-invasive techniques. Therefore, we used geometrically faithful, although rigid upper airway casts to measure Rn and simulate the effects of spontaneous breathing on this parameter *in vitro*.

Validity of R_0

We hypothesize that R_0 can be the most appropriate outcome measure for comparing patients, since it is the lowest R, unbiased by the dynamic effects of tidal breathing. Note that R_0 was assessed, instead of the pertinent unidirectional Poiseuille flow, with 16-Hz sinusoidal oscillations. This causes an overestimation of Poiseuille R (R_P) via the frequency dependence of resistance [45-47]. We could demonstrate a moderate correlation (r^2=0.41) between the Womersley number (Wo) and the ratio of measured R_0 to calculated R_P, a phenomenon already described in straight tubes by Dorkin et al [45]. (see Supplement Figure S5).

Although R_0 is the lowest oscillatory R, it can be measured only during apnea, which may limit its widespread use. R_0 values in our nasal airway casts were systematically lower than that in a previously published study in infants [27]. In the latter study, infants were measured during apnea with low-frequency oscillometry, and nasal resistance was estimated by applying a nasal cannula with a manometer. The oscillatory frequency was higher in the present study (16 Hz sine wave vs. 0.5-20 Hz pseudorandom signal) allowing us to use lower amplitude (18-20 ml/s vs 60-80 ml/s peak-to-peak) while achieving the same signal-to-noise ratio. The 60-80 ml/s amplitude represents ~70% of the flow measured during tidal breathing in infants, thus it is high enough to cause nonlinearities in the nasal airways. We tested this effect in a subgroup (n=12) of our casts. Increasing the oscillatory flow to 28-32 ml/s (peak-to-peak) resulted in an increase in R_0 of 11% (8.7-16.5%). Additionally, some extra dissipation can be produced by the collapsibility of the upper airways *in vivo* leading to even higher R values [49].

Validity of R_{eE}

If the nasal pathway acted as a pure linear resistor, the R_{eE} would be independent from respiratory rate and V' and would thus be equal to R_0. However, we found that R_{eE} increased linearly with V''_{eE} and was considerably higher than R_0 even at the lowest respiratory rate. Direct measurement of R_{eE} as well as R_{eI}, are biased by the extra dissipation due to unstable V' arising in the nasal pathway at phase transitions. This phenomenon was described previously in tracheal models by Isabey and coworkers [50], [51]. We conclude that R_{eE} alone may not be an appropriate estimate of R_0. However, serial measurements of R_{eE} at different V" values enable a fair approximation of R_0, as the coordinate intercept of the linear function.

Utility of R_n-V' segmented power-law model

We found that the relation of R_n to V' can be described by a segmented power-law equation. The first segment had an almost negligible increase until a breakpoint followed by a more abrupt elevation above the breakpoint. This non-linear behaviour of the P-V' relationship in the nasal airways may be related to a developing non-laminar flow regime [30], [50-52] and to singular pressure losses at abrupt narrowings, i.e. the so-called orifice effect [54]. Both processes may contribute to the sharper V'-dependent rise observed in R_n beyond V'_{bp}. Our data also showed that V'_{bp} has a strong linear dependence on V". Increasing V" may affect flow rheology by the re-laminarisation of turbulent flow [55].

The effect of sharp narrowings in the nasal passages is reflected in the relation between certain shape descriptors and *Re*(V'_{bp}). Upper airway casts with higher sparseness had a relatively spacious cavity with less wall irregularities and lower surface/volume ratio. Flatness on the other hand is an indicator of relative narrowness of the nasal passage, mimicking a slit between two infinite parallel plates. Sparse but not flat nasal cavities, acting as wide cylinders, had low *Re*(V'_{bp}) values, suggesting that this geometry is advantageous for the development of turbulent flow.

The nasal valve is the narrowest segment of the nasal pathway and it is considered to be responsible for 50-75% of the total Rn [56], [57]. Our results fit well with the literature data: R_0 and X_0 correlated inversely with the ECSA of the nasal valve with an r^2 value close to 0.5. The R-V' relationship was also affected by the nasal valve geometry. A power law function was found to describe the relationship between nasal valve ECSA and normalized flow-

dependent increase in R during inspiration and expiration (($R_{V'maxI}$-R_{eE}).V'_{maxI}^{-1} and $R_{V'maxE}$-R_{eI}).V'_{maxE}^{-1}, respectively). (Unpublished data.)

Despite the fact that V'_{bp} correlated well with structural variables, the utility of V'_{bp} and other parameters of the segmented power-law model remain limited in the in vivo estimation of R_0, because of the strong V" dependence. This was verified in a selected small group of healthy term newborns even though there was a strong V'_{bp}-V" relationship (Fig. 6) and the model fitted well for these *in vivo* measurements (Supplement Fig. S3).

Geometrical estimation of R_0 from a single R_n-V' loop

We propose a method for correcting the shift in R_{eE}, thus estimating R_0, by the normalized flow-dependent increase in R: ($R_{V'maxI}$-R_{eE})/V'_{maxI}. This method can be applied to a single set of intra-breath oscillometric measurements, without the need for changing respiratory rate or tidal volume, as performed in our simulations. Infant measurements showed that the effect of upper-airway non-linearities are even significant around zero V' and represent up to 33% in R_{eI} and 19% in R_{eE} (Supplement Fig. S4).

Extrapolation of R_{rs} data by using the equation derived from the cast measurements (Eq. 6) resulted in a larger decrease in R_{eI} than R_{eE}, thereby increasing the tidal difference in Rrs (ΔR). Since ΔR has been shown to be a sensitive measure of yet subtle alterations in peripheral homogeneity [31, 32], application of a correction accounting for the V"-dependent effects would further increase the utility of ΔR. While the significance of this correction procedure lies in an improved assessment of the intrapulmonary mechanics, further investigations are warranted for the implementation in studies conducted *in vivo.*

Dynamic changes in X_n and X_{rs}

We measured positive mean values of X_n, indicating the presence of inertance, an expected significant property of the upper airways. The V'-dependent decrease in X_n can be explained by the decrease in apparent inertance caused by the vortex formation at orifices [58, 59].

The patterns of X_{rs} were similar, although more variable than that of X_n, and the mean X_{rs} values were negative due to the presence of elastic forces of the total respiratory system at 16 Hz. The compliant upper airway structures must have added to this variability while the orifice effects pertained; an extreme example of inspiratory flow limitation (the Bernoulli effect) is demonstrated in Supplement Fig. S8 (infant #11).

Limitations of Study 1

This study had some limitations. Since the CT sampling time was quite short (~75-300 ms), we had to assume that the whole nasal pathway was reconstructed in the same phase of the respiratory cycle. Nevertheless, since CT acquisition was not gated with respect to the respiratory phase, the within-breath variation in the diameter of the soft tissue that may exist *in vivo* is not reflected in the 3D cast. Additionally, since more compliant structures of the upper airways, such as the vocal cord area and part of the oropharynx, were not included in the reconstructed upper airways the intra-breath changes must have been reduced substantially, imposing another limitation in the applicability of cast measurements in the interpretation of the *in vivo* infant data. A further limitation was the rigid material of the cast, as well as the surface texture is likely to be different from that of the upper airway mucosa. Non-linearity originating from the compliance of some segments of the nasal pathway cannot be modeled by this approach. Despite the rigidity of the casts, distortions in the R_n – V' relationship could be adequantly studied since the orifice effect can be considered the most important contributor to the flow-dependence of R_n during tidal breathing.

A time windowing of 0.25 s was used during intra-breath oscillatory measurements. This means that an average of 4 oscillatory cycles was used for impedance estimation. Decreasing windowing time to a minimum of two cycles excessively decreased signal-to-noise ratio, which was especially critical in the *in vivo* setting. The effect of increasing the windowing time was investigated in a subgroup of our casts (n=12; data not shown). Increasing windowing time to 0.5 s led to higher values of R_{eE} but without much change in $R_{V'maxI}$ and $R_{V'maxE}$. Although the increase in R_{eE} was systematic, the intercept of the linear R_{eE} vs V''_{eE} relationship did not change, so the estimation of R_0 seems to be insensitive to windowing time.

Discussion of Study 2

The 94% success rate in the present study confirms earlier observations on the feasibility of oscillometry in unsedated newborns [36] and infants [32, 33, 35], although its outstanding value can largely be attributed to the favourable environmental and time allocation circumstances in the neonatal ward. These factors enabled a detailed assessment of short-term variability of Zrs in healthy term neonates.

Intra-breath changes in Rrs

The characteristic effect of V' on Rrs was documented in early studies using single-frequency oscillations in orally breathing adult subjects [28, 60]. These biphasic changes in Rrs, characterised by minimum values at zero V' and local maxima at peak inspiratory and expiratory V' (V'_{maxI} and V'_{maxE}, respectively) were a marked feature in the neonates of this study, with the nonlinearity in expiration usually exceeding that of inspiration. Previous observations suggest that the nonlinear, V'-dependent increase in Rrs originates from the upper airways [39, 50, 51], obeying the classical empirical description by Rohrer [61].

An unexpected finding in the present investigation was the fact that R_{eI} was higher than R_{eE} (i.e. ΔR was negative) in almost half of the subjects. This is in contrast to previous intra-breath studies where the typically positive ΔR values were attributed to the tidal dilatation of the pulmonary airways [29, 32, 62]. One important specific factor in infancy is the large contribution of the extrathoracic pathways to Rrs, whose transmural pressures are dependent on V' rather than V and are thus opposite to that of the pulmonary airways; this may lead to narrowing of the upper airways during inspiration and possibly some residual constriction at end inspiration. Another factor, also augmented in nasal breathing is the non-steady flow patterns that develop at fast transitions of V' in the upper airways of irregular geometry. This leads to extra dissipation, which has been shown to depend on the rate of change in V' (i.e. on V") [39, 50, 51], and would add to the true "zero-flow" values of R_{eE} and R_{eI}. In the present study, the asymmetry of respiratory phase change (as characterised by the ratio $V"_{eE}/V"_{eI}$) was shown to negatively correlate with ΔR. Since the transition from inspiration to expiration is usually faster than *vice versa*, it can lead to low, or even negative values in ΔR. These factors discussed above suggest that the contributions of the upper airway to ΔR may mask the change in pulmonary airway caliber. Nevertheless, the near-zero mean value of ΔR is at variance with the results of the intra-breath measurements in infants [32] where an average of 4.43 $hPa.s.L^{-1}$ (IQR: 0.65–8.13 $hPa.s.L^{-1}$) was observed. Since the same custom-made wave-tube device was employed in both studies and the spectral Zrs measures are similar, differences between the 2 populations, such as ethnic (Caucasians *vs* Black Africans), age (newborns *vs* 6 wk old infants), gestational age (term *vs* term + late preterm) and other characteristics may explain the different ΔR values.

Intra-breath changes in Xrs

While the changes in Rrs within the respiratory cycle are dominated by the "U" shape in V' dependence of different degrees and asymmetry, Xrs exhibited qualitatively more distinct intra-breath patterns. We defined a group with the lowest V'-dependent changes in Xrs (pattern A) and considered it the control group. The rest (45%) of the examined neonates exhibited diverse and strong V' dependences of Xrs. Three additional typical V'-dependent patterns were identified qualitatively and verified by cluster analysis. Inference to the underlying mechanisms of each pattern is burdened by the lack of additional signals (e.g. nasopharyngeal pressure) unavailable in the non-invasive setting of the current study. Nevertheless, a decrease in Xrs during expiration (pattern B) is most likely caused by glottal braking that help maintain the end-expiratory lung volume in the early phase of postnatal lung and chest wall development [19]. The small but highly significant increase in the T_E/T_{Tot} ratio in this group (Table 2) supports the above argument. Intuitively, a similar change in Xrs but in inspiration (Pattern C) can be attributed to the negative pressure swings in the glossopharyngeal area, which lead via deformation of soft tissues to inspiratory V' limitation and are augmented by the large nasal component of Rrs. This suggests that the nasal impedance is not only a significant additive component in Zrs [25, 27, 63] but it may modulate the transmural pressures in the compliant structures of distal extrathoracic airways more than in the case of oral breathing. Whereas Patterns B and C describe temporary changes in Xrs, pronounced in mid-expiration or mid-inspiration, respectively (Fig. 13), Pattern D is characterised by marked positive increases in Xrs with both inspiratory and expiratory V'. This is likely to be associated with the increased impedance of the nasal pathway, in terms of both resistance and inertance, as reflected by the higher values of R and L in this group (Table 3), also manifested in the significant elevations in zero-V' Xrs (X_{eE} and X_{eI}, Table 4). Note that while the relatively low numbers of Pattern C and Pattern D subjects warrant considerations in their statistical assessments, the frequency of these patterns can be regarded as an inherent feature of the studied healthy term infants. Importantly, Xrs patterns suggesting intrapulmonary expiratory flow limitation observed in the South-African cohort of 6-wk-old infants [32] were not detected in the present study.

The respiratory pattern can undergo gradual or abrupt changes in a relatively short time (Fig. 12). After examination of individual recordings, it can be concluded that a V'-dependent Xrs pattern is not a permanent characteristic of a newborn, but a temporary feature. Sudden changes in the V'-nonlinearities might explain the huge day-to-day variability of spectral

oscillometry [36]. Therefore, measurements of both intra-breath and spectral oscillometry in the same session are recommended to detect and explain the short term changes in respiratory mechanics.

Within-session variability of oscillometry measures

The 90-s recordings allowed us to have a closer look into the short-term changes in intra-breath Zrs, which sometimes even disclosed transitions from one pattern of V' dependence into another. The within-session variability of intra-breath Zrs measures was slightly larger than that of the breathing pattern descriptors, which were obtained from the same recordings (Table 5). Although this may suggest that fluctuations in the spirogram cause changes in the intra-breath parameters, correlation analysis did not confirm such a relationship; similarly, no direct correlations were found between the tidal breathing pattern and the within-session variability of spectral oscillometry (data not reported).

The fact that the most stable spectral measures were R and $|Z_8|$ is somewhat surprising, as we expected a large variability contributed by the nasal pathway. Explanations based solely on our non-invasive measurement data would be speculative; however, there is indication that the nasal and the distal pulmonary resistances can change in opposite direction to maintain a relatively constant total resistance [63]. The highest variability was observed in Ax, which is widely considered as a robust measure of elastic properties of the respiratory system [64]. However, as the area of the negative Xrs domain is terminated by f_{res}, changes in the dominant nasal inertance would strongly influence the Ax values. Indeed, the intra-breath analysis revealing the patterns of V' dependence indicated that Ax was biased by changes in Xrs (Table 3), whereas the model fitting of Zrs spectra accounted for the changes in L and resulted in remarkably constant estimates of C for all patterns in spontaneously breathing neonates. The model-based approach supported by intra-breath analysis thus makes the values of C less influenced by the upper airway compartment and more specific to the elastic properties of the lungs.

Implications in oscillometry procedures in infants

Technical standards and protocols of spectral oscillometry have been developed for cooperating children and adults [65, 66]; these include reproducibility criteria based on repeated measurements that are separated by intervals when the subject is detached from the device. This protocol is clearly impractical to adopt in infant studies, primarily because of the

removal and replacement of the face mask may alter the breathing pattern and the sleep stage via excitation of the facial nerves [67]. Additionally, a minimum of 3 measurement epochs whose lowest-frequency Rrs values have a CoV of ≤10% (adults) or ≤15% (children) has been suggested as the reproducibility criterion [65]. The wide ranges of within-session CoV values of tidal breathing and Zrs parameters observed in the present study (Table 4) may reflect a higher degree of natural variability in respiratory mechanics in neonates [68] compared with older subjects. Therefore, more permissive reproducibility criteria combined with the equally important Xrs measures and based on longer recordings should be established for infants. On the other hand, inclusion of the nasal passages in the infant oscillometry requires careful inspection of the patency of this pathway; congestion may lead to extreme values in R and L and associated with the Xrs pattern D, as in the current measurements.

Instrumentation requirements

The spectral measures of Zrs in the present study, as expressed by the R, C and L values (Table 3), are very close to that obtained with the same technique previously [33, 35, 36] and correspond to an impedance magnitude of 40-60 hPa.s.L^{-1}. Far above these values representing *averages* for whole breathing cycles, huge *peak values* in Zrs were identified by the intra-breath tracking to occur at instances of V'_{maxE} and V'_{maxI}. As illustrated in Figs 12 and 13, and quantified by the R_{ppI}/Z_0 and R_{ppE}/Z_0 data in Table 3, Zrs often exceeded 200 hPa.s.L^{-1} in the healthy term newborns of this study. This highlights the need for accurate measurements at peak values of Zrs and not only in intra-breath analysis, as the average values obtained in the conventional spectral oscillometry would also be distorted if an upper range of Zrs is misestimated. The wave-tube principle [69] employed in the present work is particularly advantageous in the measurements of high Zrs, and it was considered as the gold standard technique in the comparison of commercially available oscillometry devices [70]. Device dependence might have been the primary reason for the large differences in the Rrs and Xrs values reported recently [40, 71], compared with that from the present and previous measurements with the wave-tube technique [32, 33, 35, 36].

Implications in tidal breathing analysis

Comparative analysis of tidal breathing and oscillometry indices has revealed generally modest interrelationships (Fig. 15) but pinpointed a strong connection between T_{PTEF}/T_E and an asymmetry measure of V" ($V"_{eE}/V"_{eI}$). T_{PTEF}/T_E can be obtained in relatively simple measurement settings and it has often been considered as a useful index to detect airway

obstruction [72-74], although the assessment of T_{PTEF}/T_E as a surrogate of mechanical tests is controversial in the literature.

In the current study, T_{PTEF}/T_E did not correlate with the intra-breath Rrs or Xrs variables, and was not different between groups of V' dependence of Xrs. However, the mean values of V''_{eE}/V''_{eI} of the subjects and the corresponding T_{PTEF}/T_E data covered wide ranges (Fig. 16) with an unexpectedlystrong linear relationship. This suggests that in healthy term newborns, such as those in the present study, marked differences in the activity of the respiratory control mechanisms rather than airway obstruction exist and determine the values of T_{PTEF}/T_E [75,76].

Limitations of Study 2

(i) The spectral and intra-breath oscillometry data were derived from recordings collected separately. In order to minimise systematic errors, the two modalities were alternated and, whenever possible, without the removal/repositioning of the face mask. Although there was good agreement in the mean 16-Hz Zrs data collected from the two modalities, the unchanged status of the respiratory mechanical system could not be guaranteed.

(ii) Although sleep state can be an important factor when interpreting lung function measurements in sleeping infants, addressing the relationship between the sleep state and respiratory mechanics was beyond the scope of the current study. Sleep states such as the active (rapid eye movement – REM) sleep and the quiet (non-REM) sleep typically last for 50-70 min in healthy newborns [77], and while we cannot exclude the possibility that a transition between sleep states took place during the measurements, it was more likely that the same state persisted during our recording sessions of typically 14-min duration. Since the estimated ratio of active and quiet sleep is approximately 2:1 in healthy term newborns [77], we can assume that a non-negligible portion of recordings was collected during active sleep. Regularity of the respiratory pattern is also known to be different during active and quiet sleep [78, 79]; from the present data it can only be inferred that the variability of T_{tot} and V_T was independent of the Xrs pattern of V' dependence (Table 2).

(iii) The measurement device imposes some impedance against the breathing, which may alter the pattern of tidal breathing without this load. In the present study, the total load including the bacterial filter, the wave-tube, the pneumotachograph and the breathing tube amounted to 6.5 $hPa.s.L^{-1}$, i.e., roughly 10-15% of Rrs. Even if this additional load does not interact with

the breathing pattern significantly, it increases the flow-dependent changes in the glossopharyngeal area and may augment the upper airway nonlinearities.

CONCLUSIONS

Study 1 investigated R-V' relationship in anatomically faithful rigid nasal airway casts during simulated respiration. We found a characteristic nonlinear relationship between R and V', exhibiting segmental power-law behavior with a prominent breakpoint. This model was reproducible in the *in vivo* study on a small group of infants. We observed a linear shift in R_{eE} which was attributable to increasing values of V". We developed a geometrical approach to quantify intra-breath nonlinearities in R_n, allowing to estimate R_0 from a single oscillometric measurement. Using this correction may reduce the masking effect of the nonlinear upper airways on the changes in the intrathoracic R in future studies.

The impedance tracking employed in Study 2 revealed marked intra-breath changes in Rrs and Xrs in healthy term neonates during natural sleep in the first few days of life. These changes were dominated by the increases in Rrs with V' in both inspiration and expiration, whereas Xrs exhibited different patterns of change, including inspiratory and expiratory flow limitations. It is suggested that these intra-breath nonlinearities are of upper airway origin, with fundamental contributions from the nasal pathways. Intra-breath changes exert a biasing effect on the conventional measures of the multi-frequency oscillometry that are intended to characterise pulmonary mechanics. It is recommended that the measurements of Zrs in infants cover longer study intervals than that required from cooperative subjects to account for the variable mechanical status of the developing respiratory system. Use of intra-breath oscillometry is proposed to gain more insight into the mechanisms determining Zrs and to properly interpret the results of conventional spectral oscillometry in infants.

Our studies demonstrated that oscillometry is a promising, noninvasive pulmonary function test achieving high success rate in infants. The single frequency (tracking) mode of oscillometry revealed considerable intra-breath changes in Zrs in healthy newborns. Our results verified the basic assumption that V'-and V"-dependent changes in Zrs develop in the upper airways. We conclude that upper airway rheology can cause non-negligible bias and can contribute to the high natural variability of respiratory oscillometry results.

REFERENCES

1 Lum, S., Hülskamp, G., Merkus, P., Baraldi, E., Hofhuis, W., & Stocks, J. (2006). Lung function tests in neonates and infants with chronic lung disease: forced expiratory maneuvers. *Pediatr Pulmonol, 41(3), 199-214.*

2 Stocks, J. (1999). Lung function testing in infants. *Pediatr Pulmonol Suppl, 18, 14-20.*

3 Jackson, E., Rabbette, P., Dezateux, C., Hatch, D., & Stocks, J. (1991). The effect of triclofos sodium sedation on respiratory rate, oxygen saturation, and heart rate in infants and young children. *Pediatr Pulmonol, 10(1), 40-5.*

4 Mayers, D., Hindmarsh, K., Sankaran, K., Gorecki, D., & Kasian, G. (1991). Chloral hydrate disposition following single-dose administration to critically ill neonates and children. *Dev Pharmacol Ther, 16(2), 71-7.*

5 Gaultier, C., Fletcher, M., Beardsmore, C., England, S., & Motoyama, E. (1995). Respiratory function measurements in infants: measurement conditions. Working Group of the European Respiratory Society and the American Thoracic Society. *Eur Respir J, 8(6), 1057-66.*

7 Schmalisch, G., Wilitzki, S., & Wauer, R. (2005). Differences in tidal breathing between infants with chronic lung diseases and healthy controls. *BMC Pediatr, 5, 36.*

8 Aston, H., Clarke, J., & Silverman, M. (1994). Are tidal breathing indices useful in infant bronchial challenge tests?. *Pediatr Pulmonol, 17(4), 225-30.*

9 Seddon, P., Davis, G., & Coates, A. (1996). Do tidal expiratory flow patterns reflect lung mechanics in infants?. *Am J Respir Crit Care Med, 153(4 Pt 1), 1248-52.*

10 Black, J., Baxter-Jones, A., Gordon, J., Findlay, A., & Helms, P. (2004). Assessment of airway function in young children with asthma: comparison of spirometry, interrupter technique, and tidal flow by inductance plethsmography. *Pediatr Pulmonol, 37(6), 548-53.*

11 Calabrese, P., Dinh, T., Eberhard, A., Bachy, J., & Benchetrit, G. (1998). Effects of resistive loading on the pattern of breathing. *Respir Physiol, 113(2), 167-79.*

12 Marsh, M., Ingram, D., & Milner, A. (1993). The effect of instrumental dead space on measurement of breathing pattern and pulmonary mechanics in the newborn. *Pediatr Pulmonol, 16(5), 316-22.*

13 Dolfin, T., Duffty, P., Wilkes, D., England, S., & Bryan, H. (1983). Effects of a face mask and pneumotachograph on breathing in sleeping infants. *Am Rev Respir Dis, 128(6), 977-9.*

14 Schmalisch, G., Foitzik, B., Wauer, R., & Stocks, J. (2001). Effect of apparatus dead space on breathing parameters in newborns: "flow-through" versus conventional techniques. *Eur Respir J, 17(1), 108-14.*

15 Dizdar, E., Bozkaya, D., Sari, F., Beser, E., Tayman, C., & Oguz, S. (2021). Tidal Breathing Parameters Measured by Structured Light Plethysmography in Newborns: Is It Feasible in Neonatal Intensive Care Unit?. *Am J Perinatol, 38(12), 1254-1258.*

16 Brown, K., Aun, C., Jackson, E., Mackersie, A., Hatch, D., & Stocks, J. (1998). Validation of respiratory inductive plethysmography using the Qualitative Diagnostic Calibration method in anaesthetized infants. *Eur Respir J, 12(4), 935-43.*

17 Motamedi-Fakhr, S., Wilson, R., & Iles, R. (2017). Tidal breathing patterns derived from structured light plethysmography in COPD patients compared with healthy subjects. *Med Devices (Auckl), 10, 1-9.*

18 Kosch, P., Davenport, P., Wozniak, J., & Stark, A. (1985). Reflex control of expiratory duration in newborn infants. *J Appl Physiol, 58(2), 575-81.*

19 Kosch, P., Hutchinson, A., Wozniak, J., Carlo, W., & Stark, A. (1988). Posterior cricoarytenoid and diaphragm activities during tidal breathing in neonates. *J Appl Physiol, 64(5), 1968-78.*

20 Kosch, P., & Stark, A. (1984). Dynamic maintenance of end-expiratory lung volume in full-term infants. *J Appl Physiol Respir Environ Exerc Physiol, 57(4), 1126-33.*

21 Harding, R., Johnson, P., & McClelland, M. (1980). Respiratory function of the larynx in developing sheep and the influence of sleep state. *Respir Physiol, 40(2), 165-79.*

22 Poets, C., Rau, G., Neuber, K., Gappa, M., & Seidenberg, J. (1997). Determinants of lung volume in spontaneously breathing preterm infants. *Am J Respir Crit Care Med, 155(2), 649-53.*

23 Stocks, J., Godfrey, S., Beardsmore, C., Bar-Yishay, E., Castile, R., & Society, E. (2001). Plethysmographic measurements of lung volume and airway resistance. ERS/ATS Task Force on Standards for Infant Respiratory Function Testing. European Respiratory Society/ American Thoracic Society. *Eur Respir J, 17(2), 302-12.*

24 Gappa, M., Pillow, J., Allen, J., Mayer, O., & Stocks, J. (2006). Lung function tests in neonates and infants with chronic lung disease: lung and chest-wall mechanics. *Pediatr Pulmonol, 41(4), 291-317.*

25 Polgar, G., & Kong, G. (1965). The nasal resistance of newborn infants. *J Pediatr, 67(4), 557-67.*

26 Stocks, J., & Godfrey, S. (1978). Nasal resistance during infancy. *Respir Physiol, 34(2), 233-46.*

27 Hall, G., Hantos, Z., Wildhaber, J., & Sly, P. (2002). Contribution of nasal pathways to low frequency respiratory impedance in infants. *Thorax, 57(5), 396-9.*

28 Davidson, R., Greig, C., Hussain, A., & Saunders, K. (1986). Within-breath changes of airway calibre in patients with airflow obstruction by continuous measurement of respiratory impedance. *Br J Dis Chest, 80(4), 335-52.*

29 Lorx, A., Czovek, D., Gingl, Z., Makan, G., Radics, B., Bartusek, D., Szigeti, S., Gal, J., Losonczy, G., Sly, P., & Hantos, Z. (2017). Airway dynamics in COPD patients by within-breath impedance tracking: effects of continuous positive airway pressure. *European Respiratory Journal, 49(2): 1601270.*

30 Peslin, R., Ying, Y., Gallina, C., Duvivier, C. (1992). Within-breath variations of forced oscillation resistance in healthy subjects. *European Respiratory Journal, 5(1), 86-92.*

31 Czovek, D., Shackleton, C., Hantos, Z., Taylor, K., Kumar, A., Chacko, A., Ware, R., Makan, G., Radics, B., Gingl, Z., & Sly, P. (2016). Tidal changes in respiratory resistance are sensitive indicators of airway obstruction in children. *Thorax, 71(10), 907-915.*

32 Gray, D., Czovek, D., McMillan, L., Turkovic, L., Stadler, J., Vanker, A., Radics, B., Gingl, Z., Hall, G., Sly, P., Zar, H., & Hantos, Z. (2019). Intra-breath measures of respiratory mechanics in healthy African infants detect risk of respiratory illness in early life. *Eur Respir J, 53(2). 1800998 , 9 p.*

33 Gray, D., Czövek, D., Smith, E., Willemse, L., Alberts, A., Gingl, Z., Hall, G., Zar, H., Sly, P., & Hantos, Z. (2015). Respiratory impedance in healthy unsedated South African infants: effects of maternal smoking. *Respirology, 20(3), 467-73.*

34 Gray, D., Willemse, L., Visagie, A., Czövek, D., Nduru, P., Vanker, A., Stein, D., Koen, N., Sly, P., Hantos, Z., Hall, G., & Zar, H. (2017). Determinants of early-life lung function in African infants. *Thorax, 72(5), 445-450.*

35 Gray, D., Willemse, L., Visagie, A., Smith, E., Czövek, D., Sly, P., Hantos, Z., Hall, G., & Zar, H. (2015). Lung function and exhaled nitric oxide in healthy unsedated African infants. *Respirology, 20(7), 1108-14.*

36 Hantos, Z., Czövek, D., Gyurkovits, Z., Szabó, H., Maár, B., Radics, B., Virág, K., Makan, G., Orvos, H., Gingl, Z., & Sly, P. (2015). Assessment of respiratory mechanics with forced oscillations in healthy newborns. *Pediatr Pulmonol, 50(4), 344-52.*

37 Desager, K., Buhr, W., Willemen, M., Bever, H., Backer, W., Vermeire, P., & Lándsér, F. (1991). Measurement of total respiratory impedance in infants by the forced oscillation technique. *J Appl Physiol, 71(2), 770-6.*

37 Hantos, Z. (2021). Intra-breath oscillometry for assessing respiratory outcomes. *Current Opinion is Physiology, 22, 100441.*

38 Solow, B., & Peitersen, B. (1991). Nasal airway resistance in the newborn. *Rhinology, 29(1), 27-33.*

39 Radics, B., Makan, G., Coppens, T., André, N., Page, C., Dégrugilliers, L., Bayat, S., Gingl, Z., Gyurkovits, Z., M Tóth, T., Hantos, Z., & Bayat, S. (2020). Effect of nasal airway nonlinearities on oscillometric resistance measurements in infants. *J Appl Physiol (1985), 129(3), 591-598.*

40 Klinger, A., Travers, C., Martin, A., Kuo, H., Alishlash, A., Harris, W., Carlo, W., & Ambalavanan, N. (2020). Non-invasive forced oscillometry to quantify respiratory mechanics in term neonates. *Pediatr Res, 88(2), 293-99.*

41 Yushkevich, P., Piven, J., Hazlett, H., Smith, R., Ho, S., Gee, J., & Gerig, G. (2006). User-guided 3D active contour segmentation of anatomical structures: significantly improved efficiency and reliability. *Neuroimage, 31(3), 1116-28.*

42 Doorly, D., Taylor, D., & Schroter, R. (2008). Mechanics of airflow in the human nasal airways. *Respir Physiol Neurobiol, 163(1-3), 100-10.*

43 Kiwanuka F. , and Wilkinson M. (2015). Cluster based vector attribute filtering. *In: Mathematical Morphology and Its Applications in Signal and Image Processing.* Edited by Benediktsson J., Chanussot J., Najman L. & Talbot H. , *277-83.*

44 Hey, E., & Price, J. (1982). Nasal conductance and effective airway diameter. *J Physiol, 330, 429-37.*

45 Dorkin, H., Jackson, A., Strieder, D., & Dawson, S. (1982). Interaction of oscillatory and unidirectional flows in straight tubes and an airway cast. *J Appl Physiol Respir Environ Exerc Physiol, 52(4), 1097-1105.*

46 Finucane, K., Dawson, S., Phelan, P., & Mead, J. (1975). Resistance of intrathoracic airways of healthy subjects during periodic flow. *J Appl Physiol, 38(3), 517-30.*

47 Franken, H., Clément, J., Cauberghs, M., & Woestijne, K. (1981). Oscillating flow of a viscous compressible fluid through a rigid tube: a theoretical model. *IEEE Trans Biomed Eng, 28(5), 416-20.*

48 Peták, F., Hayden, M., Hantos, Z., & Sly, P. (1997). Volume dependence of respiratory impedance in infants. *Am J Respir Crit Care Med, 156(4 Pt 1), 1172-7.*

49 Jaeger, M., & Matthys, H. (1968). The pattern of flow in the upper human airways. *Respir Physiol, 6(1), 113-27.*

50 Isabey, D., & Chang, H. (1981). Steady and unsteady pressure-flow relationships in central airways. *J Appl Physiol Respir Environ Exerc Physiol, 51(5), 1338-48.*

51 Isabey, D., Chang, H., Delpuech, C., Harf, A., & Hatzfeld, C. (1986). Dependence of central airway resistance on frequency and tidal volume: a model study. *J Appl Physiol (1985), 61(1), 113-26.*

52 Pedley, T., Schroter, R., & Sudlow, M. (1970). Energy losses and pressure drop in models of human airways. *Respir Physiol, 9(3), 371-86.*

53 Schroter, R., & Sudlow, M. (1969). Velocity profiles in models of human airways. *J Physiol, 202(1), 36P-37P.*

54 Ingram, O. and Pedley T. (2011). Pressure-flow relationships in the lungs. (2011). *Comprehensive Physiology 1(1): 277-93.*

55 Iida, O. and Nagano Y. (1998). The relaminarization mechanisms of turbulent channelflow at low Reynolds numbers. *Flow, Turbulence and Combustion, 60(1), 193-213.*

56 Proctor, D., & Adams, G. (1976). Physiology and pharmacology of nasal function and mucus secretion. *Pharmacol Ther B, 2(3), 493-509.*

57 Yu, S., Liu, Y., Sun, X., & Li, S. (2008). Influence of nasal structure on the distribution of airflow in nasal cavity. *Rhinology, 46(2), 137-43.*

58 Ingard U., Ising H. (1967). Acoustic nonlinearity of an orifice. *J Acoust Soc Am, 42, 6-1*.

59 Jing X., Sun X. (2002). Sound-excited flow and acoustic nonlinearity at an orifice. *Physics of Fluids 14, 268–76.*

60 Peslin, R., Hixon, T., & Mead, J. (1971). Variations of thoraco-pulmonary resistance during the respiratory cycle studied by the oscillation method. *Bull Physiopathol Respir (Nancy), 7(1), 173-88.*

61 Rohrer, F. (1915). Der Strömungswiderstand in den menschlichen Atemwegen und der Einfluss der unregelmässigen Verzweigung des Bronchialsystems auf den Atmungsverlauf in verschiedenen Lungenbezirken. *Pflüger's Archiv für die gesamte Physiologie des Menschen und der Tiere.* 162: 225-99.

62 Chiabai, J., Friedrich, F., Fernandes, M., Serpa, F., Antunes, M., Neto, F., Makan, G., Hantos, Z., Sly, P., & Jones, M. (2021). Intrabreath oscillometry is a sensitive test for assessing disease control in adults with severe asthma. *Ann Allergy Asthma Immunol, 127(3), 372-377.*

63 Lacourt, G., & Polgar, G. (1971). Interaction between nasal and pulmonary resistance in newborn infants. *J Appl Physiol, 30(6), 870-3.*

64 Goldman, M. (2001). Clinical application of forced oscillation. *Pulm Pharmacol Ther, 14(5), 341-50.*

65 King, G., Bates, J., Berger, K., Calverley, P., Melo, P., Dellacà, R., Farré, R., Hall, G., Ioan, I., Irvin, C., Kaczka, D., Kaminsky, D., Kurosawa, H., Lombardi, E., Maksym, G., Marchal, F., Oppenheimer, B., Simpson, S., Thamrin, C., Berge, M., & Oostveen, E. (2020). Technical standards for respiratory oscillometry. *Eur Respir J, 55(2).*

66 Oostveen, E., MacLeod, D., Lorino, H., Farré, R., Hantos, Z., Desager, K., Marchal, F., & Measurements, E. (2003). The forced oscillation technique in clinical practice: methodology, recommendations and future developments. *Eur Respir J, 22(6), 1026-41.*

67 Kuypers, K., Martherus, T., Lamberska, T., Dekker, J., Hooper, S., & Te Pas, A. (2020). Reflexes that impact spontaneous breathing of preterm infants at birth: a narrative review. *Arch Dis Child Fetal Neonatal Ed, 105(6), 675-679.*

68 Beydon, N., Davis, S., Lombardi, E., Allen, J., Arets, H., Aurora, P., Bisgaard, H., Davis, G., Ducharme, F., Eigen, H., Gappa, M., Gaultier, C., Gustafsson, P., Hall, G., Hantos, Z., Healy, M., Jones, M., Klug, B., Lødrup Carlsen, K., McKenzie, S., Marchal, F., Mayer, O., Merkus, P., Morris, M., Oostveen, E., Pillow, J., Seddon, P., Silverman, M., Sly, P., Stocks, J., Tepper, R., Vilozni, D., Wilson, N., Testing, A., & Young Children Pulmonary Function (2007). An official American Thoracic Society/European Respiratory Society statement: pulmonary function testing in preschool children. *Am J Respir Crit Care Med, 175(12), 1304-45.*

69 Van de Woestijne K., Franken H., Cauberghs M., Làndsér F., Clément J. (1981). A modification of the forced oscillation technique. *In: 28th International Congress of Physiological Sciences*. Editors: Hutás I, Debreczeni L. Budapest, Hungary: Akadémiai Kiadó; p. 655-660

70 Dandurand, R., Lavoie, J., Lands, L., Hantos, Z., & Group, O. (2019). Comparison of oscillometry devices using active mechanical test loads. *ERJ Open Res, 5(4).*

71 Travers, C., Klinger, A., Aban, I., Hoover, W., Carlo, W., & Ambalavanan, N. (2021). Noninvasive Oscillometry to Measure Pulmonary Mechanics in Preterm Infants. *Am J Respir Crit Care Med, 204(4), 485-488.*

72 Baldwin, D., Pillow, J., Stocks, J., & Frey, U. (2006). Lung-function tests in neonates and infants with chronic lung disease: tidal breathing and respiratory control. *Pediatr Pulmonol, 41(5), 391-419.*

73 Banovcin, P., Seidenberg, J., & Hardt, H. (1995). Assessment of tidal breathing patterns for monitoring of bronchial obstruction in infants. *Pediatr Res, 38(2), 218-20.*

74 Çelik, E., & Uysal, P. (2021). Pulmonary function testing with tidal breath analyze technique is useful in predicting persistant small airway damage in infants with acute bronchiolitis. *Pediatr Allergy Immunol, 32(1), 60-66.*

75 Hutten, G., Eykern, L., Latzin, P., Kyburz, M., Aalderen, W., & Frey, U. (2008). Relative impact of respiratory muscle activity on tidal flow and end expiratory volume in healthy neonates. *Pediatr Pulmonol, 43(9), 882-91.*

76 van der Ent, C., Grinten, C., Meessen, N., Luijendijk, S., Mulder, P., & Bogaard, J. (1998). Time to peak tidal expiratory flow and the neuromuscular control of expiration. *Eur Respir J, 12(3), 646-52.*

77 Curzi-Dascalova, L., Peirano, P., & Morel-Kahn, F. (1988). Development of sleep states in normal premature and full-term newborns. *Dev Psychobiol, 21(5), 431-44.*

78 Curzi-Dascalova, L., Lebrun, F., & Korn, G. (1983). Respiratory frequency according to sleep states and age in normal premature infants: a comparison with full term infants. *Pediatr Res, 17(2), 152-6.*

79 Hoppenbrouwers, T., Harper, R., Hodgman, J., Sterman, M., & McGinty, D. (1978). Polygraphic studies on normal infants during the first six months of life. II. Respiratory rate and variability as a function of state. *Pediatr Res, 12(2), 120-5.*

80 Miller, T., & Pimmel, R. (1982). Forced noise mechanical parameters during inspiration and expiration. *J Appl Physiol Respir Environ Exerc Physiol, 52(6), 1530-4.*

ACKNOWLEDGEMENTS

First and foremost, I would like to say thank you to my PhD supervisor, Professor Zoltán Hantos. You not only taught me the basics of research but gave me essential lessons from the hidden curriculum of science.

In addition to my supervisor I would like to say thank you to Professor Zoltán Gingl and Gergely Makan for their seminal contribution to the development of infant oscillometry.

I would like to say thank you to Prof. Sam Bayat and his team from University of Amiens for providing the 3-D-printed upper airway casts to our experiments.

I want to express my gratitude to Dr. Zita Gyurkovits for all the entrustment and her persistence during the long hours of lung function measurements.

I have no words for the amount and intensity of the love, support and patience coming from my wife, Orsolya. This work would have never got finished without you. Thank you for believing me during my darkest moments.

I would like to say thank you for my sons Gergő and Vince. You really brought a new meaning to my life. It was worth to finish this work for you.

I am really grateful for my mother, Helga, my father Béla, and my brother Bélus. You created a true home: a safe and creative environment where I could enjoy studying and getting to know the world as a child.

There is not enough space here to list the innumerable friends, family members and colleagues who helped me to complete my Ph.D. studies. Thank you!

I would like to thank the colleagues at the Department of Medical Physics and Informatics, the NoiseLab in the Department of Technical Informatics, the Neonatal Ward in the Clinics of Obstetrics and Gynaecology, the Department of Pulmonology and the Department of Pathology at University of Szeged for their support.

SUPPLEMENTARY TABLES AND FIGURES

Table S1. Mean (SE) values of segmented power-law model parameters estimated in rigid nasal pathway casts of infants with a superimposed breathing of 0.75 Hz and individually calculated tidal volumes. Data show parameters calculated for the expiratory limb. V'bp: flow at the breakpoint, k1: steepness of the first segment (when V'≤ V'bp); k2: steepness of the second segment (when V'>V'bp).

ID	ln V'_{bp} (SE)	intercept (SE)	k1 (SE)	k2 (SE)	adjusted r^2
cast 001	3.25	2.19	0.073	1.169	0.990
	(0.017)	(0.03)	(0.013)	(0.031)	
cast 003	3.57	1.81	0.022	0.976	0.984
	(0.023)	(0.03)	(0.010)	(0.029)	
cast 005	3.87	0.41	0.021	0.843	0.986
	(0.024)	(0.03)	(0.009)	(0.025)	
cast 006	3.78	2.92	0.024	1.506	0.983
	(0.018)	(0.05)	(0.015)	(0.045)	
cast 007	3.55	0.62	0.039	0.779	0.974
	(0.034)	(0.03)	(0.011)	(0.034)	
cast 008	3.93	2.16	0.005	0.930	0.985
	(0.023)	(0.03)	(0.008)	(0.025)	
cast 009	4.21	1.82	0.132	1.160	0.976
	(0.027)	(0.07)	(0.020)	(0.052)	
cast 010	4.11	0.74	0.036	1.060	0.983
	(0.021)	(0.03)	(0.010)	(0.034)	
cast 012	4.15	1.75	0.018	1.064	0.969
	(0.031)	(0.08)	(0.022)	(0.050)	
cast 014	3.50	1.27	0.042	0.911	0.989
	(0.021)	(0.03)	(0.010)	(0.024)	
cast 015	4.19	2.12	-0.032	1.042	0.979
	(0.026)	(0.07)	(0.020)	(0.037)	
cast 016	3.34	1.10	0.075	1.026	0.988
	(0.022)	(0.03)	(0.012)	(0.029)	
cast 017	4.30	2.16	0.012	1.215	0.985
	(0.019)	(0.06)	(0.015)	(0.037)	
cast 018	3.82	1.80	0.031	0.935	0.991
	(0.02)	(0.05)	(0.016)	(0.024)	
cast 019	3.96	0.83	0.062	0.874	0.989
	(0.019)	(0.03)	(0.010)	(0.026)	
cast 021	4.02	1.70	0.045	1.140	0.986
	(0.019)	(0.03)	(0.011)	(0.032)	
cast 022	4.35	2.04	0.059	1.306	0.977
	(0.023)	(0.09)	(0.024)	(0.051)	
cast 025	4.20	1.30	0.055	1.058	0.985
	(0.020)	(0.03)	(0.010)	(0.033)	
cast 026	3.88	2.73	0.033	1.223	0.984
	(0.02)	(0.03)	(0.010)	(0.036)	
cast 027	3.84	0.20	0.044	0.897	0.987
	(0.022)	(0.04)	(0.013)	(0.027)	
cast 028	3.92	0.84	0.047	0.910	0.986
	(0.025)	(0.05)	(0.014)	(0.029)	
cast 030	3.92	2.65	0.007	0.944	0.979
	(0.026)	(0.05)	(0.016)	(0.034)	

cast 032	3.69	1.09	0.033	0.892	0.991
	(0.019)	(0.02)	(0.007)	(0.022)	
cast_034	4.19	0.75	0.028	1.052	0.974
	(0.03)	(0.04)	(0.012)	(0.044)	
cast_035	3.39	0.29	0.043	0.888	0.988
	(0.022)	(0.02)	(0.009)	(0.026)	
cast 039	3.88	1.88	0.017	1.160	0.980
	(0.026)	(0.06)	(0.020)	(0.041)	
cast 040	3.87	0.41	0.014	0.889	0.979
	(0.026)	(0.03)	(0.009)	(0.032)	
cast 041	3.90	-0.02	0.040	0.856	0.975
	(0.033)	(0.04)	(0.015)	(0.036)	
cast 042	4.40	1.38	0.086	1.055	0.979
	(0.026)	(0.06)	(0.017)	(0.043)	
cast 043	4.48	1.10	0.080	0.981	0.989
	(0.019)	(0.04)	(0.012)	(0.028)	
cast 051	4.30	0.54	0.031	0.788	0.951
	(0.045)	(0.06)	(0.018)	(0.044)	
cast 175	4.03	0.97	0.053	0.897	0.988
	(0.024)	(0.06)	(0.017)	(0.029)	
cast 220	4.35	2.20	0.009	1.348	0.981
	(0.021)	(0.06)	(0.016)	(0.043)	
cast 300	4.30	1.09	0.092	0.968	0.985
	(0.024)	(0.04)	(0.012)	(0.034)	
cast 398	4.68	0.66	0.016	0.855	0.982
	(0.021)	(0.03)	(0.008)	(0.027)	
cast 444	4.24	0.19	0.061	0.976	0.985
	(0.022)	(0.05)	(0.013)	(0.033)	
cast 457	3.25	2.13	0.066	0.993	0.990
	(0.017)	(0.03)	(0.011)	(0.028)	
cast 609	4.22	2.34	0.035	1.056	0.985
	(0.019)	(0.03)	(0.008)	(0.034)	
cast 619	4.11	2.49	0.021	1.261	0.985
	(0.019)	(0.06)	(0.017)	(0.040)	
cast 651	4.42	1.32	0.139	1.005	0.985
	(0.023)	(0.07)	(0.019)	(0.039)	
cast 832	4.04	0.73	0.057	0.875	0.977
	(0.029)	(0.04)	(0.013)	(0.038)	
cast 955	4.37	1.69	0.021	1.015	0.984
	(0.021)	(0.05)	(0.014)	(0.033)	
cast 968	4.38	1.86	0.050	1.354	0.981
	(0.020)	(0.04)	(0.011)	(0.047)	
cast 7418	4.23	1.89	0.053	1.171	0.977
	(0.028)	(0.10)	(0.028)	(0.052)	
cast 9025	4.50	1.57	0.117	1.244	0.986
	(0.020)	(0.07)	(0.019)	(0.042)	

Table S2. The characteristics of newborns involved in oscillatory mechanics measurements. PVN: per vias naturalis, SC: Caesarean section, M: male, F: female.

ID	Measurement after delivery (hours)	Length (cm)	Weight (g)	Gestational age (week)	Delivery	Sex
#1	3	45	2820	38	PVN	M
#2	8	47	2870	39	PVN	F
#3	56	46	2400	39	PVN	F
#4	62	53	3900	39	PVN	F
#5	39	48	2760	37	SC	F
#6	42	50	3120	41	SC	M
#7	30	50	3380	38-5	SC	F
#8	34	50	2650	39-2	PVN	M
#9	31	47	2800	39-2	SC	F
#10	26	52	3130	39-5	SC	M
#11	91	47	2340	36-2	SC	F
#12	58	48	3190	38	PVN	F
#13	40	47	2680	40-6	PVN	F
#14	75	52	3460	40	SC	M
#15	25	49	3070	39	SC	F

Table S3. Model parameters estimated in newborns (SE: standard error). V'bp: flow at the breakpoint, k1: steepness of the first segment (when V'≤ V'bp); k2: steepness of the second segment (when V'>V'bp).

ID	ln V'_{bp} (SE)	intercept (SE)	k1 (SE)	k2 (SE)	adjusted r^2
#1	3.71	3.52	0.104	0.788	0.93
	(0.052)	(0.07)	(0.023)	(0.053)	
#2	3.87	3.43	0.022	0.450	0.86
	(0.082)	(0.05)	(0.016)	(0.043)	
#3	3.18	4.04	-0.007	0.443	0.69
	(0.129)	(0.07)	(0.028)	(0.047)	
#4	4.11	3.72	-0.016	0.775	0.72
	(0.14)	(0.20)	(0.063)	(0.127)	
#5	3.63	3.52	0.013	0.446	0.84
	(0.056)	(0.03)	(0.011)	(0.034)	
#6	4.07	3.67	0.000	0.506	0.75
	(0.126)	(0.07)	(0.024)	(0.075)	
#7	3.60	3.96	0.027	0.617	0.87
	(0.071)	(0.05)	(0.019)	(0.047)	
#8	3.91	2.70	0.076	0.393	0.91
	(0.074)	(0.08)	(0.024)	(0.058)	
#9	3.37	3.72	0.018	0.681	0.87
	(0.070)	(0.07)	(0.028)	(0.054)	
#10	3.98	3.88	0.054	0.728	0.92
	(0.052)	(0.06)	(0.018)	(0.056)	
#11	3.37	4.88	-0.174	0.746	0.63
	(0.13)	(0.29)	(0.104)	(0.123)	
#12	3.94	4.47	0.019	0.561	0.62
	(0.155)	(0.10)	(0.031)	(0.121)	
#13	3.66	3.53	0.073	0.385	0.80
	(0.148)	(0.11)	(0.034)	(0.074)	
#14	3.79	3.06	0.026	0.644	0.88
	(0.063)	(0.08)	(0.024)	(0.056)	
#15	4.22	3.85	0.038	0.793	0.66
	(0.095)	(0.09)	(0.027)	(0.167)	

Table S4. Indication for CT examination.

Subject #	Indication	Radionology Report
0001	Meningitis	Normal CT
0002	Seizure	Normal CT
0003	Meningitis	Normal CT
0005	Rule out brain hemorrhage	Normal CT
0006	Rule out brain hemorrhage	Normal CT
0007	Head Trauma	Normal CT
0008	Rule out brain hemorrhage	Normal CT
0009	Rule out brain tumor	Normal CT
0010	Seizure	Normal CT
0012	Fever of unknown origin	Normal CT
0014	Rule out brain hemorrhage	Normal CT
0015	Seizure	Normal CT
0016	Rule out brain tumor	Frontal ischemic lesion
0017	Head Trauma	Normal CT
0018	Rule out brain tumor	Normal CT
0019	Head Trauma	Meningial Hemorrhage
0021	Rule out brain abcess	Normal CT
0022	Rule out brain tumor	Normal CT
0025	Seizure	Normal CT
0026	Hydrocephalus	NA
0027	NA	NA
0028	Rule out brain hemorrhage	Normal CT
0030	Rule out brain tumor	Subcutaneous parietal hematoma
0032	Seizure	Normal CT
0034	Rule out brain hemorrhage	Normal CT
0035	Seizure	Normal CT
0039	Epidural hematoma	Post-surgical epidural thickenning
0040	Seizure	Normal CT
0041	Rule out craniostenosis	Normal CT
0042	NA	NA
0043	NA	NA
0051	Rule out brain hemorrhage	NA
0175	NA	NA
0220	NA	NA
0300	NA	NA
0398	Cervical adenopathy	NA
0444	Head Trauma	NA
0457	NA	NA
0609	NA	NA
0619	NA	NA
0651	Abnormal gait	NA
7418	NA	NA
0832	NA	NA
9025	Head Trauma	NA
0955	Head Trauma	NA
0968	Head Trauma	NA

Figure S1. This figure shows the first (minor) and second (major) semi-axis of the ellipsoid fitted around the three-dimensional segmented image of the nasal airway. The eigen vectors that give the vectors of the ellipsoid and the eigen values used to compute the radii of the ellipsoid are computed from this matrix, according to the author of the code (Thomas Boudier). Sphericity was computed from the volume and sur**f**ace area of the segmented airways, not the ellipse.

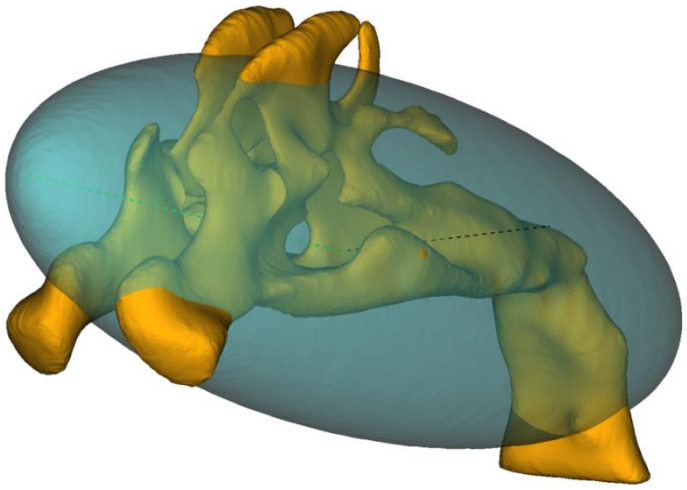

Figure S2. Nasal resistance (R_n) versus volume acceleration (V") in 8 randomly selected upper airway casts. Different colours correspond to different respiratory rates and/or tidal volumes (V_T) of simulated breathing pattern. Solid line is the linear regression fitted to the end-expiratory point of resistance (R_{eE}) and that of V" ($V"_{eE}$), while dotted line is fitted to the end-inspiratory points (R_{eI} and $V"_{eI}$). The intercept of the linear regression is a close estimate of the lowest oscillatory R (R_0) measured at baseline conditions.

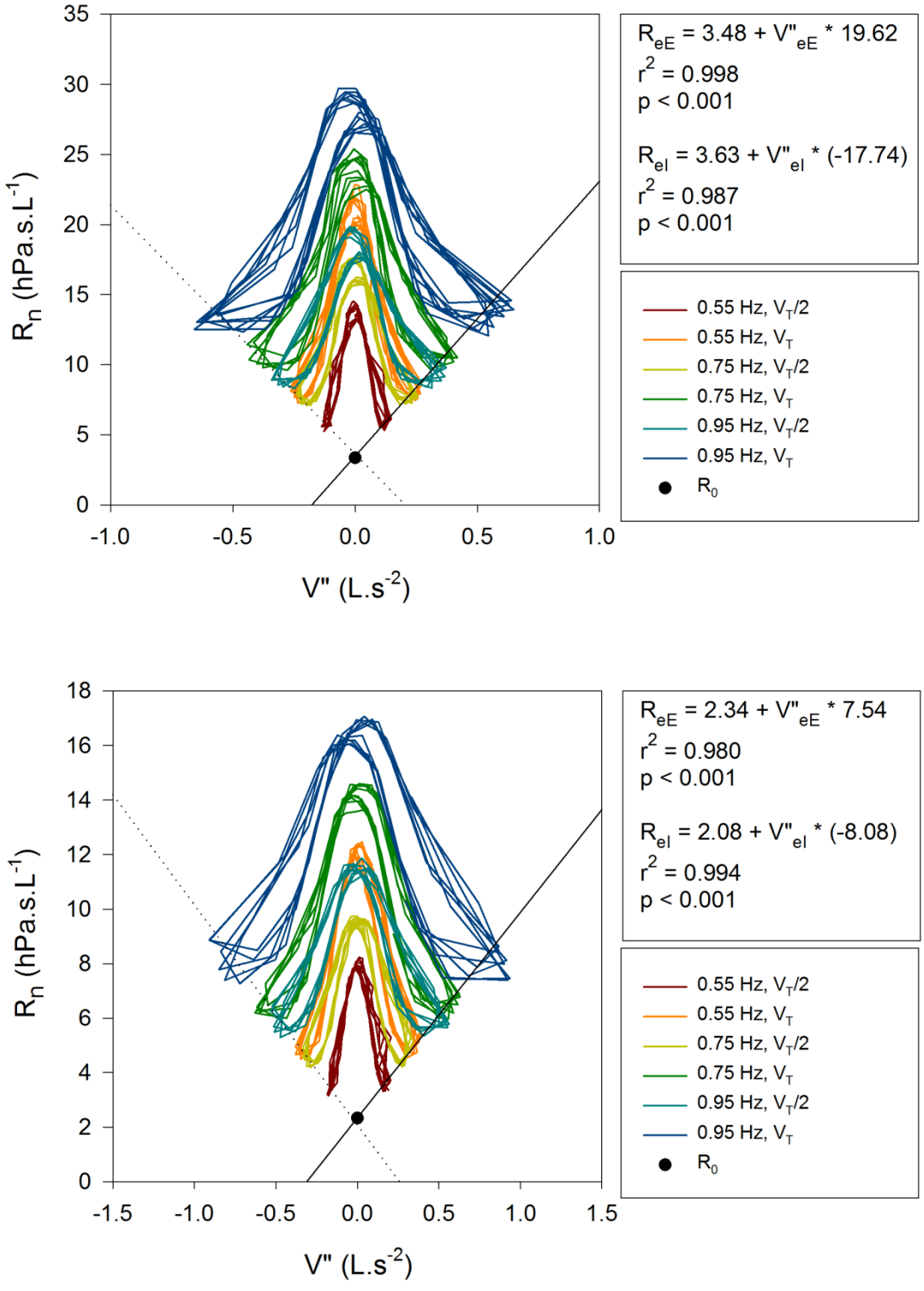

Figure S2 continued

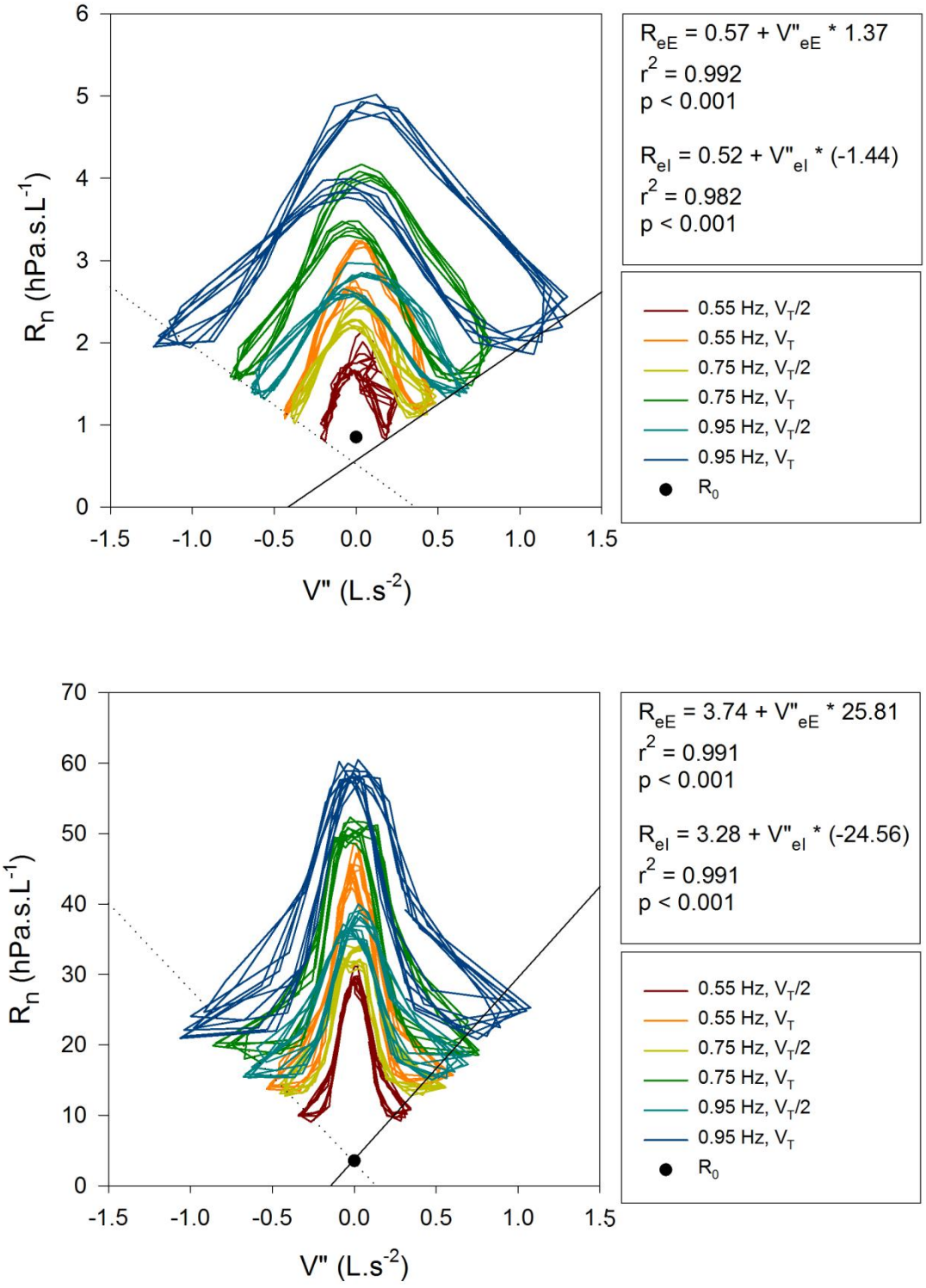

Figure S2 continued

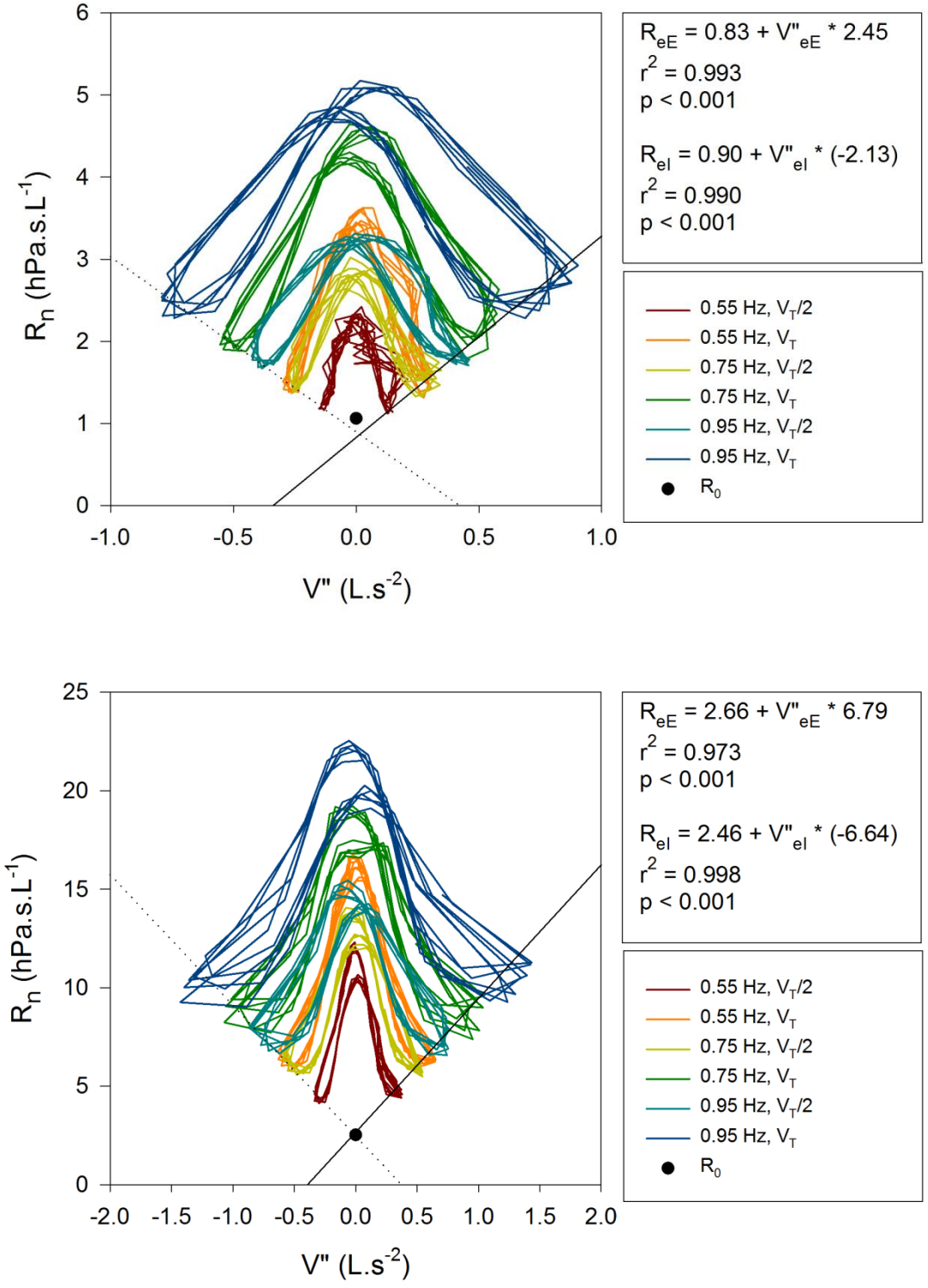

Figure S2 continued

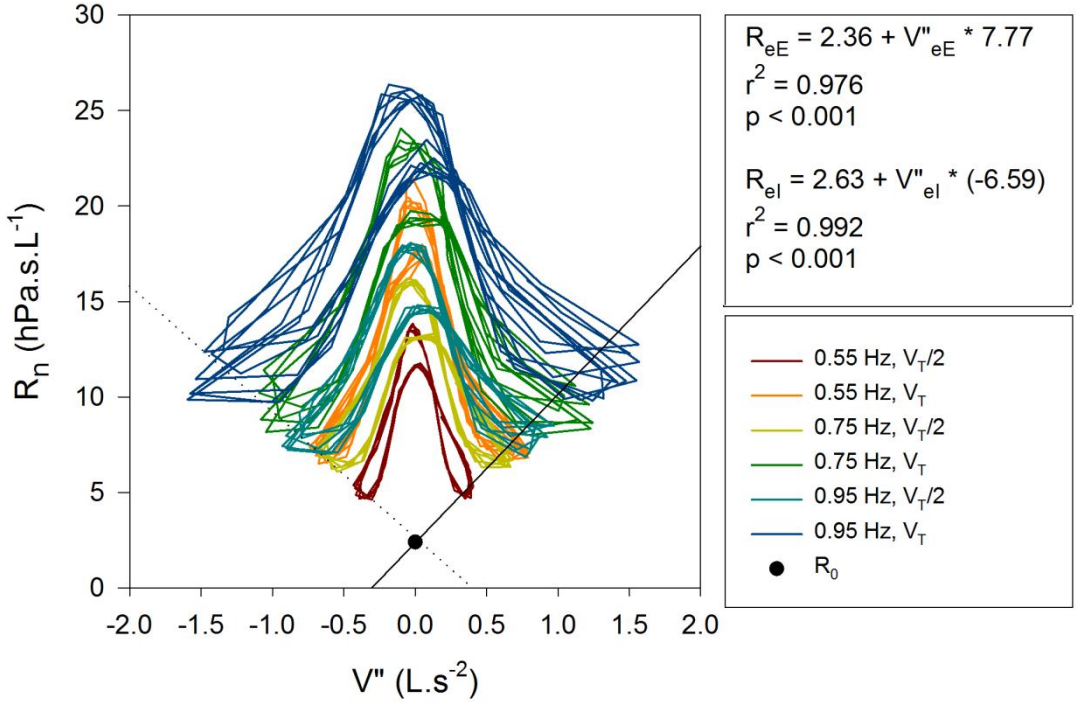

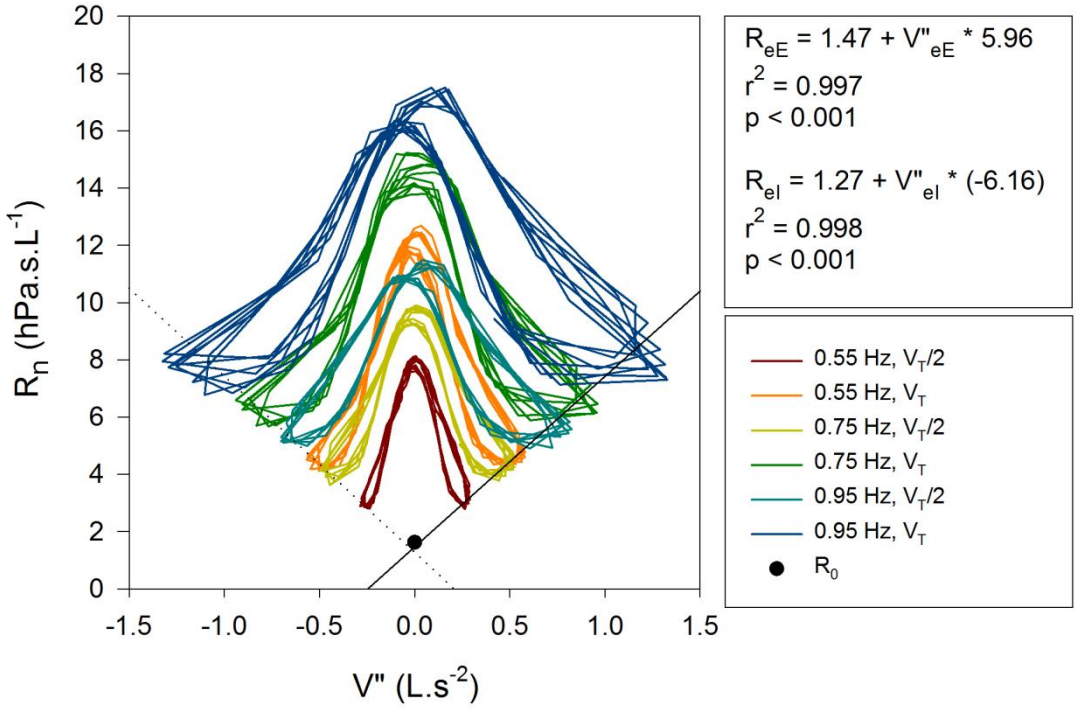

Figure S3. Respiratory system resistance (R_{rs}) vs flow (V') graphs of 15 newborns with the segmented- model fitting. Only the expiratory limb is visualised. Note the logarithmic scale.

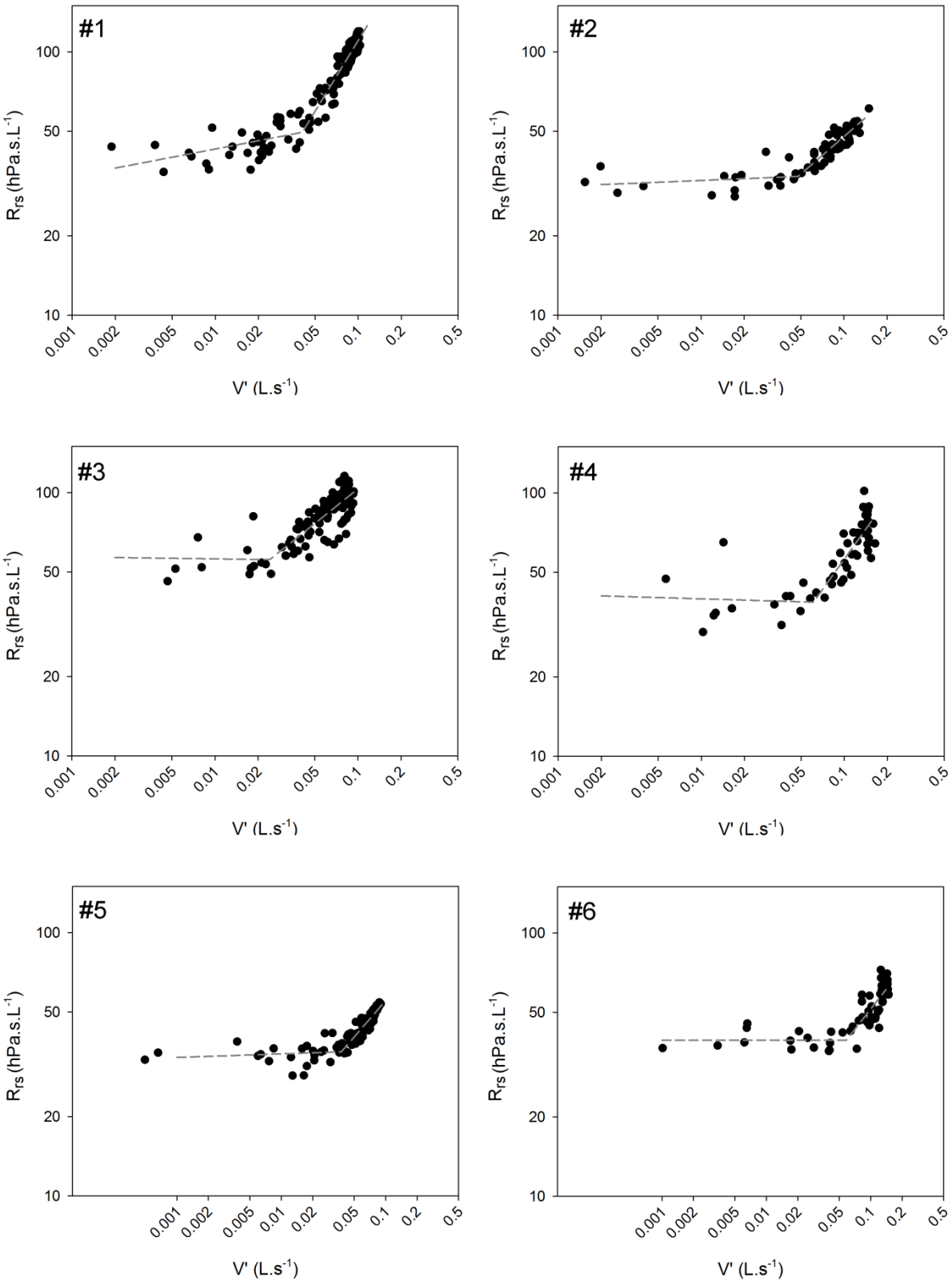

Figure S3 Continued

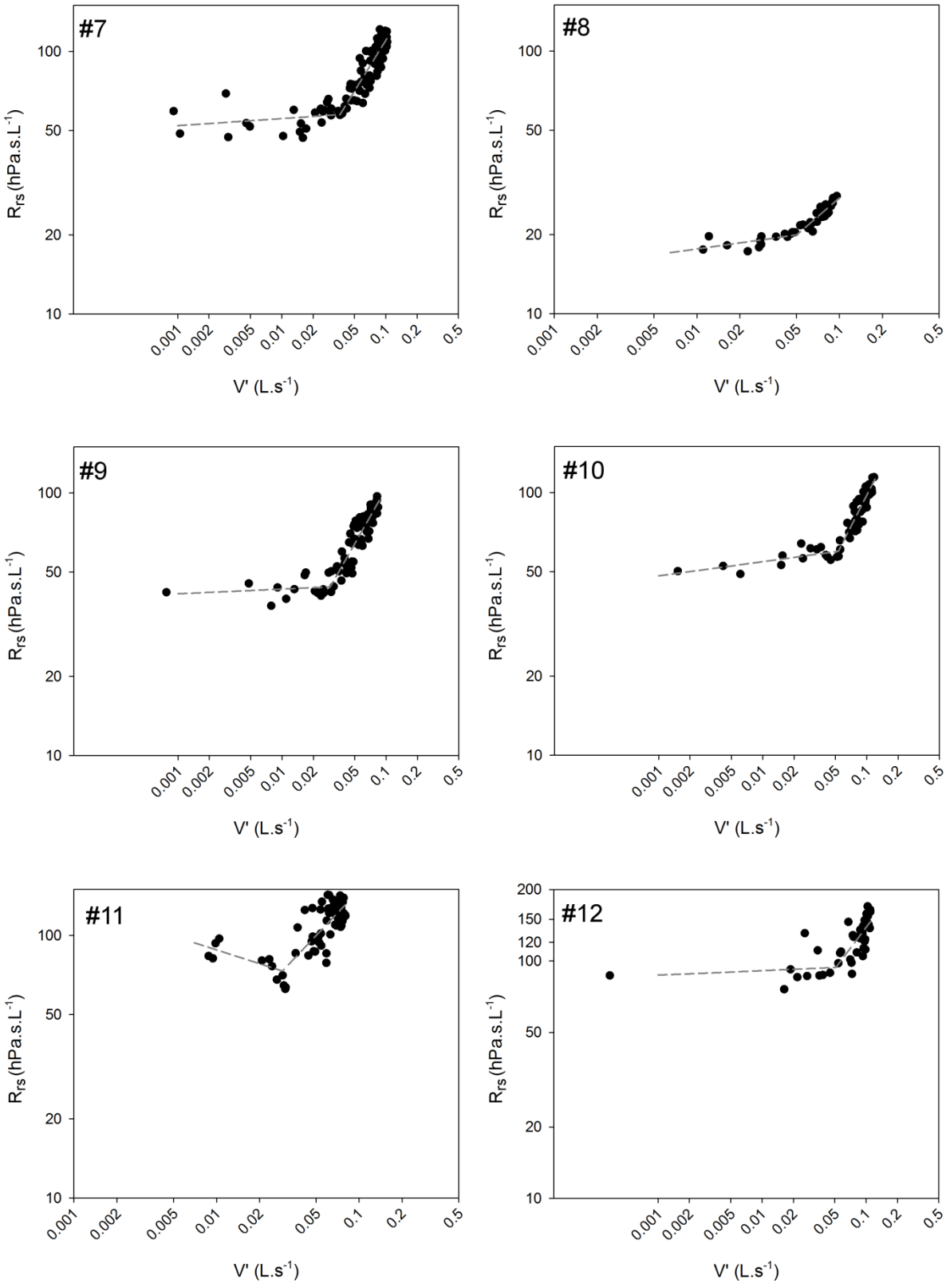

Figure S3 Continued

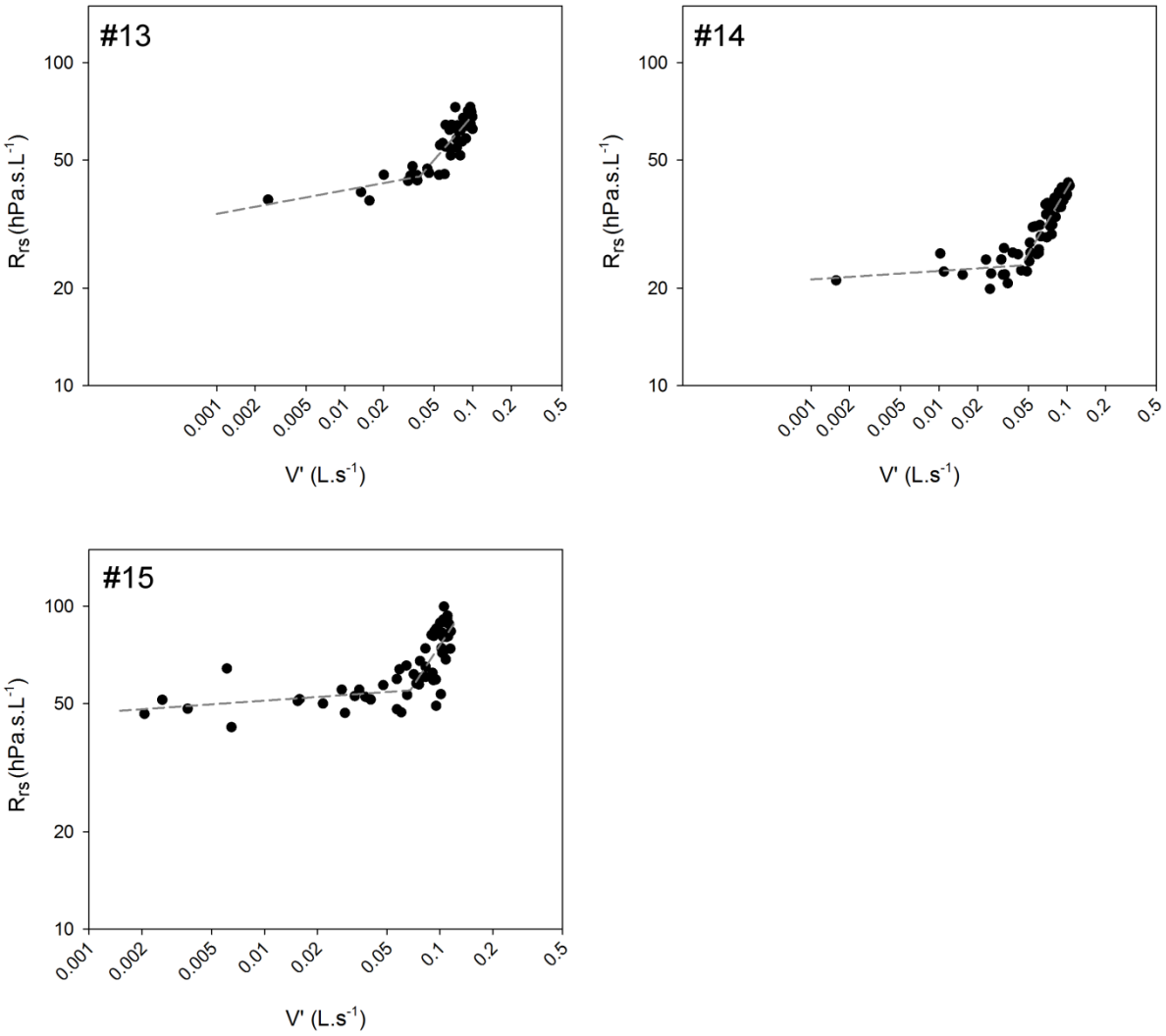

Figure S4. The effect of the geometrical correction on end-expiratory and end-inspiratory resistance (R_{eE} and R_{eI}, respectively), and the difference between ReE and ReI (ΔR) in healthy newborns (n=15). ΔR values are more realistic after correction, indicating less bias from the dynamic nonlinearities arising in the upper airways.

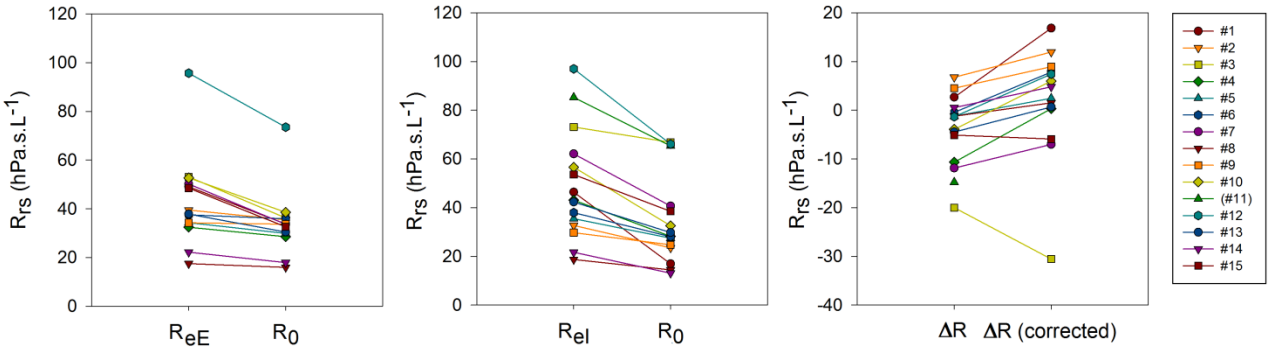

Figure S5. Relationshiph between the ratio of (measured) lowest oscillatory nasal resistance at 16 Hz (R_0) and Poiseuille R (R_P) (calculated) versus Womersley number (Wo) (calculated) of the casts without superimposed breathing. Each symbol represents a cast (n=45). Note the logarithmic scales. R_0 values are typically 10-30 times higher than R_P. Our data have a good agreement with the relationship measured in straight tubes by Dorkin et al. (Ref. 4.).

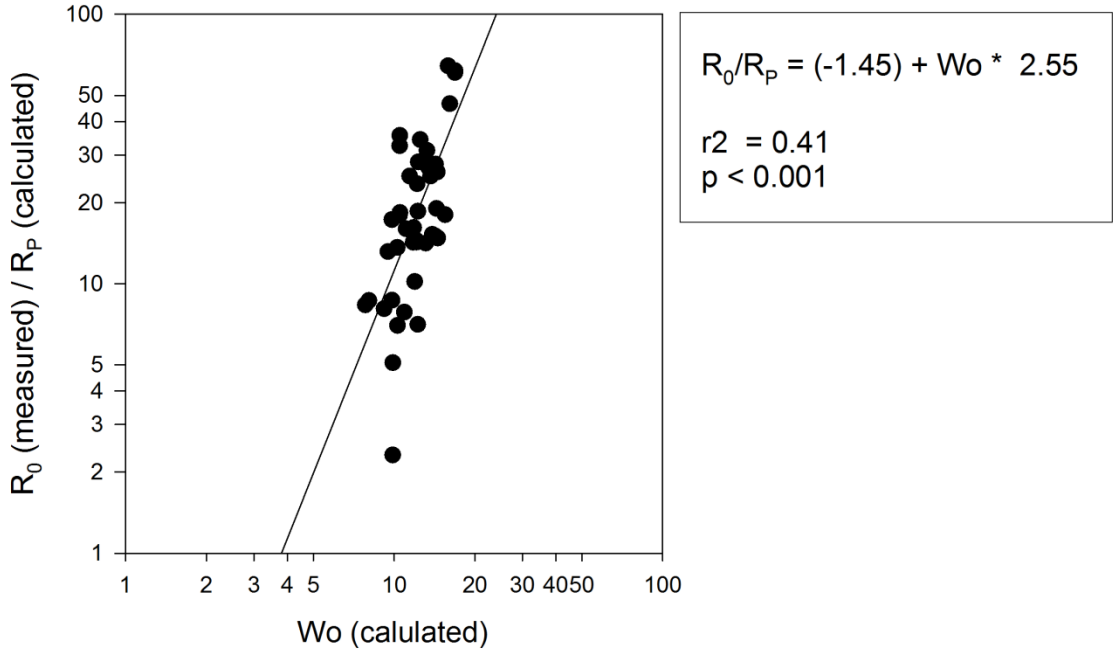

Figure S6. Nasal resistance (R_n) and reactance (X_n) versus flow (V') in randomly selected upper airway casts. Different colours indicate different respiratory rates and/or tidal volumes (V_T) of simulated breathing pattern. Lowest oscillatory R (R_0) and X (X_0) are labelled with closed and open symbols, respectively. Note the marked V'-dependent increase in R_n and the „mirroring" nature of X_n.

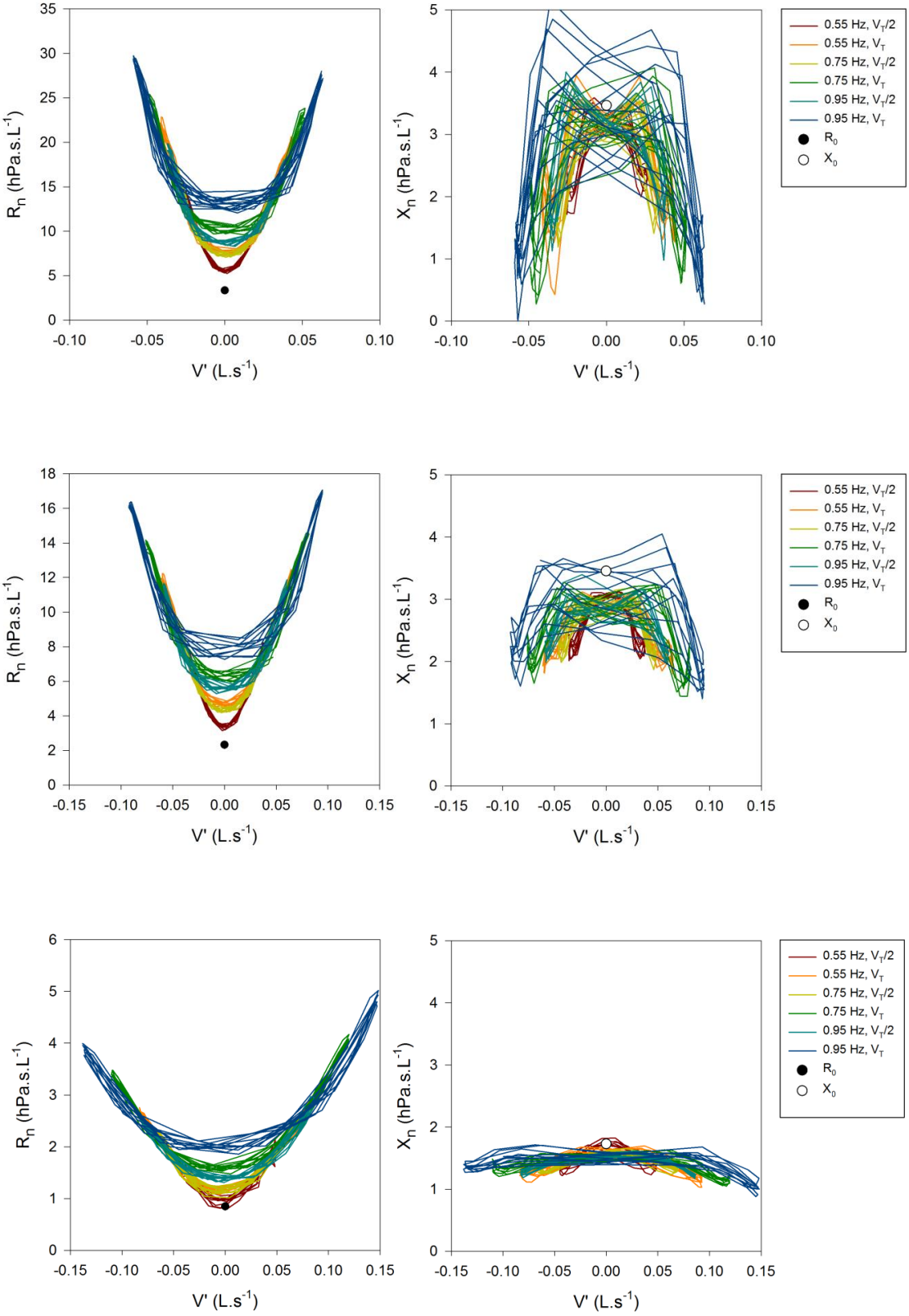

Figure S6 Continued

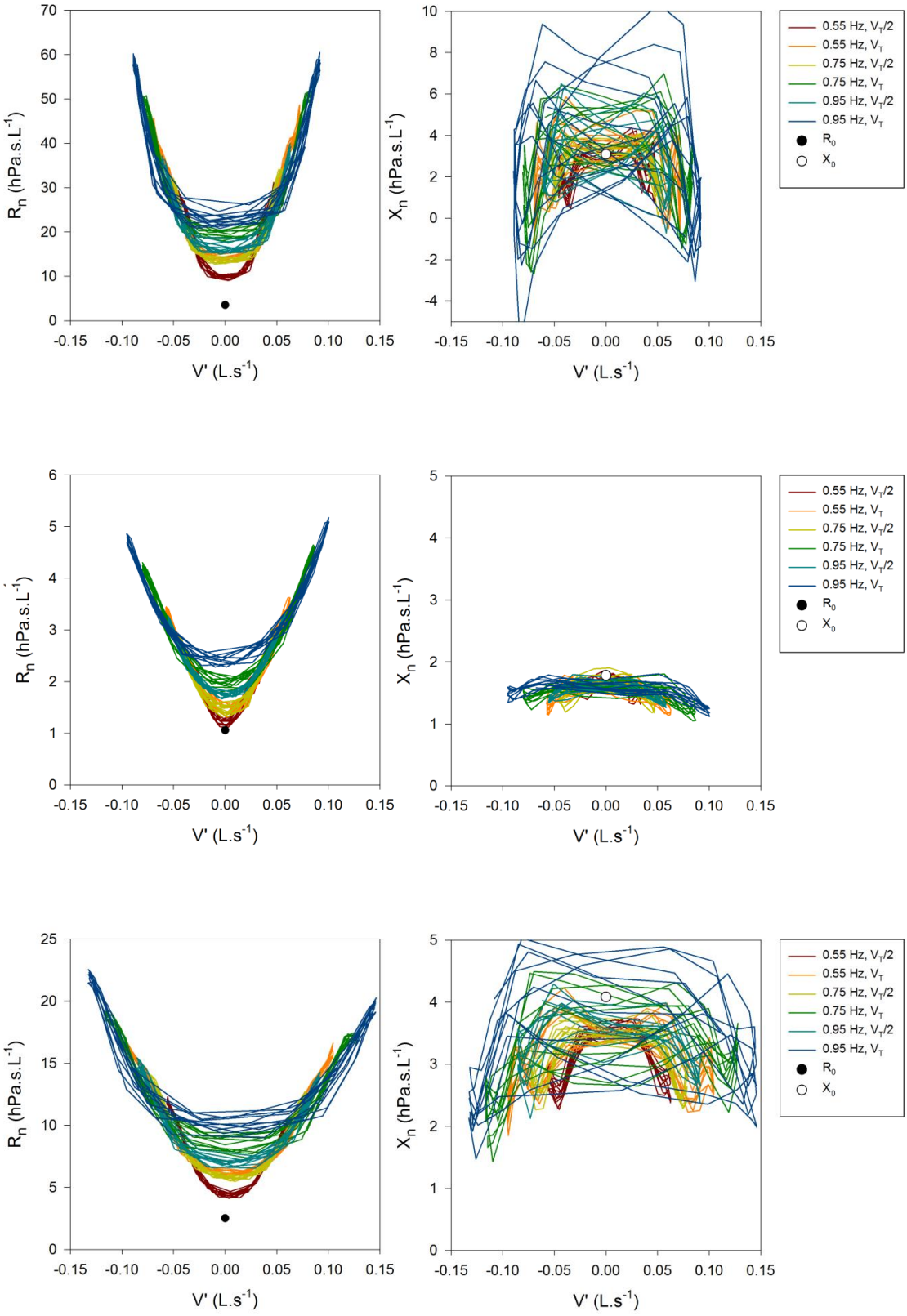

Figure S6 Continued

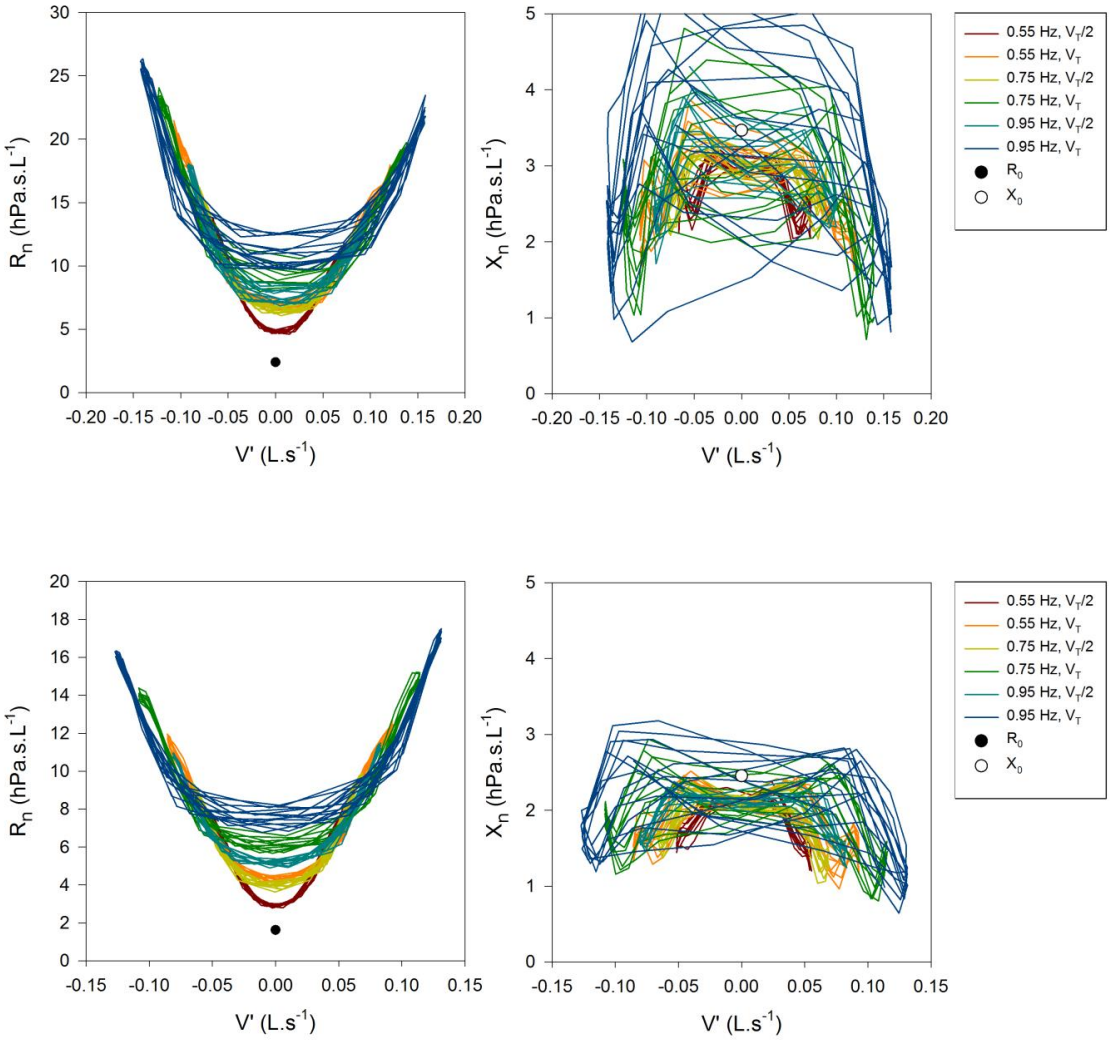

Figure S7. Boxplots showing dynamic changes in nasal reactance (X_n) values. X_n measured in baseline conditions (X_0) decreased significantly ($p<0.05$) when simulated breathing was applied. X_n measured at end-expiration (X_{eE}) had lower values than X_0, showing some effect of volume accelaration (V") on X_n. Lowest values of X_n occured at expiratory peak flows ($X_{V'maxE}$). Respiratory rate was set between 0.55 Hz to 0.95 Hz with halved tidal volumes ($V_T/2$ – first table) or full V_T (second table). Tables show the q values of pairwise statistical comparison (Repeated ANOVA on ranks with Tukey post hoc test). Numbers in bold represent a significant ($p<0.05$) difference.

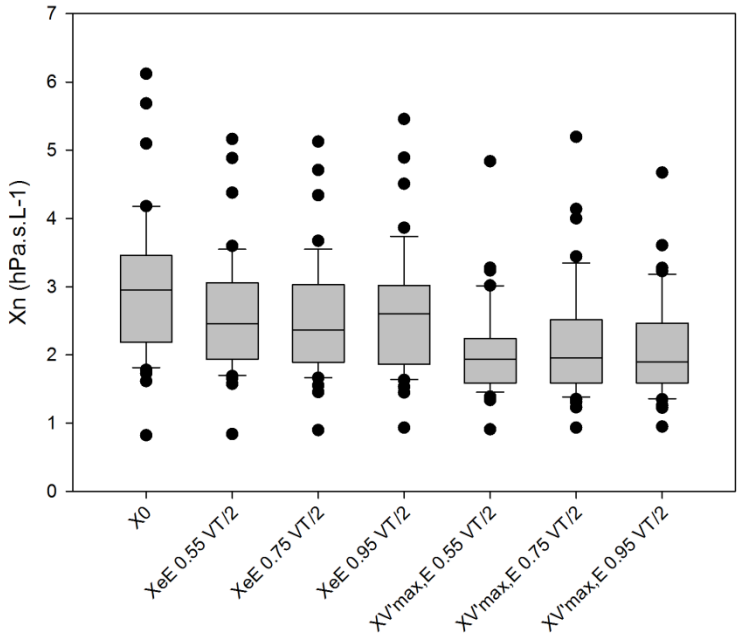

q-values	X_0	X_{eE} (0.55 Hz, $V_T/2$)	X_{eE} (0.75 Hz, $V_T/2$)	X_{eE} (0.95 Hz, $V_T/2$)	$X_{V'maxE}$ (0.55 Hz, $V_T/2$)	$X_{V'maxE}$ (0.75 Hz, $V_T/2$)	$X_{V'maxE}$ (0.95 Hz, $V_T/2$)
X_0		**4.55**	**7.77**	**5.78**	**14.836**	**13.318**	**14.353**
X_{eE} (0.55 Hz, $V_T/2$)			3.105	1.104	**10.282**	**8.76**	**9.799**
X_{eE} (0.75 Hz, $V_T/2$)				1.99	**7.18**	**5.659**	**6.694**
X_{eE} (0.95 Hz, $V_T/2$)					**9.178**	**7.66**	**8.695**
$X_{V'maxE}$ (0.55 Hz, $V_T/2$)						1.518	0.483
$X_{V'maxE}$ (0.75 Hz, $V_T/2$)							1.035
$X_{V'maxE}$ (0.95 Hz, $V_T/2$)							

Figure S7 continued

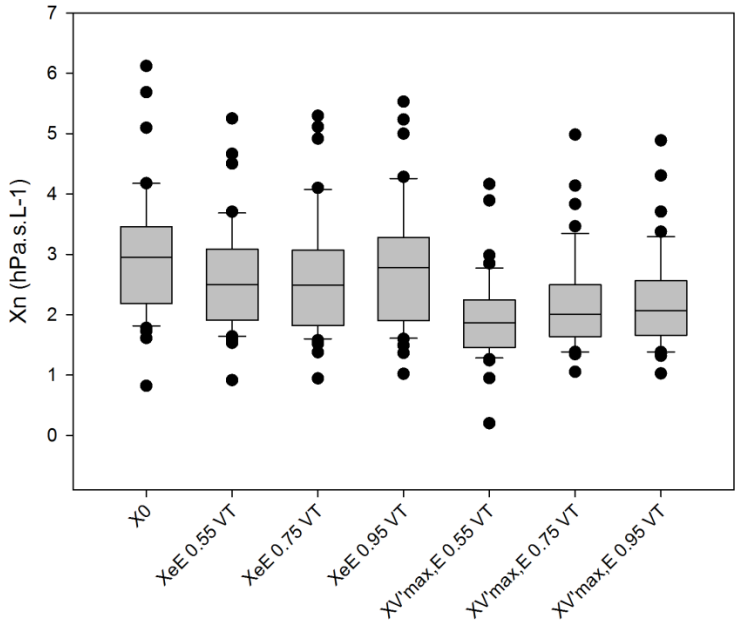

q-values	X_0	X_{eE} (0.55 Hz, V_T)	X_{eE} (0.75 Hz, V_T)	X_{eE} (0.95 Hz, V_T)	$X_{V'maxE}$ (0.55 Hz, V_T)	$X_{V'maxE}$ (0.75 Hz, V_T)	$X_{V'maxE}$ (0.95 Hz, V_T)
X_0		**6.28**	**7.798**	3.795	**15.043**	**12.835**	**12.214**
X_{eE} (0.55 Hz, V_T)			1.518	2.484	**8.764**	**6.56**	**5.935**
X_{eE} (0.75 Hz, V_T)				4.002	**7.25**	**5.037**	**4.416**
X_{eE} (0.95 Hz, V_T)					**11.248**	**9.04**	**8.419**
$X_{V'maxE}$ (0.55 Hz, V_T)						2.208	2.829
$X_{V'maxE}$ (0.75 Hz, V_T)							0.621
$X_{V'maxE}$ (0.95 Hz, V_T)							

Figure S8. Respiratory system resistance (R_{rs}) and reactance (X_{rs}) vs flow (V') graphs of newborns - in vivo measurements. Note that the mean value of Xrs is usually negative. Xrs „mirrors" the changes in Rrs in most cases, but there are several exceptions (sometimes even with increasing Xrs – a pattern never observed during the in vitro experiment).

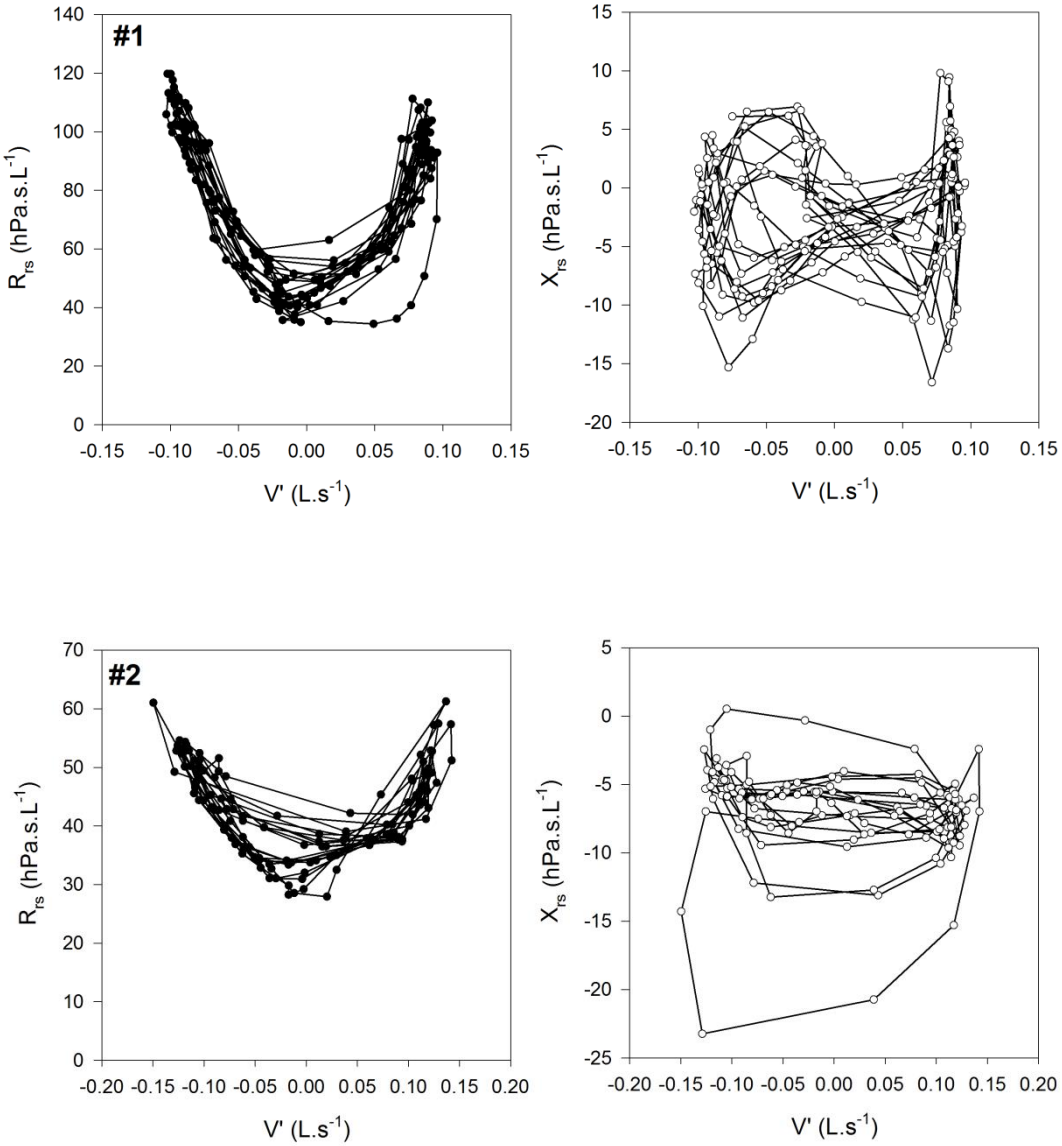

Figure S8 Continued

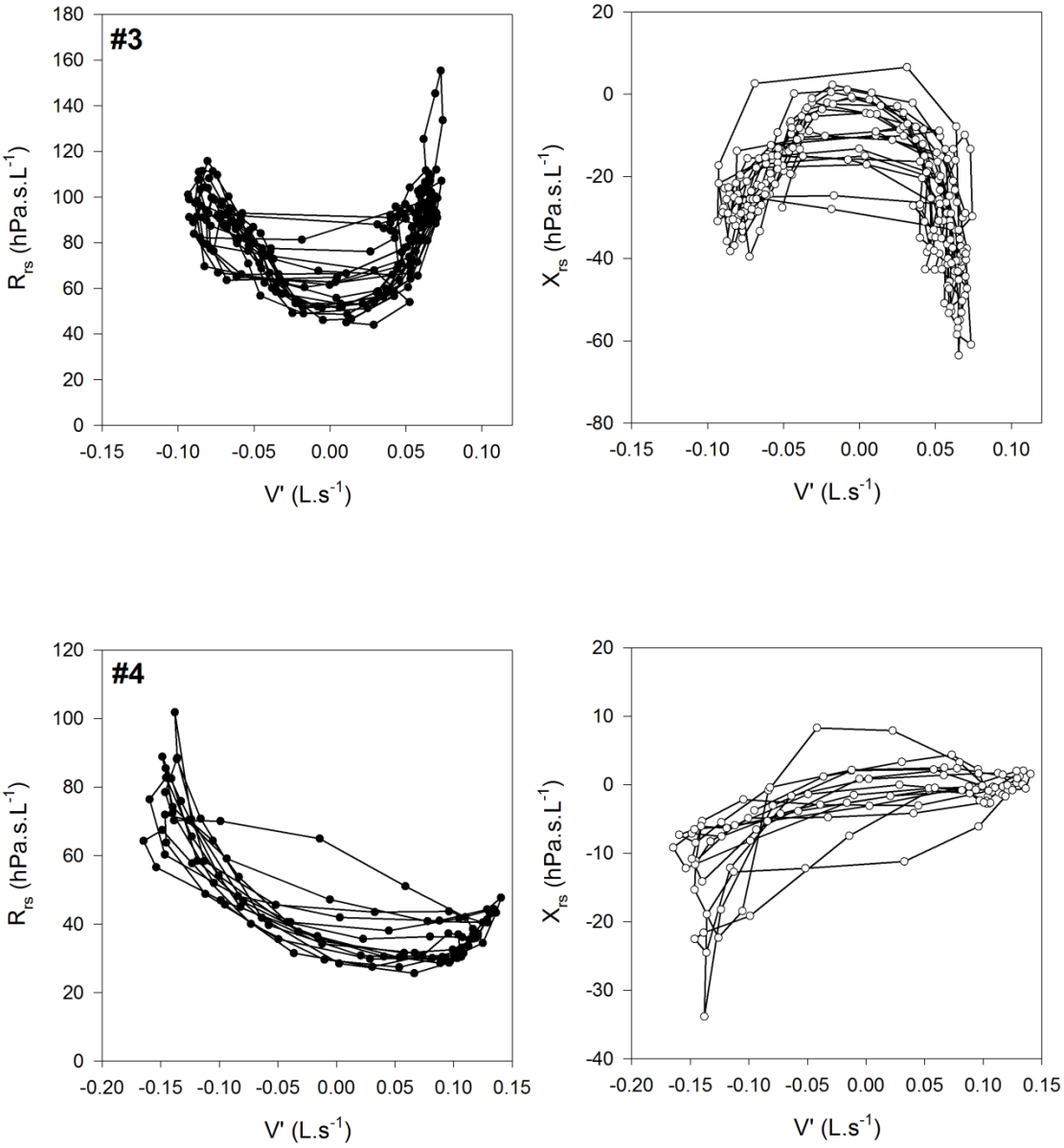

Figure S8 Continued

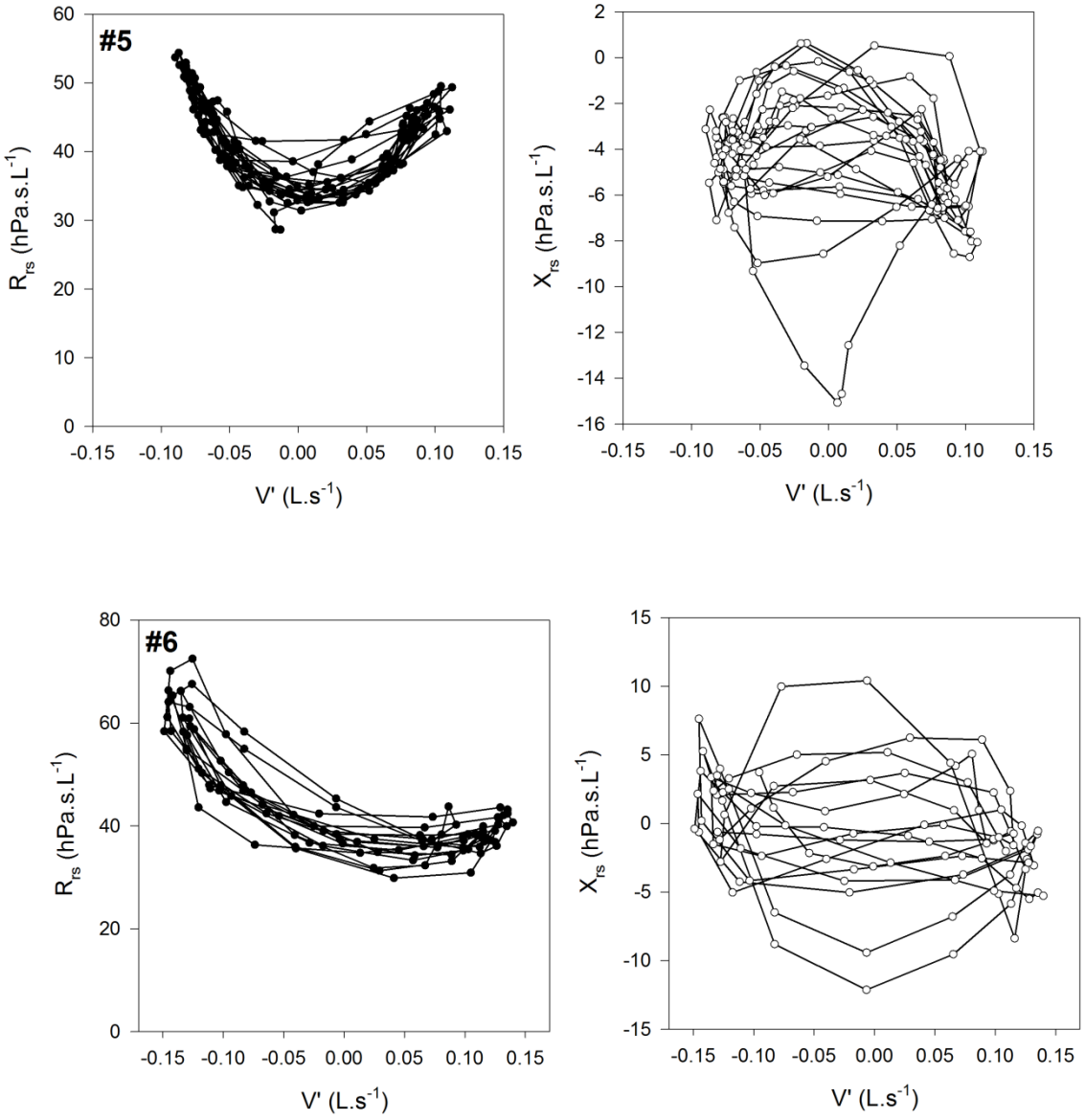

Figure S8 Continued

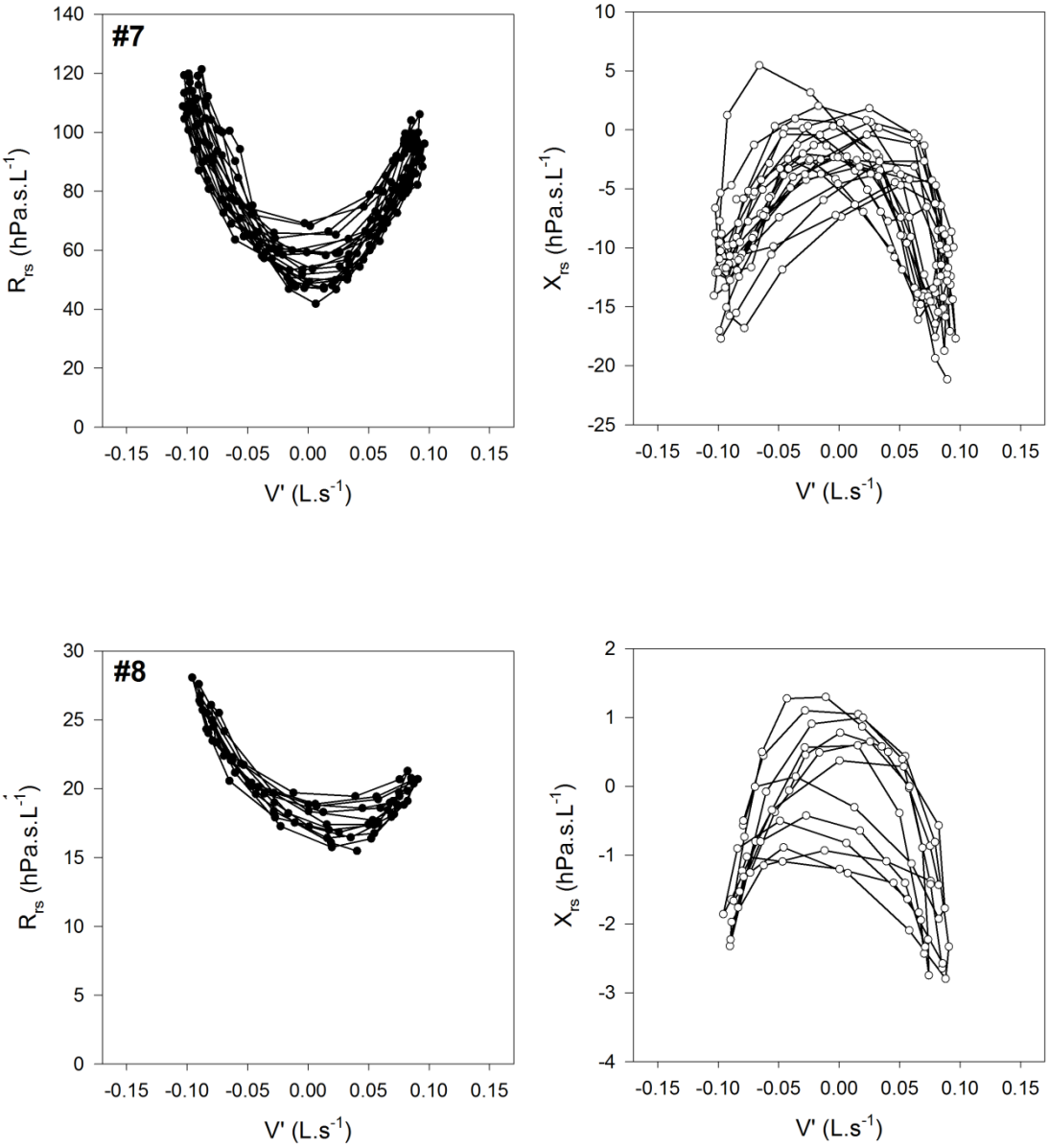

Figure S8 Continued

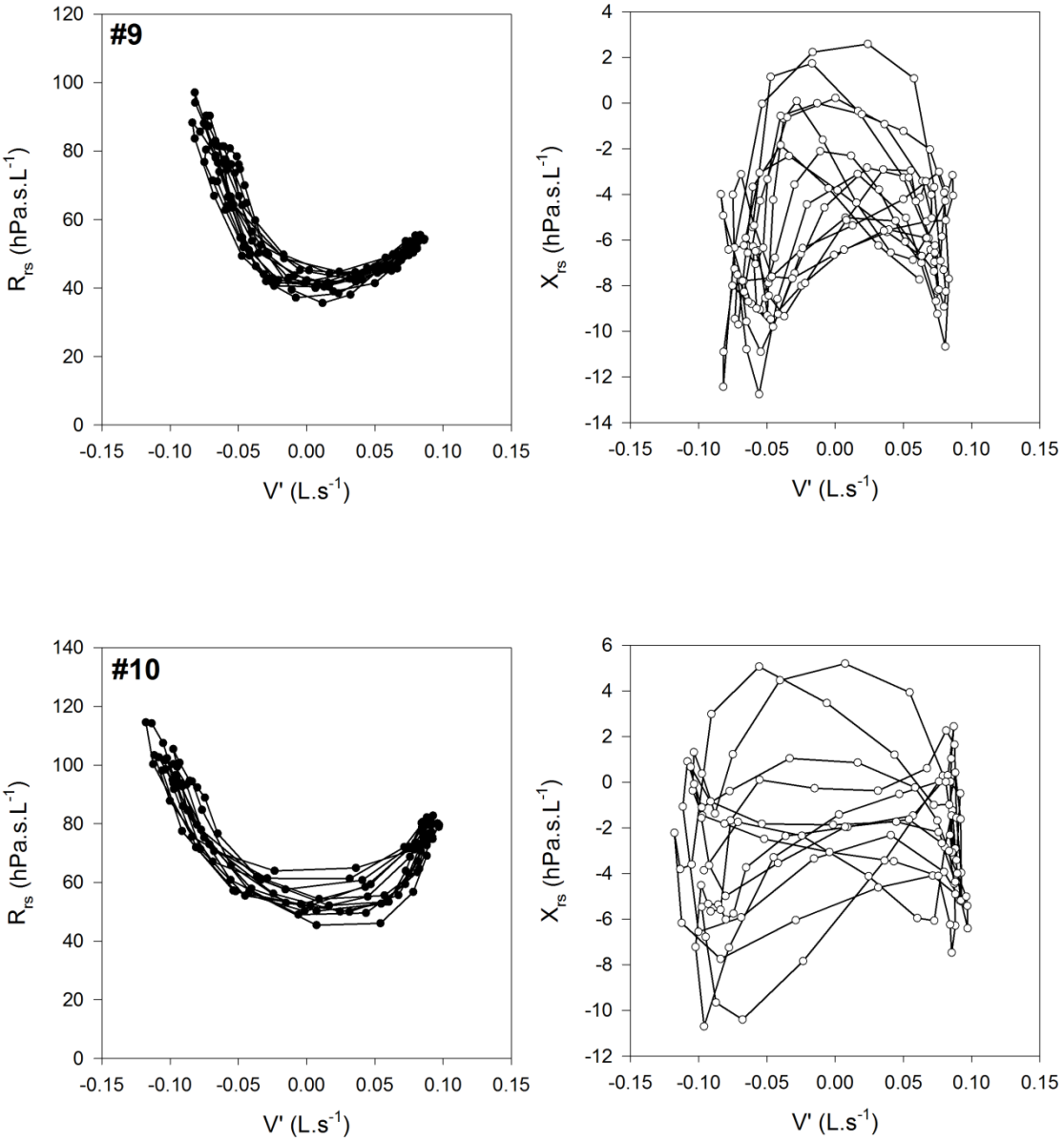

Figure S8 Continued

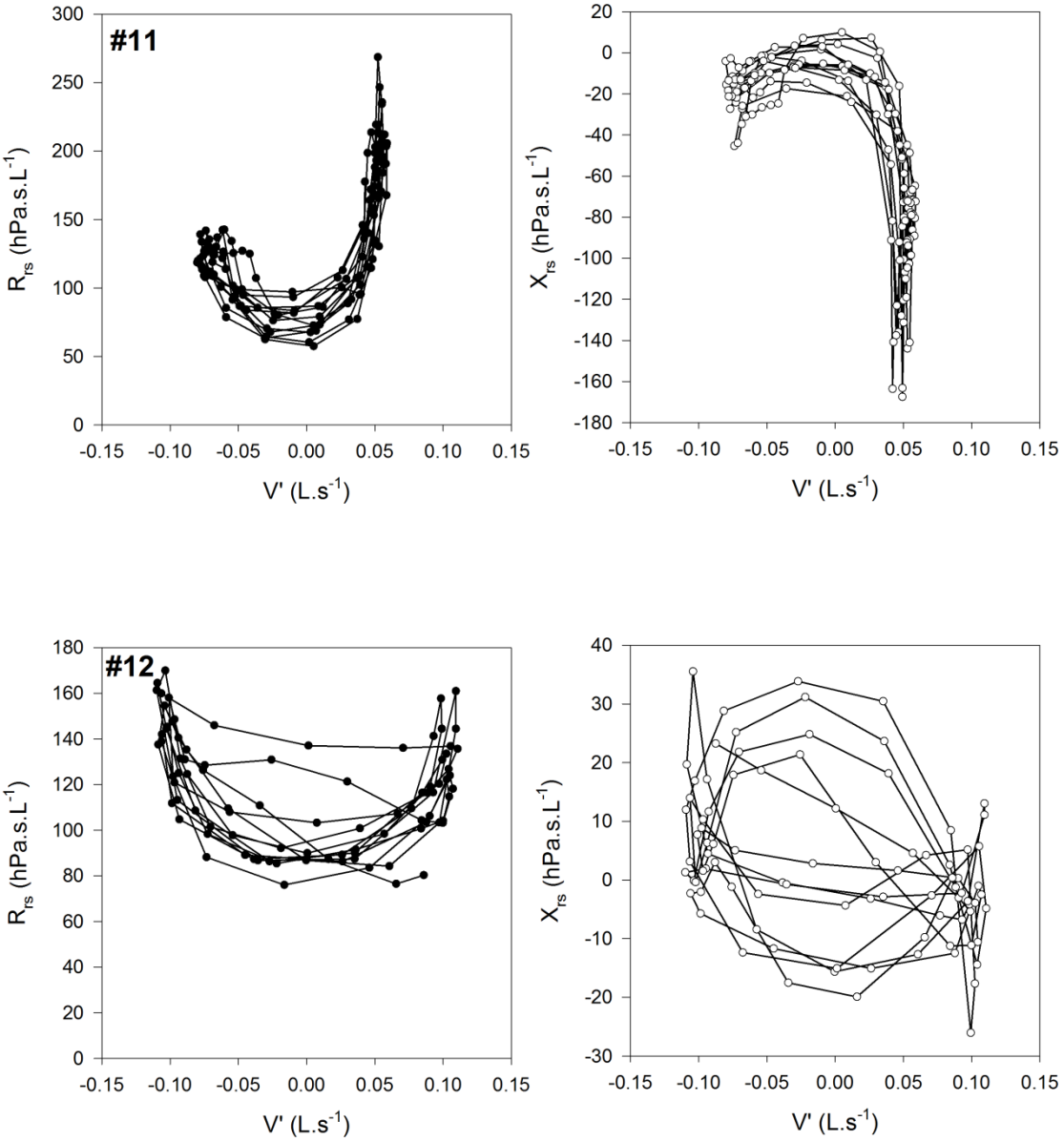

Figure S8 Continued

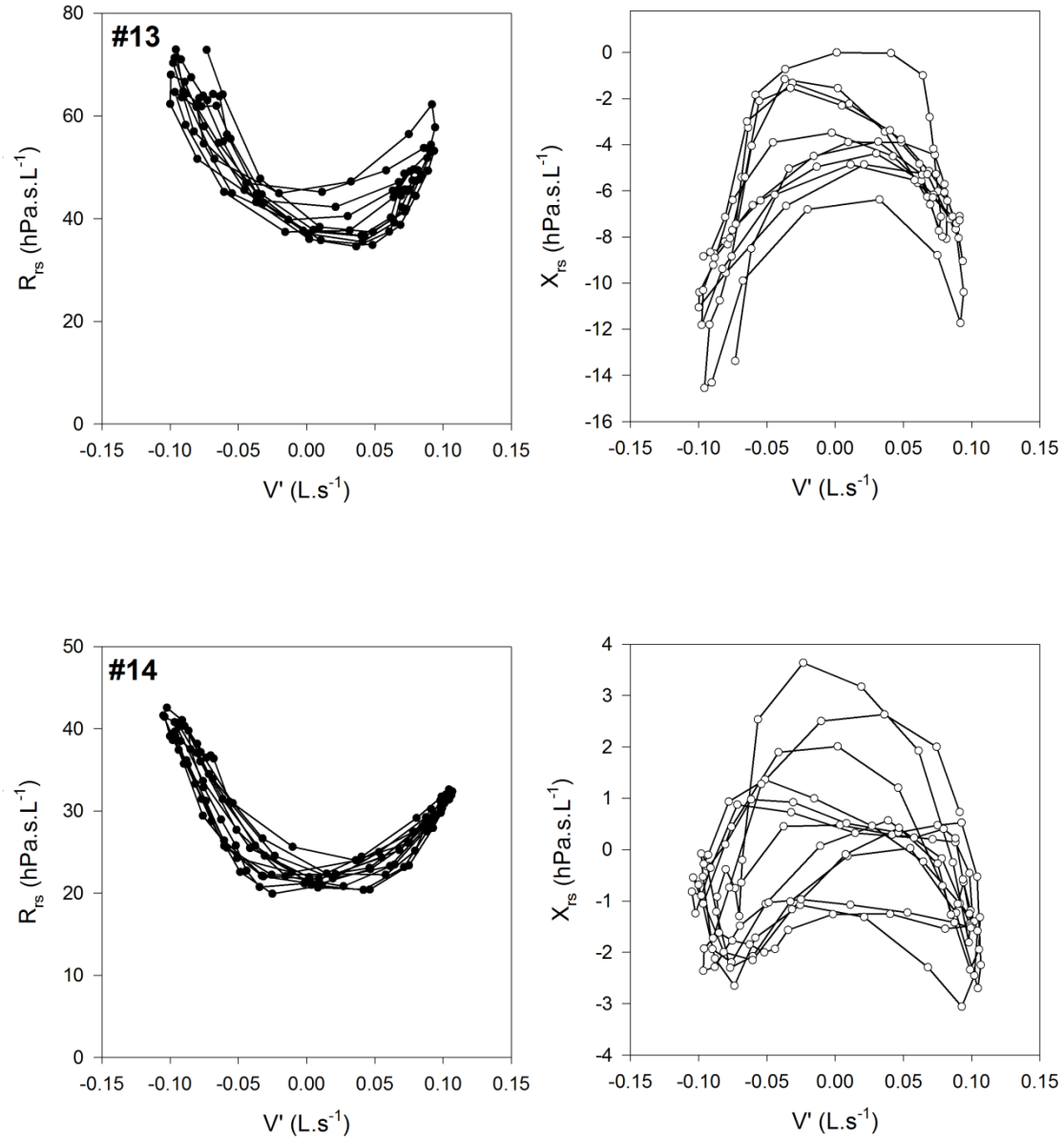

Figure S8 Continued

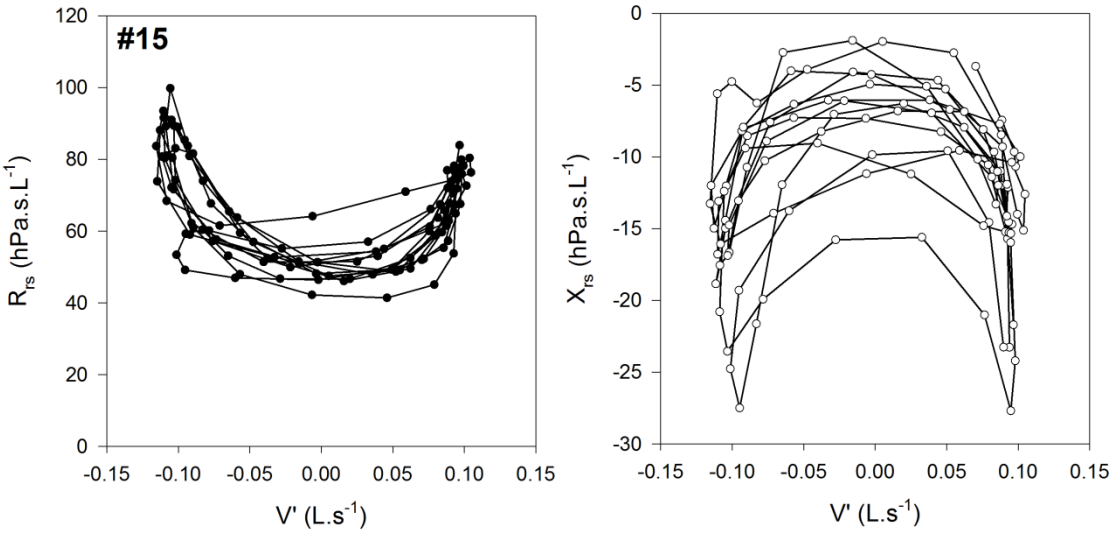

SUPPLEMENT 2.

PAPERS UNDERLYING THE PHD THESIS

I.

J Appl Physiol 129: 591–598, 2020.
First published July 23, 2020; doi:10.1152/japplphysiol.00128.2020.

RESEARCH ARTICLE

Effect of nasal airway nonlinearities on oscillometric resistance measurements in infants

Bence L. Radics,[1] Gergely Makan,[2] Thibault Coppens,[3] Nicolas André,[4] Cyril Page,[4] Loïc Dégrugilliers,[5] S. Kianoush Bayat,[6] Zoltán Gingl,[2] Zita Gyurkovits,[7] Tivadar M. Tóth,[8] Zoltan Hantos,[9,10]* and Sam Bayat[11,12]*

[1]*Department of Pulmonology, University of Szeged, Szeged, Hungary;* [2]*Department of Technical Informatics, University of Szeged, Szeged, Hungary;* [3]*St-Luc University Hospital, Brussels, Belgium;* [4]*Department of Otorhinolaryngology, Amiens University Hospital, Amiens, France;* [5]*Department of Pediatric Intensive Care, Amiens University Hospital, Amiens, France;* [6]*Inria Grenoble, Equipex Amiqual4Home, Grenoble, France;* [7]*Department of Obstetrics and Gynaecology, University of Szeged, Szeged, Hungary;* [8]*Department of Mineralogy, Geochemistry, and Petrology, University of Szeged, Szeged, Hungary;* [9]*County Hospital for Chest Diseases, Deszk, Hungary;* [10]*Department of Anaesthesiology and Intensive Therapy, Semmelweis University, Budapest, Hungary;* [11]*Department of Pulmonology and Physiology, Grenoble University Hospital, Grenoble, France; and* [12]*Inserm UA7 STROBE Laboratory, Grenoble, France*

Submitted 21 February 2020; accepted in final form 18 July 2020

Radics BL, Makan G, Coppens T, André N, Page C, Dégrugilliers L, Bayat K, Gingl Z, Gyurkovits Z, Tóth TM, Hantos Z, Bayat S. Effect of nasal airway nonlinearities on oscillometric resistance measurements in infants. *J Appl Physiol* 129: 591–598, 2020. First published July 23, 2020; doi:10.1152/japplphysiol.00128.2020.—Oscillometric measurements of respiratory system resistance (R_{rs}) in infants are usually made via the nasal pathways, which not only significantly contribute to overall R_{rs} but also introduce marked flow (V')-dependent changes. We employed intrabreath oscillometry in casts of the upper airways constructed from head CT images of 46 infants. We examined oscillometric nasal resistance (R_n) in upper airway casts with no respiratory flow (R_0) and the effect of varying V' on R_n by simulating tidal breathing. A characteristic nonlinear relationship was found between R_n and V', exhibiting segmental linearity and a prominent breakpoint (V'_{bp}) after log-log transformation. V'_{bp} was linearly related to the preceding value of end-expiratory volume acceleration (V''_{eE}; on average $r^2 = 0.96$, $P < 0.001$). R_n depended on V', and R at end-expiration (R_{eE}) showed a strong dependence on V''_{eE} in every cast ($r^2 = 0.994$, $P < 001$) with considerable interindividual variability. The intercept of the linear regression of R_{eE} versus V''_{eE} was found to be a close estimate of R_0. These findings were utilized in reanalyzed R_{rs} data acquired in vivo in a small group of infants ($n = 15$). Using a graphical method to estimate R_0 from R_{eE}, we found a relative contribution of V'-dependent nonlinearity to total resistance of up to 33%. In conclusion, we propose a method for correcting the acceleration-dependent nonlinearity error in R_{eE}. This correction can be adapted to estimate R_0 from a single intrabreath oscillometric measurement, which would reduce the masking effects of the upper airways on the changes in the intrathoracic resistance.

NEW & NOTEWORTHY Oscillometric measurements of respiratory system resistance (R_{rs}) in infants are usually made via the nasal pathways, which not only significantly contribute to overall R_{rs} but also introduce marked flow acceleration-dependent distortions. Here, we propose a method for correcting flow acceleration-dependent nonlinearity error based on in vitro measurements in 3D-printed upper airway casts of infants as well as in vivo measurements. This correction can be adapted to estimate R_{rs} from a single intrabreath oscillometric measurement.

forced oscillations; respiratory mechanics; upper airway casts

INTRODUCTION

The contribution of nasal airway resistance (R_n) to total respiratory system resistance (R_{rs}) is a central problem in infant pulmonary function testing, since infants are obligate nasal breathers during the first several months of life. Therefore, measurements of lung function in this population are usually performed through a facemask, unlike in older children and adults.

The contribution of R_n to that of the R_{rs} in infants has been studied previously by posterior rhinomanometry. Using this technique, Polgar and Kong (23) estimated this contribution to be 26%, whereas Stocks and Godfrey (25) found a higher value of 49%. Using low-frequency oscillometry during apneic periods, Hall et al. (8) studied the impedance of the nasal pathways in infants by measuring nasal pressure with a miniature catheter-tip transducer inserted through a nostril. They found a 45% contribution of the nasal impedance to R_{rs}.

Although some discrepancy in previous estimates of the contribution of R_n to R_{rs} may be attributed to differences in methodology and population, measurement and interpretation of R_n are profoundly complicated by the anatomic irregularity and complex flow rheology of the nasal passages. The nonlinear pressure (P)-flow (V') relationship in the upper airways contributes to the dynamic changes in R_{rs}, which have been well documented with intrabreath oscillometry in adults (2, 19, 21), children (1), and infants (7). Measurement of R_{rs} at points of zero V' [namely at end expiration (R_{eE}) and end inspiration (R_{eI})] minimizes the nonlinear contribution of the nasal pathways and the consequent bias in the estimation of R of the lower respiratory tract. Intrabreath oscillometry is a unique lung function technique that is able to identify these zero-flow values of R_{rs}.

The aim of this study was to use intrabreath oscillometry in anatomically faithful casts of the nasal pathways of infants

* Z. Hantos and S. Bayat are senior co-authors of this article.
Correspondence: S. Bayat (sbayat@chu-grenoble.fr).

from birth to 2 yr, reconstructed from computed tomography (CT) images. We assessed the lowest oscillatory R without superimposed breathing (R_0) as well as the effect of varying V' on R_n by simulating breathing through the casts. We characterized the relationships of R_n to V' and volume acceleration (V''). Based on these relationships, we propose a graphical method to correct the error in intrabreath oscillometric R_{rs} measurements that results from V'-dependent nonlinearities. The relative contribution of these nonlinearities to R_{rs} was further assessed in a set of intrabreath oscillometric measurements in infants.

METHODS

Study population. Data of head CT examinations of infants from birth to 24 mo, available in the Department of Radiology of the Amiens University Hospital database, performed between October 2011 and August 2014, were collected for analysis. The requirement for written, informed consent was waived for this retrospective study by the Internal Review Board of the Amiens University Hospital. Cases not including the entire nasal passages from the nares to the tip of the epiglottis, and those with craniofacial abnormalities or upper airway mass based on the radiologist's report, were excluded. Forty-six image sets met these criteria. Indication for head CT examination is summarized in the online supplement (Supplemental Table S4; all Supplemental Material for this article is available online at https://doi.org/10.5281/zenodo.3676456). Weight data were available in all cases from the electronic medical records. Height and sex difference data were recorded in 28 and 38 infants, respectively. A tidal volume (V_T) of 7 mL/kg was used to ventilate the casts, in one case based on ideal weight due to a lower than normal real weight.

Image analysis. All images were anonymized for analysis. Native Dicom images were converted to Nifti format. The nasal airway structures were segmented from the nares to the epiglottis, using an active contour algorithm in itk-SNAP software (26) (www.itksnap.org). A representative example is shown in Fig. 1. The accuracy of the segmentation was visually examined and manually edited when necessary by an ear-nose-throat specialist (NA). The resulting segmented image was converted to a mesh. A three-dimensional (3D) model of the nasal airways was then produced with a 3D printer (Makerbot; Replicator2) with polylactide using Meshmixer software (www.meshmixer.com), with an accuracy as follows: xy, 11 μm; z, 2.5 μm. The accuracy of the 3D-printed casts compared with the initial CT image was verified in one case by CT scanning the cast, followed by image segmentation (3). Comparison with the initially segmented image, qualitatively by overlaying images, showed a quasi-perfect match and a volume difference of 0.3%.

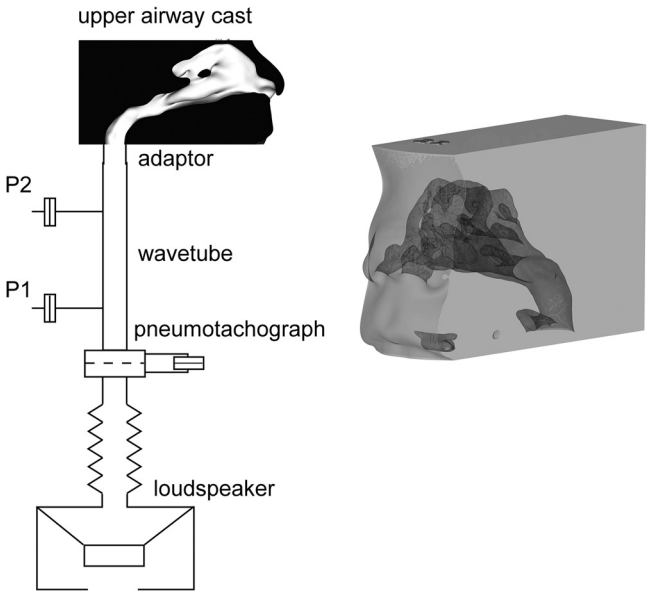

Fig. 1. *Left*: schematic illustration of the experimental setup. *Right*: transparent 3-dimensional (3D) reconstruction of the upper airways, used as a sample for 3D printing. P1 and P2, respectively, denote the inlet and outlet pressures of the wave tube.

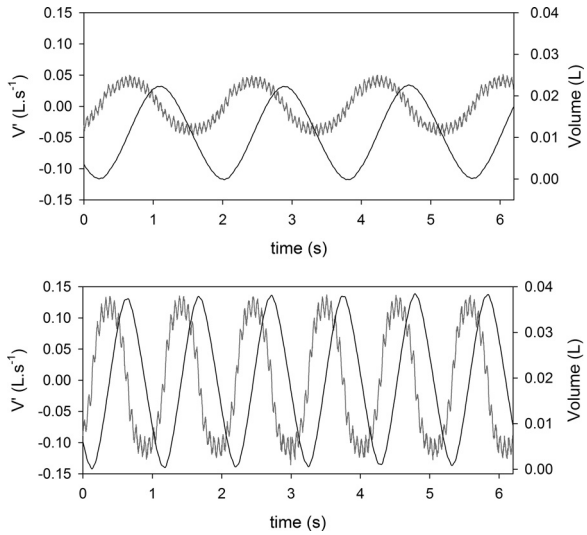

Fig. 2. Time series of 2 representative measurement settings. Small-amplitude oscillatory signal (16 Hz) superimposed on the simulated tidal breathing. *Top*: 0.55-Hz breathing frequency with halved tidal volume ($V_T/2$). *Bottom*: 0.95-Hz respiratory rate with normal tidal volume (V_T). Black lines, volume; gray lines, flow (V').

The nasal airway passages were segmented, and the volume, surface area, and various shape descriptors were measured with ImageJ software (https://imagej.nih.gov), using the "3D ImageJ Suite" plugins (https://github.com/mcib3d). Sparseness was defined as the ratio of the volume of a fitted ellipsoid (to that of the 3D-segmented image; Supplemental Fig. S1). Flatness was defined as the ratio of the second axis to the third axis of the ellipsoid. Elongation was defined as the ratio of the first to the second axis of the ellipsoid. Sphericity was defined as

$$\text{Sphericity} = \frac{\pi^{\frac{1}{3}}\left(6V_{aw}\right)^{\frac{2}{3}}}{S_{aw}}, \qquad (1)$$

where V_{aw} is the volume of the segmented upper airways and S_{aw} is the surface area. The theoretical background of these measures is given in Ref. 18.

Experimental setup. Rheological measurements of the upper airway casts were performed with custom-made equipment (Fig. 1). Baseline measurements were recorded with the oscillatory signal only, without simulated breathing (R_0). Tidal excursions were generated by a 20-cm-diameter subwoofer loudspeaker (SRP 2030; Somogyi Audio Line, Budapest, Hungary) at three different respiratory rates (33, 45,

Table 1. *Upper airway model subject characteristics*

	Median (Q1, Q3)	Range
Age, wk	25.4 (9.3, 46.3)	0.3–86.7
Weight, kg	6.5 (5.4, 8.9)	2.3–12
Height, cm	59.4 (56.8, 62.1)	49–80.5
Sex (females/males)	0.81	

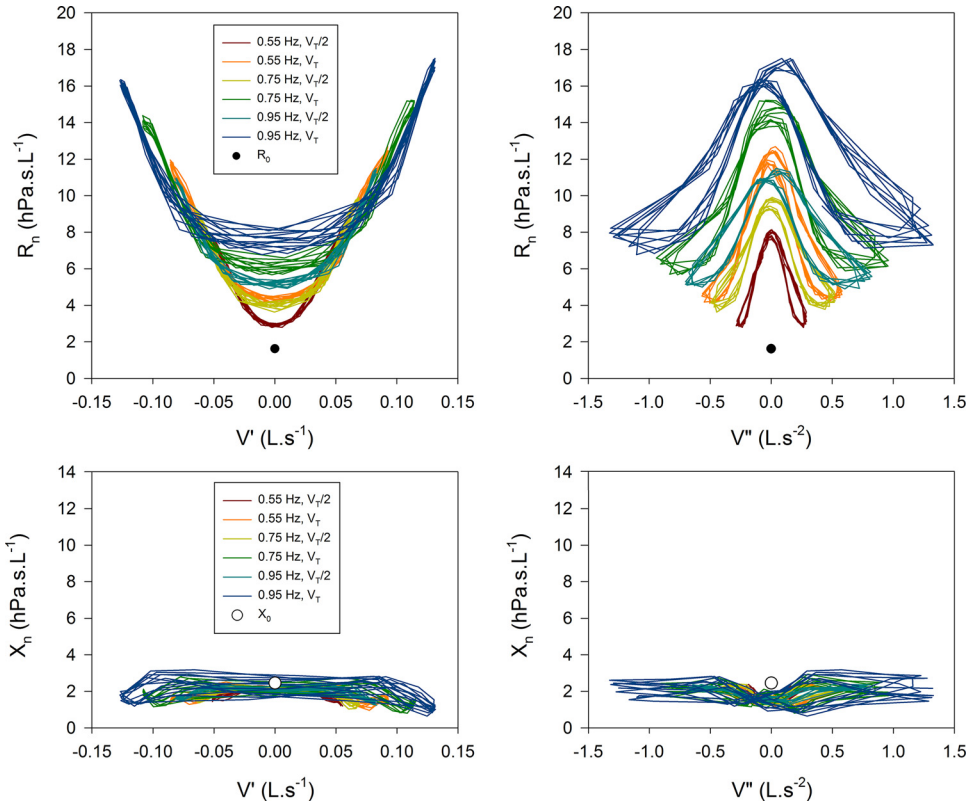

Fig. 3. Resistance (R_n) and reactance (X_n) plotted against flow (V′; *left*) and volume acceleration (V″; *right*) from a representative cast. Each set of colored loops (see *insets*) corresponds to preset breathing frequencies (0.55, 0.75, and 0.95 Hz) and tidal volumes (V_T and $V_T/2$). Lowest oscillatory R (R_0; ●) and lowest oscillatory X (X_0; ○), determined without tidal flow (V′ = 0).

and 57 cycles/min). An estimated V_T (7 mL/kg) was applied at each rate. Measurements were repeated at half of the estimated V_T (Fig. 2).

Small-amplitude (0.5 hPa) oscillations at 16 Hz and the superimposed simulated breathing pattern were generated by the loudspeaker. The combined V′ signal was delivered to the pharyngeal opening of the cast via a custom-made pneumotachograph and a modification of the wave tube oscillometer for infants (length: 10 cm; internal diameter: 8 mm) (9), measuring the input impedance of the naso-pharyngeal cast through a conic adaptor (length: 30 mm; average diameter: 10 mm). Leakage was prevented by a thin rim of silicone putty applied at the ends of the conic adaptor. Difference in the cross-sectional areas between the adaptor and the pharyngeal opening of the cast was negligible. The wave tube and the pneumotachograph were equipped by identical pressure sensors (model 26PCAFA6D; Honeywell, Golden Valley, MN). The pressure and flow signals were low-pass filtered at 50 Hz and sampled at a rate of 512 s^{-1}.

Data analysis. Input impedance of the cast (Z_n) was calculated based on the auto- and cross-power spectra of the wave tube's lateral pressures using the fast Fourier transform. The pressure signals were bandpass-filtered in the 16 ± 2 Hz frequency range of the spectra. The Z_n values were computed for four oscillation cycles (0.0625 s each), and a moving average was calculated over the time span of 0.25 s. Z_n is expressed in terms of resistance (R_n) and reactance (X_n). Volume (V) was integrated from V′ using the trapezoidal approach, whereas V″ was calculated as the derivative of V′ from individual data points by simple, one-sided difference quotients.

To characterize the relation between R_n and V′ (Fig. 4), two separate linear equations were fitted below and above a characteristic breakpoint. For the segment below, the breakpoint (1 mL/s < V′ ≤ V'_{bp}) was

$$\ln R = k_1 \times \ln V' + k_0. \quad (2)$$

For the segment above the breakpoint (V′> V'_{bp}),

$$\ln R = (k_1 + k_2) \times (\ln V' - \ln V'_{bp}) + \ln R_{bp}, \quad (3)$$

where R_{bp} is the breakpoint resistance at V′ = V'_{bp}

Estimation of Reynolds number. The volume (V) of each cast was divided by the characteristic pathway length (*l*), resulting in a rough estimate of average cross-sectional area (*A*; *Eq. 4*). Volumetric flow rate at breakpoint or at peak V′ was divided by *A* to obtain linear velocity (*u*; *Eq. 5*). Reynolds number (Re) was calculated with the equation for smooth cylindrical tubes, taking kinematic viscosity (ν) of air as $1.849 \cdot 10^{-5} \cdot m^2 \cdot s^{-1}$ (at 25°C) (*Eq. 6*):

$$A = \frac{V}{l} \quad (4)$$

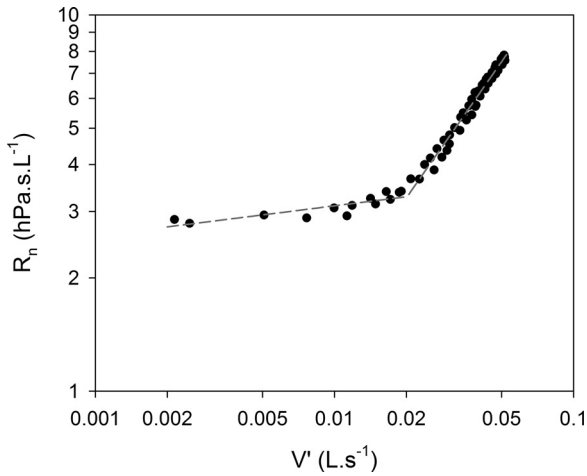

Fig. 4. Log-log plot of resistance (R_n) vs. absolute value of flow (V′) during expiration from a representative measurement [setting: 0.55 Hz, halved tidal volume ($V_T/2$)]. A segmented linear model with a breakpoint is fitted to the data, indicating power-law relationship with 2 exponents: a lower exponent for the 1st segment and a higher exponent for the 2nd segment (below and above breakpoint, respectively).

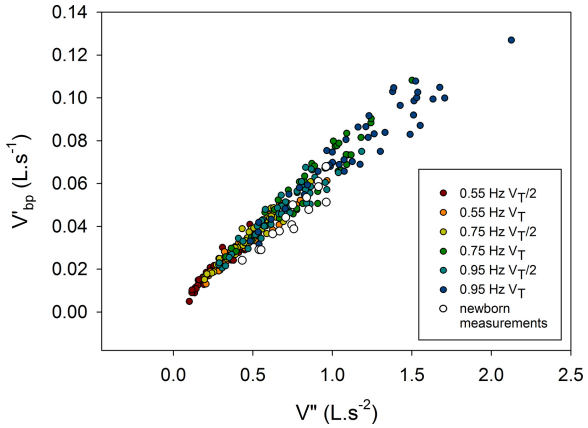

Fig. 5. Relationship between volume acceleration (V″) and flow at breakpoint (V'_{bp}) estimated at different simulated breathing settings. Each colored circle represents a single measurement from all ($n = 45$) casts. In vivo measurement from each newborn ($n = 15$; ○) recorded during the first 3 days of life.

$$u = \frac{V'}{A} \quad (5)$$

$$\mathrm{Re} = \frac{u \times l}{\nu}. \quad (6)$$

In vivo measurements. Oscillometric measurements of the respiratory system impedance (Z_{rs}) were performed in healthy term newborns with a custom-made wave tube setup in a setting similar to that described previously (7, 9). The study protocol was approved by the Institutional Clinical Ethics Committee of the University of Szeged (91/2011). Written, informed consent and assent were obtained from all parents before data collection. A 16-Hz sine wave was applied as the oscillatory signal, and Z_{rs} was estimated with the same signal-processing technique as that used in the casts (see above) and expressed as total respiratory resistance (R_{rs}) and reactance (X_{rs}). The measurements were performed before the 4th postpartum day during quiet natural sleep. Exclusion criteria were *1*) poor cooperation, *2*) lack of steady-state breathing, *3*) nasal obstruction before or during measurement, *4*) leakage around the face mask during measurement, and *5*) laryngeal breaking or inspiratory flow limitation detected during the measurements. A minimum of five steady-state, artifact-free breathing cycles were taken for analysis. A piecewise linear regression equation was fitted to the relationship between respiratory resistance (R_{rs}) and V′ in the same manner as for the nasal airway casts.

Statistical analysis. Data are expressed as median (interquartile range) unless stated otherwise. Relationships between R_n and V′ and V″ were examined by linear regression and piecewise linear regression for expiratory and inspiratory data (10). The relationship between structural and impedance data was assessed by Pearson's correlation coefficient. Statistical analysis was performed using the open-source R 3.5.1 software (R Foundation for Statistical Computing, Vienna, Austria, 2019), using the standard built-in and "segmented" (1.0-0) packages. A P value of <0.05 was considered as significant.

RESULTS

A total of 46 casts were measured. The study population characteristics are summarized in Table 1. One cast was excluded because of apparent bilateral nasal obstruction, confirmed by reassessment of the CT images, which resulted in extremely high R_n values.

Intrabreath changes in R_n and X_n as functions of V′ and V″ are illustrated in Fig. 3. R_{eE} shifted to higher values from R_0 even at the smallest V″. The fluctuations of X_n were small and largely unaffected by changes in V′ and V″ (see also Supplemental Fig. S6). For all casts, a median value of shift in R_{eE} of 47% (range 41–52%) was observed at the lowest respiratory rate and V_T. A very strong linear relationship was observed between R_{eE} and V''_{eE} in each set of cast measurements; $r^2 = 0.994$ (Q1–Q3: 0.988–0.996, $P < 0.001$) with considerable inter-individual variability in the coefficients of regression (Supplemental Fig. S2). The intercept of the linear regression was found to be a close estimate of R_0, characterized by a median of relative bias of −4.5% (−12 to 6%).

A characteristic nonlinear relationship was found between R_n and V′, exhibiting segmental linearity and a prominent breakpoint after logarithmic transformation (Fig. 4). The adjusted r^2 values for the fitted piecewise linear model were 0.984 (0.974–0.989) and 0.984 (0.974–0.988) for the expiratory and inspiratory phase, respectively, with all frequencies and volumes included. V'_{bp} during the expiratory phase had a median value of 0.041 L/s (0.028–0.058) for the entire data set. The slope of the first segment (k_1) was 0.0426 (0.0262–0.0649), whereas slope of the second segment ($k_1 + k_2$) was steeper, with a median of 0.9572 (0.857–1.101). Similar piece-

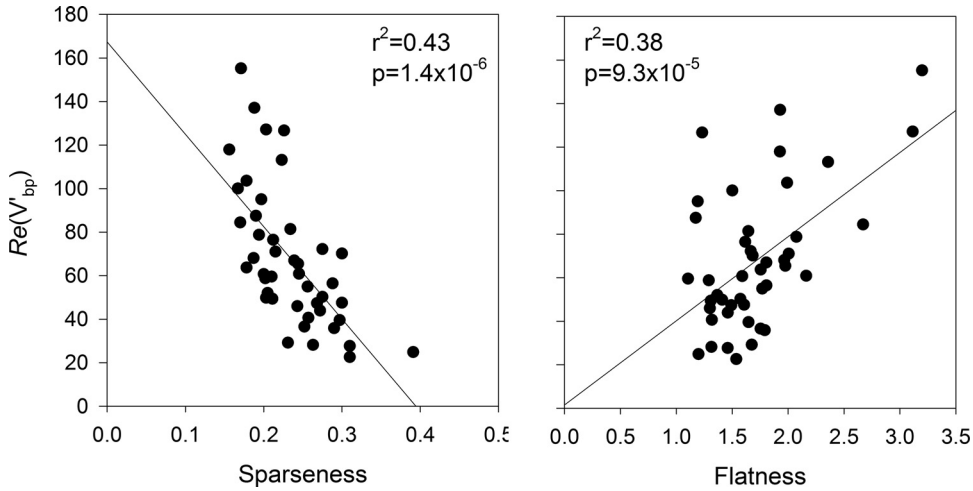

Fig. 6. Correlation between the Reynolds number at breakpoint flow Re(V'_{bp}) vs. sparseness (*left*) and flatness (*right*) of the casts. High Re can be found for casts characterized by low sparseness and high flatness, indicating that flow transition is delayed in narrow and flat upper airways (dominance of viscous forces). Each point corresponds to an individual cast (setting: 0.95 Hz, normal tidal volume).

wise linear R_{rs} versus V' relationships were observed in the in vivo measurements (Supplemental Fig. S3).

V'_{bp} was found to be linearly related to V'' ($r^2 = 0.96$, $P < 0.001$), with increasing residual errors at higher values (Fig. 5). The in vivo data exhibited a similar V'_{bp} versus V'' relationship at slightly lower values of V'_{bp}.

The estimated Re at maximal flow was 118.4 (91.3–154.9), whereas Re at V'_{bp} at maximum respiratory rate (0.95 Hz) and V_T was 60.8 (47.3–81.4). Figure 6 shows the relationships between the shape indices of the nasal airways and Re. The Re at V'_{bp} [$Re(V'_{bp})$] was found to be inversely proportional to the sparseness of the airway ($r^2 = 0.43$, $P < 0.001$) and directly proportional to its flatness ($r^2 = 0.31$, $P < 0.001$). Other structural descriptors (tortuosity, elongation, or sphericity) had no connection with $Re(V'_{bp})$ ($P > 0.10$). X_0 showed moderate correlation with sparseness and was found to be inversely proportional to flatness ($r^2 = 0.24$ and $r^2 = 0.14$, respectively, $P < 0.05$). R_0 correlated weakly with sparseness ($r^2 = 0.09$, $P < 0.05$) and had no correlation with flatness ($r^2 = 0.05$, $P > 0.10$).

To estimate R_0 based on the intrabreath R-V' loops (Fig. 7, *top*) the slope of the fitted line was determined between R_{eI} and R_n at maximum expiratory flow ($R_{V'maxE}$). The slope of this linear fit remained constant across the different respiratory rates and V_Ts. When this linearly approximated V'-dependent increase in R_n was compared with the V''-dependent shift in R_{eE} (Fig. 7, *bottom*), a strong linear relationship was found. By utilizing this relationship, R_0 can be estimated from a single intrabreath impedance measurement:

$$R_0 = R_{eI} - V''_{eI} \times c \times \frac{R_{V'maxE} - R_{eI}}{V'_{maxE}}, \qquad (7)$$

where c is a correction factor with a value of 0.0646 s^{-1} that is the slope determined from the expiratory limb in Fig. 7, *bottom*. A strong relationship with a similar slope (0.0709 s^{-1}, $P < 0.001$) was also observed for the inspiratory limb (data not shown). This estimation of R_0 is hence independent of respiratory rate and tidal volume.

The relative error of measured and corrected R_{eE} with respect to the R_0 at each setting of the respirator is shown in Fig. 8. Measured R_{eE} was significantly ($P < 0.001$) higher than corrected R_{eE} at each setting with increasing differences at higher frequency and V_T. After the mathematical correction in R_{eE} was applied to the in vivo measurements, the end-inspiratory R (R_{eI}) decreased by 33% (9.5–70%, $P < 0.001$), whereas R_{eE} dropped 19% (1.6–33%, $P < 0.001$) (Supplemental Fig. S3).

X_0 had positive values in all casts, indicating the presence of inertance in the rigid upper airway casts. The overall shape of X_n-V' loops mirrored the pattern of R_n-V' loops (Supplemental Fig. S6); however, the changes in X_n were smaller and not as regular as seen for R_n. X_n decreased significantly ($P < 0.001$) when simulated breathing was applied (Supplemental Fig. S7). End-expiratory X_n (X_{eE}) was found to be somewhat lower than X_0, indicating that V'' has some effect on X_n; however, this effect cannot be described by a simple linear relationship, as was demonstrated for R_{eE}. X_n was found to be V' dependent; the lowest values of X_n were measured at peak inspiratory and expiratory flows ($X_{V'maxI}$ and $X_{V'maxE}$). However, the decrease was independent from the actual values of V'max.

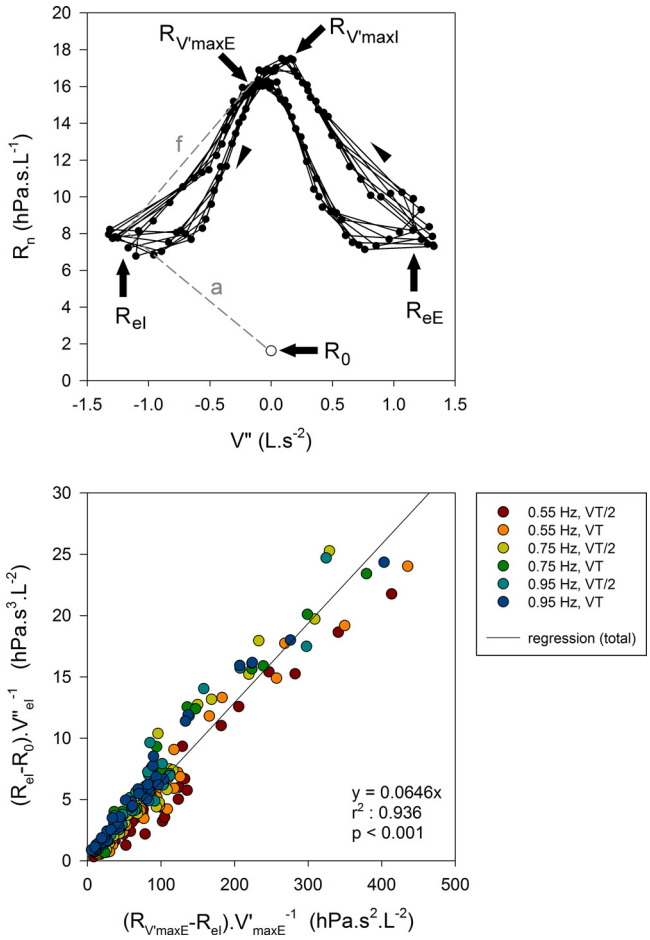

Fig. 7. *Top*: resistance (R_n) vs. volume acceleration (V'') plot from a representative cast. Lowest oscillatory R (R_0; ○) and R_n measured with superimposed breathing at 0.95 Hz with full tidal volume (V_T) (black line and ●). Each data point is marked with a closed symbol. Dashed line marked with the letter "f" shows the slope of V'-dependent increase in R; dashed line marked with the letter "a" represents the shift in the minimal resistance (R_0) due to V''. Arrowheads indicate inspiratory limb of the loops. Highest resistances occur at peak inspiratory flow ($R_{V'maxI}$) and at peak expiratory flow ($R_{V'maxE}$). *Bottom*: V''- dependent shift in ReI [$(R_{eI} - R_0)\cdot V''_{eI}{}^{-1}$], i.e., slope "a" at *top*, plotted against V'-dependent increase in R_n [$(R_{V'maxE} - R_{eI})\cdot V'_{maxE}{}^{-1}$], slope "f", reflecting a strong linear relationship. Each symbol represents a cast measured at different respiratory rates at full or halved tidal volume (V_T and $V_T/2$).

The "mirroring" pattern of X_{rs}-V' loops was visible for most of the in vivo measurements in healthy newborns (Supplemental Fig. S8) despite the fact that the mean X_{rs} values are usually negative at 16 Hz. Sometimes we observed increasing (less negative) X_{rs} values at peak V'-s, a phenomenon never found in vitro.

DISCUSSION

The primary aim of this study was to examine the confounding effect of the nasal pathway during oscillometric assessment of lung mechanics. The contribution of R_n to R_{rs} (especially during tidal breathing) is a main problem in infant pulmonary function testing, but examining this effect is difficult with noninvasive techniques. Therefore, we used anatomically faithful, albeit rigid, upper airway casts to measure R_n and simulate the effects of spontaneous breathing on this parameter in vitro.

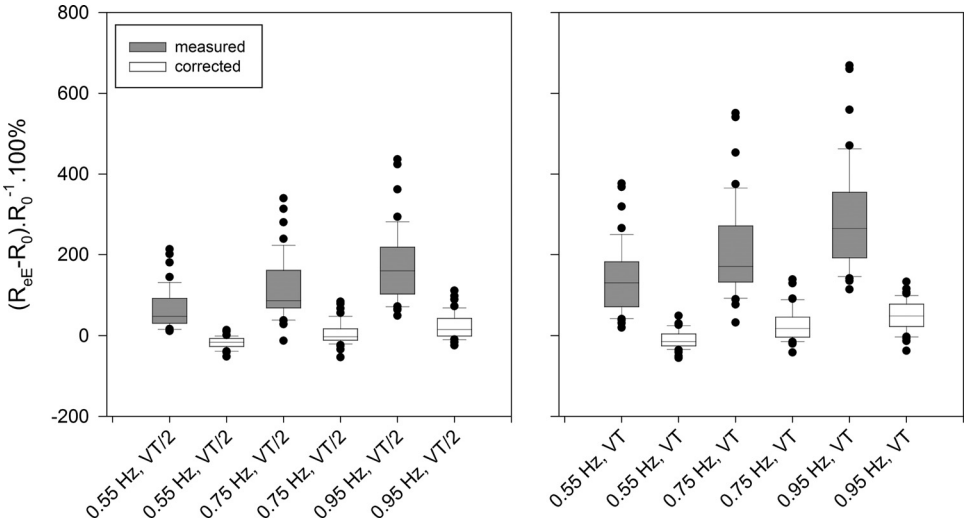

Fig. 8. Relative error of measured (gray box) and corrected (open box) lowest resistances (R_{eE}) with respect to the oscillatory resistance without superimposed breathing (R_0) at each setting of the respirator. Respiratory rate varied from 0.55 Hz to 0.95 Hz at full (V_T; *right* panel) and halved ($V_T/2$; *left*) tidal volume. Measured R_{eE} was significantly ($P < 0.001$) higher than calculated R at each setting.

Validity of R_0. We hypothesize that R_0 can be the most appropriate outcome measure for comparing patients, since it is the lowest R, unbiased by the dynamic effects of tidal breathing. Note that R_0 was assessed, instead of the unidirectional Poiseuille flow, with 16-Hz sinusoidal oscillations. This causes an overestimation of Poiseuille R (R_P) via the frequency dependence of resistance (4–6). We could demonstrate a moderate correlation ($r^2 = 0.41$) between the Womersley number and the ratio of measured R_0 to calculated R_P, a phenomenon already described in straight tubes by Dorkin et al. (4). In fact, the R_0 values were typically 10–30 times higher than R_P (see Supplemental Fig. S5).

Although R_0 is the lowest oscillatory R, it can be measured only during apnea, which may limit its widespread use. R_0 values in our nasal airway casts were systematically lower than a previously published study in infants (8, 22). In these studies, infants were measured during apnea with low-frequency oscillometry, and nasal resistance was estimated by applying a nasal cannula with a manometer. The oscillatory frequency was higher in the present study (16-Hz sine wave vs. 0.5- to 20-Hz pseudorandom signal), allowing us to use lower amplitude (18–20 mL/s vs. 60–80 mL/s peak to peak) while achieving the same signal-to-noise ratio. This amplitude represents ~70% of the flow measured during tidal breathing in infants; thus it is high enough to cause nonlinearities in the nasal airways. We tested this effect in a subgroup ($n = 12$) of our casts. Increasing the oscillatory flow to 28–32 mL/s (peak to peak) resulted in an increase in R_0 of 11% (8.7–16.5%). Additionally, some extra dissipation can be produced by the collapsibility of the upper airways in vivo, leading to even higher R values (16).

Validity of R_{eE}. If the nasal pathway acted as a pure linear resistor, the R_{eE} would be independent from respiratory rate and V″ and would thus be equal to R_0. However, we found that R_{eE} increased linearly with V''_{eE} and was considerably higher than R_0 even at the lowest respiratory rate. Direct measurement of R_{eE}, as well as R_{eI}, is biased by the extra dissipation due to unstable V′ arising in the nasal pathway at phase transitions. This phenomenon was described previously in tracheal models by Isabey and colleagues (14, 15). We conclude that R_{eE} alone may not be an appropriate estimate of R_0. However, serial measurements of R_{eE} at different V″ values enable a fair approximation as the ordinate intercept of the linear function.

Utility of R_n-V′-segmented power law model. We found that the relation of R_n with V′ can be described by a segmented power law equation. The first segment had an almost negligible increase until a breakpoint followed by a more abrupt elevation above the breakpoint. This nonlinear behavior of the P-V′ relationship in the nasal airways may be related to a developing nonlaminar flow regime (15, 20, 21, 24) and to singular pressure losses at abrupt narrowings, or the so-called orifice effect (13). Both processes may contribute to the sharper V′-dependent rise observed in R_n beyond V'_{bp}. Our data also showed that V'_{bp} has a strong linear dependence on V″. Increasing V″ may affect flow rheology by the relaminarization of turbulent flow (11).

The effect of sharp narrowings in the nasal passages is reflected in the relation between certain shape descriptors and $Re(V'_{bp})$. Upper airway casts with higher sparseness had a relatively spacious cavity with fewer wall irregularities and lower surface/volume ratio. Flatness, on the other hand, is an indicator of relative narrowness of the nasal passage, mimicking a slit between two infinite parallel plates. Sparse but not flat nasal cavities, acting as wide cylinders, had low $Re(V'_{bp})$ values, suggesting that sparse geometry is advantageous for the development of turbulent flow.

Despite the fact that V'_{bp} correlated well with structural variables, the utility of V'_{bp} and other parameters of the segmented power law model remains limited in the estimation of R_0 because of the strong V″-dependence. This was verified in a small and selected group of healthy-term newborns, although there was a strong V'_{bp}-V″ relationship (Fig. 5), and the model fitted well for these in vivo measurements (Supplemental Fig. S3).

Geometrical estimation of R_0 from a single R_n-V′ loop. We propose a method for correcting the shift in R_{eE}, thus estimating R_0, by the normalized flow-dependent increase in R: $(R_{V'maxE}-R_{eI})/V'_{maxE}$. This method can be applied to a single set of intrabreath oscillometric measurements without the necessity of changing respiratory rate or tidal volume, as performed in our simulations. Infant measurements showed that the effect of upper airway nonlinearities is significant and

represents up to 33% in R_{eI} and 19% in R_{eE} (Supplemental Fig. S4).

Extrapolation of R_{rs} data by using the equation derived from the cast measurements (*Eq. 6*) resulted in a larger decrease in R_{eI} than in R_{eE}, thereby increasing the tidal difference in R_{rs} (ΔR). Because ΔR has been shown to be a sensitive measure of subtle alterations in peripheral homogeneity (1, 7), application of a correction accounting for the V″-dependent effects would further increase the utility of ΔR.

Dynamic changes in X_n and X_{rs}. We measured positive mean values of X_n, indicating the presence of inertance, an expected property of the upper airways. The V′-dependent decrease in X_n can be explained by the decrease in apparent inertance caused by the vortex formation at orifices (12, 17).

The patterns of X_{rs} change during the respiratory cycle were similar in the in vivo measurements, albeit more variable than that of X_n, and the mean X_{rs} values were negative due to the presence of elastic forces of the total respiratory system at 16 Hz. The compliant upper airway structures may have added to this variability (whereas the orifice effects were still present); an extreme example of inspiratory flow limitation (the Bernoulli effect) is demonstrated in Supplemental Fig. S8 (*infant no. 11*).

Study limitations. This study had some limitations. Because the CT sampling time was quite short (~75–300 ms), we can assume that the whole nasal pathway was reconstructed in the same phase of the respiratory cycle. Nevertheless, because CT acquisition was not gated with respect to the respiratory phase, the within-breath variation in the diameter of the soft tissue that may exist in vivo is not reflected in the 3D cast. Although the fact that the vocal chord area and part of the oropharynx, more compliant structures of the upper airways, were not included in the reconstructed upper airways must have substantially reduced the intrabreath changes, this in turn imposed another limitation in the applicability of cast measurements in the interpretation of the in vivo infant data. A further limitation was the rigid material of the cast as well as the surface texture that can be different from that of the upper airway mucosa. Nonlinearity originating from the compliance of some segments of the nasal pathway cannot be modeled by this approach. Despite the rigidity of the casts, distortions in the R_n-V′ relationship could be adequately studied since the orifice effect can be considered the most important contributor to the flow dependence of R_n during tidal breathing.

A time windowing of 0.25 s was used during intrabreath oscillatory measurements. This means that an average of four oscillatory cycles was used for impedance estimation. Decreasing windowing time to a minimum of two cycles excessively decreased signal-to-noise ratio, which was especially critical in the in vivo setting. The effect of increasing the windowing time was investigated in a subgroup of our casts ($n = 12$; data not shown). Increasing windowing time to 0.5 s led to higher values of R_{eE}, but without much change in $R_{V'maxI}$ and $R_{V'maxE}$. Although the increase in R_{eE} was systematic, the intercept of the linear R_{eE} versus V''_{eE} relationship did not change, so the estimation of R_0 seems to be insensitive to windowing time.

Conclusions. We studied the R-V′ relationship in anatomically faithful rigid nasal airway casts during simulated respiration. We found a characteristic nonlinear relationship between R and V′, exhibiting segmental power law behavior with a prominent breakpoint. This model was reproducible in a small group of infants in vivo. We found a linear shift in R_{eE} that was attributable to increasing values of V″. We developed a geometrical approach to quantify intrabreath nonlinearities in R_n, allowing us to estimate R_0 from a single oscillometric measurement. Using the correction may reduce the masking effect of the nonlinear upper airways on the changes in the intrathoracic R in future studies.

ACKNOWLEDGMENTS

We thank Raffaella Balzarini and Stanislas Borkowski for help with 3D printing of upper airway casts.

GRANTS

This work was supported by Hungarian Scientific Research Fund Grants K105403 and K128701 and by the Amiqual4Home Equipex via the ANR-11-EQPX-0002 grant.

DISCLOSURES

No conflicts of interest, financial or otherwise, are declared by the authors.

AUTHOR CONTRIBUTIONS

B.L.R., G.M., T.C., N.A., C.P., S.K.B., Z. Gingl, Z. Gyurkovits, T.M.T., Z.H., and S.B. conceived and designed research; B.L.R., G.M., T.C., N.A., C.P., L.D., S.K.B., Z. Gingl, Z. Gyurkovits, T.M.T., Z.H., and S.B. performed experiments; B.L.R., G.M., T.C., N.A., C.P., L.D., S.K.B., Z. Gingl, Z. Gyurkovits, T.M.T., Z.H., and S.B. analyzed data; B.L.R., G.M., T.C., N.A., T.M.T., Z.H., and S.B. interpreted results of experiments; B.L.R., G.M., T.C., T.M.T., and Z.H. prepared figures; B.L.R., G.M., T.C., T.M.T., Z.H., and S.B. drafted manuscript; B.L.R., G.M., T.C., N.A., L.D., S.K.B., Z. Gingl, Z. Gyurkovits, T.M.T., Z.H., and S.B. edited and revised manuscript; B.L.R., G.M., T.C., N.A., C.P., L.D., S.K.B., Z. Gingl, Z. Gyurkovits, T.M.T., Z.H., and S.B. approved final version of manuscript.

REFERENCES

1. **Czövek D, Shackleton C, Hantos Z, Taylor K, Kumar A, Chacko A, Ware RS, Makan G, Radics B, Gingl Z, Sly PD.** Tidal changes in respiratory resistance are sensitive indicators of airway obstruction in children. *Thorax* 71: 907–915, 2016. doi:10.1136/thoraxjnl-2015-208182.
2. **Davidson RN, Greig CA, Hussain A, Saunders KB.** Within-breath changes of airway calibre in patients with airflow obstruction by continuous measurement of respiratory impedance. *Br J Dis Chest* 80: 335–352, 1986. doi:10.1016/0007-0971(86)90087-2.
3. **Doorly DJ, Taylor DJ, Schroter RC.** Mechanics of airflow in the human nasal airways. *Respir Physiol Neurobiol* 163: 100–110, 2008. doi:10.1016/j.resp.2008.07.027.
4. **Dorkin HL, Jackson AC, Strieder DJ, Dawson SV.** Interaction of oscillatory and unidirectional flows in straight tubes and an airway cast. *J Appl Physiol* 52: 1097–1105, 1982. doi:10.1152/jappl.1982.52.4.1097.
5. **Finucane KE, Dawson SV, Phelan PD, Mead J.** Resistance of intrathoracic airways of healthy subjects during periodic flow. *J Appl Physiol* 38: 517–530, 1975. doi:10.1152/jappl.1975.38.3.517.
6. **Franken H, Clément J, Cauberghs M, Van de Woestijne KP.** Oscillating flow of a viscous compressible fluid through a rigid tube: a theoretical model. *IEEE Trans Biomed Eng* 28: 416–420, 1981. doi:10.1109/TBME.1981.324725.
7. **Gray DM, Czovek D, McMillan L, Turkovic L, Stadler JAM, Vanker A, Radics BL, Gingl Z, Hall GL, Sly PD, Zar HJ, Hantos Z.** Intrabreath measures of respiratory mechanics in healthy African infants detect risk of respiratory illness in early life. *Eur Respir J* 53: 1800998, 2019. doi:10.1183/13993003.00998-2018.
8. **Hall GL, Hantos Z, Wildhaber JH, Sly PD.** Contribution of nasal pathways to low frequency respiratory impedance in infants. *Thorax* 57: 396–399, 2002. doi:10.1136/thorax.57.5.396.
9. **Hantos Z, Czövek D, Gyurkovits Z, Szabó H, Maár BA, Radics B, Virág K, Makan G, Orvos H, Gingl Z, Sly PD.** Assessment of respiratory mechanics with forced oscillations in healthy newborns. *Pediatr Pulmonol* 50: 344–352, 2015. doi:10.1002/ppul.23103.
10. **Hey EN, Price JF.** Nasal conductance and effective airway diameter. *J Physiol* 330: 429–437, 1982. doi:10.1113/jphysiol.1982.sp014349.

11. **Iida O, Nagano Y.** The relaminarization mechanisms of turbulent channel flow at low Reynolds numbers. *Flow Turbul Combus* 60: 193–213, 1998. doi:10.1023/A:1009999606355.
12. **Ingard U, Ising H.** Acoustic nonlinearity of an orifice. *J Acoust Soc Am* 42: 6–17, 1967. doi:10.1121/1.1910576.
13. **Ingram RH Jr, Pedley TJ.** Pressure-flow relationships in the lungs. *Compr Physiol*: 277–293, 2011. doi:10.1002/cphy.cp030318
14. **Isabey D, Chang HK.** Steady and unsteady pressure-flow relationships in central airways. *J Appl Physiol* 51: 1338–1348, 1981. doi:10.1152/jappl.1981.51.5.1338.
15. **Isabey D, Chang HK, Delpuech C, Harf A, Hatzfeld C.** Dependence of central airway resistance on frequency and tidal volume: a model study. *J Appl Physiol (1985)* 61: 113–126, 1986. doi:10.1152/jappl.1986.61.1.113.
16. **Jaeger MJ, Matthys H.** The pattern of flow in the upper human airways. *Respir Physiol* 6: 113–127, 1968. doi:10.1016/0034-5687(68)90021-2.
17. **Jing X, Sun X.** Sound-excited flow and acoustic nonlinearity at an orifice. *Phys Fluids* 14: 268–276, 2002. doi:10.1063/1.1423934.
18. **Kiwanuka FN, Wilkinson MHF.** Cluster based vector attribute filtering. In: *Mathematical Morphology and Its Applications to Signal and Image Processing*, edited by Benediktsson JA, Chanussot J, Najman L, and Talbot H. Cham, Switzerland: Springer International Publishing, 2015, p. 277–288.
19. **Lorx A, Czövek D, Gingl Z, Makan G, Radics B, Bartusek D, Szigeti S, Gál J, Losonczy G, Sly PD, Hantos Z.** Airway dynamics in COPD patients by within-breath impedance tracking: effects of continuous positive airway pressure. *Eur Respir J* 49: 1601270, 2017. doi:10.1183/13993003.01270-2016.
20. **Pedley TJ, Schroter RC, Sudlow MF.** Energy losses and pressure drop in models of human airways. *Respir Physiol* 9: 371–386, 1970. doi:10.1016/0034-5687(70)90093-9.
21. **Peslin R, Ying Y, Gallina C, Duvivier C.** Within-breath variations of forced oscillation resistance in healthy subjects. *Eur Respir J* 5: 86–92, 1992.
22. **Peták F, Hayden MJ, Hantos Z, Sly PD.** Volume dependence of respiratory impedance in infants. *Am J Respir Crit Care Med* 156: 1172–1177, 1997. doi:10.1164/ajrccm.156.4.9701049.
23. **Polgar G, Kong GP.** The nasal resistance of newborn infants. *J Pediatr* 67: 557–567, 1965. doi:10.1016/S0022-3476(65)80425-5.
24. **Schroter RC, Sudlow MF.** Velocity profiles in models of human airways. *J Physiol* 202: 36P–37P, 1969.
25. **Stocks J, Godfrey S.** Nasal resistance during infancy. *Respir Physiol* 34: 233–246, 1978. doi:10.1016/0034-5687(78)90031-2.
26. **Yushkevich PA, Piven J, Hazlett HC, Smith RG, Ho S, Gee JC, Gerig G.** User-guided 3D active contour segmentation of anatomical structures: significantly improved efficiency and reliability. *Neuroimage* 31: 1116–1128, 2006. doi:10.1016/j.neuroimage.2006.01.015.

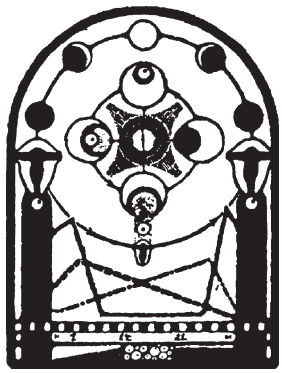

II.

frontiers | Frontiers in Pediatrics

ORIGINAL RESEARCH
published: 04 April 2022
doi: 10.3389/fped.2022.867883

Respiratory Oscillometry in Newborn Infants: Conventional and Intra-Breath Approaches

*Bence L. Radics[1], Zita Gyurkovits[2], Gergely Makan[3], Zoltán Gingl[3], Dorottya Czövek[4] and Zoltán Hantos[5]**

[1] Department of Pathology, University of Szeged, Szeged, Hungary, [2] Department of Obstetrics and Gynecology, University of Szeged, Szeged, Hungary, [3] Department of Technical Informatics, University of Szeged, Szeged, Hungary, [4] 1st Department of Pediatrics, Semmelweis University, Budapest, Hungary, [5] Department of Anesthesiology and Intensive Therapy, Semmelweis University, Budapest, Hungary

Background: Oscillometry has been employed widely as a non-invasive and standardized measurement of respiratory function in children and adults; however, limited information is available on infants.

Aims: To establish the within-session variability of respiratory impedance (Zrs), to characterize the degree and profile of intra-breath changes in Zrs and to assess their impact on conventional oscillometry in newborns.

Methods: 109 healthy newborns were enrolled in the study conducted in the first 5 postpartum days during natural sleep. A custom-made wave-tube oscillometry setup was used, with an 8–48 Hz pseudorandom and a 16 Hz sinusoidal signal used for spectral and intra-breath oscillometry, respectively. A resistance-compliance-inertance (R-C-L) model was fitted to average Zrs spectra obtained from successive 30-s recordings. Intra-breath measures, such as resistance (Rrs) and reactance (Xrs) at the end-expiratory, end-inspiratory and maximum-flow points were estimated from three 90-s recordings. All natural and artifact-free breaths were included in the analysis.

Results: Within-session changes in the mean R, C and L values, respectively, were large (mean coefficients of variation: 10.3, 20.3, and 26.6%); the fluctuations of the intra-breath measures were of similar degree (20–24%). Intra-breath analysis also revealed large swings in Rrs and Xrs within the breathing cycle: the peak-to-peak changes amounted to 93% (range: 32–218%) and 41% (9–212%), respectively, of the zero-flow Zrs magnitude.

Discussion: Intra-breath tracking of Zrs provides new insight into the determinants of the dynamics of respiratory system, and highlights the biasing effects of mechanical non-linearities on the average Zrs data obtained from the conventional spectral oscillometry.

Keywords: infant oscillometry, respiratory resistance, respiratory reactance, respiratory compliance, nasal resistance, intra-breath method

OPEN ACCESS

Edited by:
Anne B. Chang,
Charles Darwin University, Australia

Reviewed by:
Margaret Sarolta McElrea,
Children's Health Queensland, Australia
Tamara Blake,
University of Queensland, Australia

****Correspondence:***
Zoltán Hantos
hantos.zoltan@med.u-szeged.hu

Specialty section:
This article was submitted to Pediatric Pulmonology, a section of the journal Frontiers in Pediatrics

Received: *01 February 2022*
Accepted: *02 March 2022*
Published: *04 April 2022*

Citation:
Radics BL, Gyurkovits Z, Makan G, Gingl Z, Czövek D and Hantos Z (2022) Respiratory Oscillometry in Newborn Infants: Conventional and Intra-Breath Approaches. Front. Pediatr. 10:867883. doi: 10.3389/fped.2022.867883

Motto:
"Accurate assessment of lung function in infants is no mean undertaking – requiring not only the highest specifications from equipment . . . but infinite patience and meticulous attention to detail from the operators."

Janet Stocks, 2004
Pediatric Anesthesia 14: 537–540

INTRODUCTION

The burdens of infant pulmonary function testing (PFT) imposed by the lack of active cooperation, the requirement for sleep, the obligatory nasal breathing, the high impedance of the respiratory system and several other factors have prevented the establishment of a gold standard in infant PFT. Respiratory oscillometry measures the mechanical impedance of the respiratory system (Zrs), and it has been shown as a promising method in different measurement settings (1). Recent work has demonstrated its feasibility in normally breathing unsedated infants with a high success rate (2–5). Additionally, a new tracking modality of oscillometry (6) has revealed disease-specific patterns of intra-breath changes in Zrs and has proven unique in predicting lower respiratory tract illness during infancy (7). However, a comprehensive analysis is still needed to fully characterize the intra-breath dynamics of Zrs in infants, with special regard to the substantial contribution of the upper airways (8–12). Confrontation of the novel intra-breath oscillometry with conventional spectral oscillometry is also lacking. While some data on the day-to-day Zrs changes in newborn infants are available (5, 13), the within-session reproducibility of oscillometry measures has not been studied.

The aims of the present study were (a) to measure Zrs in healthy term newborns to characterize the physiological flow (V')- and volume (V)-dependent changes *via* intra-breath oscillometry, (b) to examine the potentially confounding effects of intra-breath changes on average Zrs spectra obtained from conventional multi-frequency measurements and (c) to determine the within-session variability of conventional and intra-breath oscillometry variables.

MATERIALS AND METHODS

The study protocol was approved by the Institutional Clinical Ethics Committee of the University of Szeged (91/2011, renewed in 2017). A written informed consent and assent was obtained from all mothers prior to the subject recruitment. The data collection period started in January 2017 and ended in May 2017. All measurements were performed in the Neonatal Unit, Department of Obstetrics and Gynecology, University of Szeged.

Healthy term infants (> 37th week of gestation, birthweight > 2,500 g, APGAR score at 5 min ≥ 8, uninterrupted early adaptation) were included in the study. Lung function was measured between the 2nd–5th postpartum day on a single occasion, during natural sleep. Newborns were excluded from the study if steady-state breathing was not reached or leakage persisted around the face mask despite multiple trials.

Measurement Setup

Oscillometric measurement of input Zrs was made with a custom-made wave-tube setup (length: 20 cm, internal diameter: 8 mm), in a setting similar to that described previously (5, 7). Small-amplitude (0.5 hPa) oscillations were generated by the loudspeaker and superimposed on the breathing. Spectral oscillometric recordings were 30 s long, and five different pseudorandom signal specimens containing components at every 4 Hz between 8 and 48 Hz were applied. Intra-breath oscillometric recordings lasted for 90 s, and a single 16 Hz sinusoid was used. Multiple measurements were performed with both modalities in random order, without removing the face mask between recordings if the sleep stage was uninterrupted.

Airflow (V') was measured with a custom-made pneumotachograph. The wave-tube and the pneumotachograph were equipped with identical pressure sensors (Honeywell model 26PCAFA6D, Golden Valley, MN, United States). Single-use bacterial filter (Gibeck, Humid-Vent filter, small straight type, No. 19502 Teleflex Medical, Athlone, Ireland) and face mask (Hudson RCI, air-cushion mask with inflation valve, neonate size, No. 41277, Teleflex Medical) were attached to the setup. The equipment's dead space was flushed by medical air at a rate of 2 $L.min^{-1}$ to avoid hypercapnia.

Transcutaneous monitoring of peripheral hemoglobin oxygen-saturation was done (Edan M50, Bell Medical, Inc., St. Louis, MO, United States) during the recordings for safety reasons. No desaturation episode was detected during data collection. Oxygen saturation data were not stored for further analysis.

Signal Processing

Pressure and V' signals were sampled at a rate of 512 s^{-1}, bandpass filtered in the 4–50 Hz range for spectral oscillometry and the 14–18 Hz range for the intra-breath measurements. Zrs was calculated based on the auto- and cross-correlation spectra of the wave-tube's lateral pressures using the fast Fourier transform, and expressed as resistance (Rrs) and reactance (Xrs). The intra-breath Zrs values were computed for each oscillation cycle (0.0625 s) and a moving average was calculated over a time window of 0.25 s. The signals of volume (V) and volume acceleration (V"), respectively, were obtained by numerical integration and differentiation of V'.

Analysis of Zrs Spectra

An average spectrum was calculated from a minimum of 3 recordings of lowest Rrs. Recordings or segments thereof containing artifacts, such as glottis closure, vocalization, body movements and leaks around the mask were discarded. No criteria relating to tidal volume (V_T) were set and sighs *per se* were not considered as artifacts. A simple resistance (R)—compliance (C)—inertance (L) model (14) was fit to the average Zrs data, as described in detail previously (5). Conventional spectral oscillometry measures, such as the lowest-frequency (8-Hz) values of Zrs magnitude ($|Z_8|$), resonance frequency (f_{res}) and reactance area below f_{res} (Ax) were also calculated; the frequency

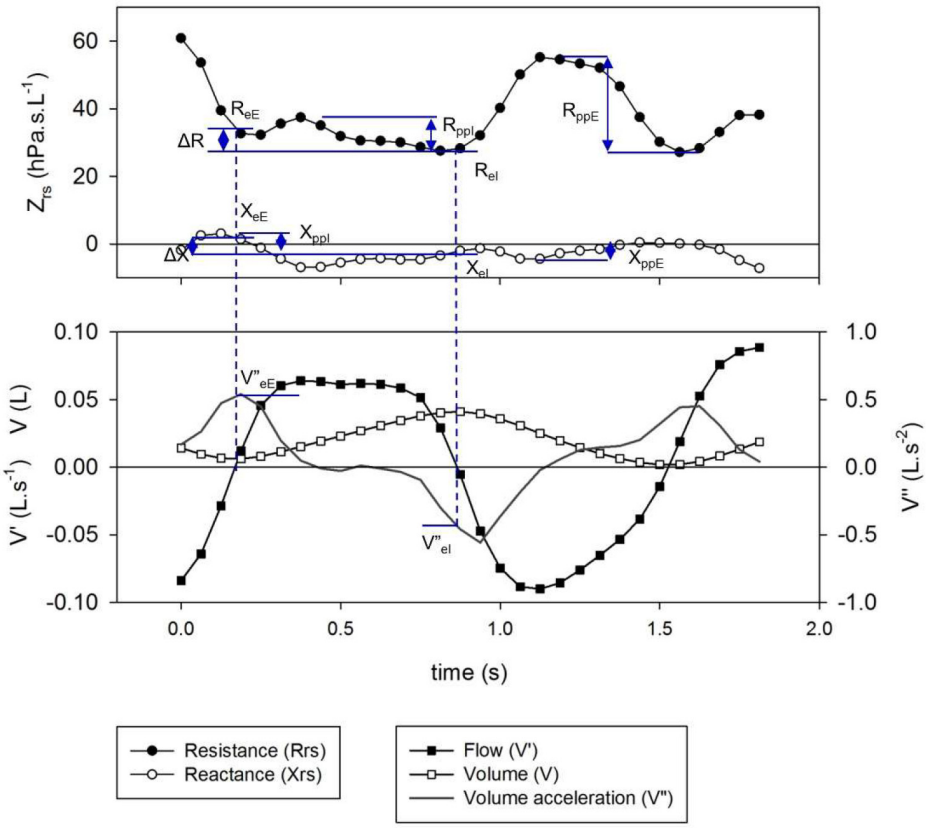

FIGURE 1 | Definition of specific intra-breath measures of resistance (Rrs) and reactance (Xrs). Shown are the time points of end inspiration (eI)- and end expiration (eE) (indicated by dotted lines), their differences (Δ) and peak-to-peak changes in inspiration (ppI) and expiration (ppE).

dependence of Rrs was characterized by the difference in Rrs between 8 Hz and 32 Hz (R_{8-32}).

Intra-Breath Measures

All regular artifact-free breaths (see previous section) except sighs were included in the analysis. Specific points of the respiratory cycle were selected to characterize the intra-breath dynamics of Zrs (**Figure 1**). Values of Rrs at end-expiration and end-inspiration (R_{eE} and R_{eI}, respectively) were calculated from the closest data points to zero V' obtained with linear interpolation. Tidal change in Rrs (ΔR) was determined as R_{eE}-R_{eI}. Peak-to-peak changes in Rrs during inspiration (R_{ppI}) and expiration (R_{ppE}) were determined. The corresponding parameters of Xrs (X_{eE}, X_{eI}, ΔX, X_{ppE} and X_{ppI}) and the average zero-flow impedance magnitude, $|Z_0| = |1/2(Z_{eE} + Z_{eI})|$ were also calculated.

Tidal Breathing Parameters

Simple tidal breath descriptors, such as V_T, respiratory rate (f_{br}), ratio of expiratory time over cycle time (T_E/T_{tot}), and the ratio of time to peak expiratory flow (V'_{maxE}) and T_E (T_{PTEF}/T_E) were obtained from the spirogram. Volume acceleration at end-expiration and end-inspiration ($V"_{eE}$ and $V"_{eI}$, respectively) were determined from pairs of V" data adjacent to the zero crossing.

Statistical Analysis and Graphics

Data are presented as mean ± standard deviation (SD). Two sample *t*-test, correlation analysis with Pearson's correlation coefficients were performed with the open-source RStudio software[1] based on R language (R.4.1). Cluster analysis was also performed in R using Euclidean distances and Ward's hierarchical method. Graphs were prepared with SigmaPlot 13.5 (Systat Software Inc., San José, CA, United States).

RESULTS

A total of 109 newborns were enrolled in the study. Six subjects were excluded due to technical reasons (see pre-defined exclusion criteria in the "Materials and Methods" section). Although the measurements were technically acceptable, 17 of the remaining 103 subjects were excluded on the basis of physiologically unrealistic values of Zrs parameters, such as negative L (n = 4), low C (< 0.5 mL.hPa^{-1}) (n = 6) or high RL product (>10 hPa^2.s^3.L^{-2}) suggestive for nasal obstruction (n = 7); in 4 of these 17 subjects, two exclusion criteria applied. Most of these subjects were also identified as

[1]https://www.rstudio.com

TABLE 1 | Comparison of anthropometry and spirogram data between subject groups of different patterns of flow dependence of reactance.

	All (n = 86)	Pattern A (n = 47)	Pattern B (n = 27)	Pattern C (n = 5)	Pattern D (n = 7)
GA (weeks)	38.7 ± 1.3	38.9 ± 1.2	38.6 ± 1.2	38.0 ± 2.1	38.3 ± 1.4
BL (cm)	49.5 ± 2.4	50.0 ± 2.5	49.3 ± 2.3	48.0 ± 2.7	47.7 ± 1.5**
BW (g)	3,269 ± 546	3,365 ± 569	3,293 ± 490	2,694 ± 491*	2,931 ± 210**
f_{br} (min^{-1})	62.0 ± 11.4	65.3 ± 12.2	58.2 ± 9.5**	57.9 ± 5.0*	57.5 ± 10.1
V_T (mL)	29.3 ± 5.5	29.3 ± 5.9	29.7 ± 4.6	26.2 ± 3.6	30.6 ± 6.5
V'_{maxE} ($mL.s^{-1}$)	90 ± 17	93 ± 17	81 ± 15**	77 ± 15	81 ± 16
T_E/T_{tot}	0.50 ± 0.03	0.50 ± 0.03	0.52 ± 0.03**	0.47 ± 0.03	0.51 ± 0.01
T_{PTEF}/T_E	0.47 ± 0.07	0.47 ± 0.07	0.45 ± 0.09	0.49 ± 0.07	0.49 ± 0.07
CoV[T_{tot}]	0.155 ± 0.058	0.155 ± 0.059	0.168 ± 0.055	0.132 ± 0.032	0.118 ± 0.058
CoV[V_T]	0.219 ± 0.092	0.231 ± 0.07	0.212 ± 0.069	0.162 ± 0.072	0.202 ± 0.097

Mean ± SD values.
Pattern A: minimal dependence of reactance (Xrs) on flow (V').
Pattern B: marked V'-dependent decrease in Xrs during expiration.
Pattern C: marked V'-dependent decrease during inspiration.
Pattern D: marked V'-dependent increases in Xrs.
GA, gestational age; BL, birth length; BW, birth weight; f_{br}, respiratory rate; V_T, tidal volume; V'_{maxE}, peak expiratory flow; T_E, expiratory time; T_{tot}, total respiratory cycle time; T_{PTEF}, time to peak tidal expiratory flow; CoV, coefficient of variation.
**$p < 0.05$ vs. Pattern A.*
***$p < 0.01$ vs. Pattern A.*

outliers during regression diagnostics, and therefore they were omitted from further analysis. Statistical analysis was performed on the data of the remaining 86 newborns (41 females, 45 males; spontaneous delivery: 41, caesarean section: 45) whose anthropometric characteristics are summarized in **Table 1**.

The mean total recording time in the 103 subjects was 14 min (range: 8–21 min); the recordings were suspended for 3–10 min in 13 subjects, and the measurements were successful only on the following day in 3 neonates. On the average, 48 (range: 15–105) respiratory cycles were analyzed from the intra-breath oscillometry in each newborn; these were collected as segments of steady-state breathing from a minimum of three 90-s recordings. The average values of spectral outcomes were calculated from 6 (3–11) recordings of a mean length of 26 s (12–30 s).

Overall, the intra-breath changes in Zrs, dominated by the V' dependence, were remarkably large. R_{ppE} and R_{ppI} amounted to 91.4 ± 33.3% and 55.9 ± 27.6%, respectively, of the average zero-flow impedance magnitude, i.e., $Z_0 = 1/2(Z_{eE} + Z_{eI})$. The maximum Rrs was usually located near the peak V', while the minimum was found around V' = 0. The corresponding changes in Xrs (X_{ppE} and X_{ppI}) were roughly half as large (44.9 ± 26.8% and 32.7 ± 19.3%, respectively). Tidal change in Rrs was on the average close to zero ($\Delta R = -0.4 \pm 6.5$ hPa.s.L^{-1}), with negative values of ΔR were observed in 51% of the subjects, whereas the decreases in Xrs between end expiration and end inspiration were more uniform ($\Delta X = 2.39 \pm 3.44$ hPa.s.L^{-1}).

Short-term changes in Zrs are illustrated with a few selected segments of intra-breath recordings (**Figure 2**). These examples are not intended to be exhaustive; they only highlight epochs where (i) regular intra-breath fluctuations in Rrs and Xrs are observed despite a slightly irregular spirogram (**Figure 2A**), (ii) a slow negative drift in Xrs occurs (**Figure 2B**) or (iii) increasing fluctuations in both Rrs and Xrs take place (**Figure 2C**) at virtually even tidal volumes, and (iv) the large expiratory increases in Rrs and decreases in Xrs are reduced following a sigh (**Figure 2D**).

Whereas Rrs exhibited positive V' dependences during inspiration and expiration, the intra-breath changes in Xrs were more diverse. Four typical patterns were determined qualitatively and are exemplified in **Figure 3** where Rrs and Xrs are plotted against V and V'. These patterns are characterized as minimal dependence of Xrs on V' (Pattern A), marked V'-dependent decrease in Xrs during expiration (Pattern B), marked V'-dependent decrease during inspiration (Pattern C) and marked V'-dependent increases in Xrs (Pattern D). Each newborn was classified into one group according to the V'-dependence of Xrs by cluster analysis, presuming that four different patterns exist (**Figure 4**). Subjects with the lowest V'-dependence in Xrs (Pattern A) were considered the control group. **Tables 1–3**, respectively, contain the anthropometrical and tidal breathing data, the spectral oscillometry measures and the intra-breath variables in the 4 clusters. Slightly lower body measures were found in the Pattern C and D groups and lower f_{br} values in Pattern B-D groups compared to the Pattern A data (**Table 1**). L was the highest while f_{res} and Ax were the lowest in the positive V' dependence (Pattern D) group (**Table 2**). L was significantly ($p < 0.05$) lower and Ax was higher in subjects with negative expiratory swings in Xrs (Pattern B) compared to Pattern A. Unlike the values of X_8, parameter C was found to be not different between groups. The overall fitting error of the R -C-L model to the Zrs data was 7.4 ± 2.8%; its components broken down to Rrs and Xrs were 6.3 ± 2.7% and 3.7 ± 1.6%, respectively.

Comparison of intra-breath measures (**Table 3**) revealed mild elevations in R_{eE} and R_{eI} in the C and D groups but no differences in ΔR between the different patterns. ΔX reached significantly higher values in the Pattern B group than in the rest of groups. Differences in the V' dependence of Rrs measures (R_{ppE} and R_{ppI}) were milder between groups than that of Xrs

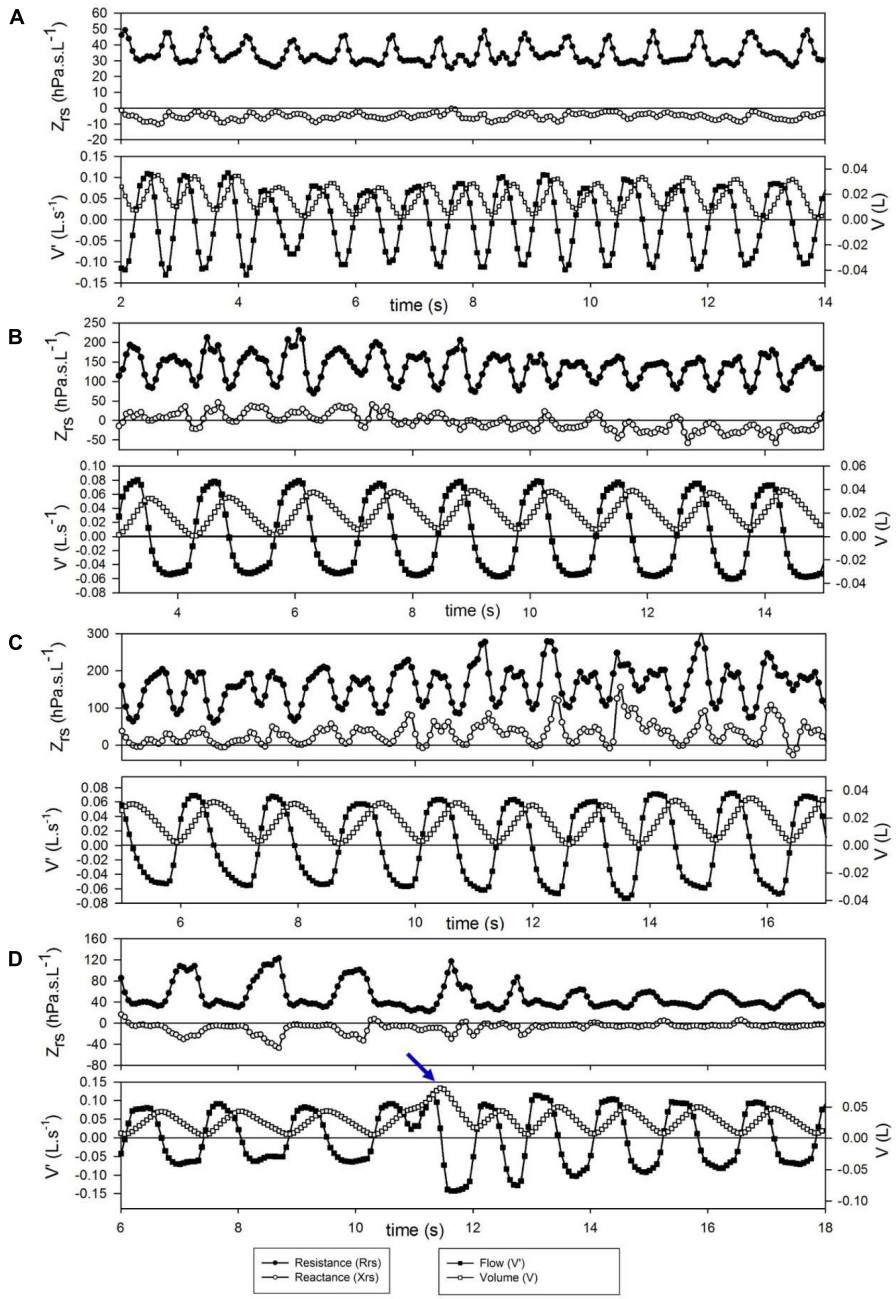

FIGURE 2 | Examples of short term changes in impedance (Zrs) and breathing pattern. Each graph represents a 12-s period. **(A)** Slightly irregular tidal flow but stable and low Zrs. **(B)** Slow downward drift in reactance (Xrs) during regular breathing. **(C)** Increasing flow dependence of Zrs during steady-state breathing; this probably reflects spontaneous development of nasal obstruction. **(D)** Transient decrease of expiratory flow limitation after a spontaneous sigh (arrow).

measures (X_{ppE} and X_{ppI}) as the latter are related to the clustering variables (**Figure 4**).

Figure 5 gives an overview on the correlations between selected indices of the spirogram, spectral oscillometry and intrabreath analysis. Among the between-category comparisons, high correlation coefficients were found between R and the intra-breath Rrs measures and between the spectral (L, f_{res} and Ax) and intra-breath Xrs measures, except C which was most correlated with Ax and X_8 but not with intra-breath Xrs data. A weak although statistically significant (r = 0.39, $p < 0.001$) linear correlation was found between ΔR and $|V''_{eE}/V''_{eI}|$. T_{PTEF}/T_E was not correlated with any of the spectral and intra-breath Rrs or Xrs outcomes, but exhibited a very strong relationship (r = 0.84, $p < 0.001$) with $|V''_{eE}/V''_{eI}|$, apparently unrelated to the pattern of V' dependence of Xrs (**Figure 6**).

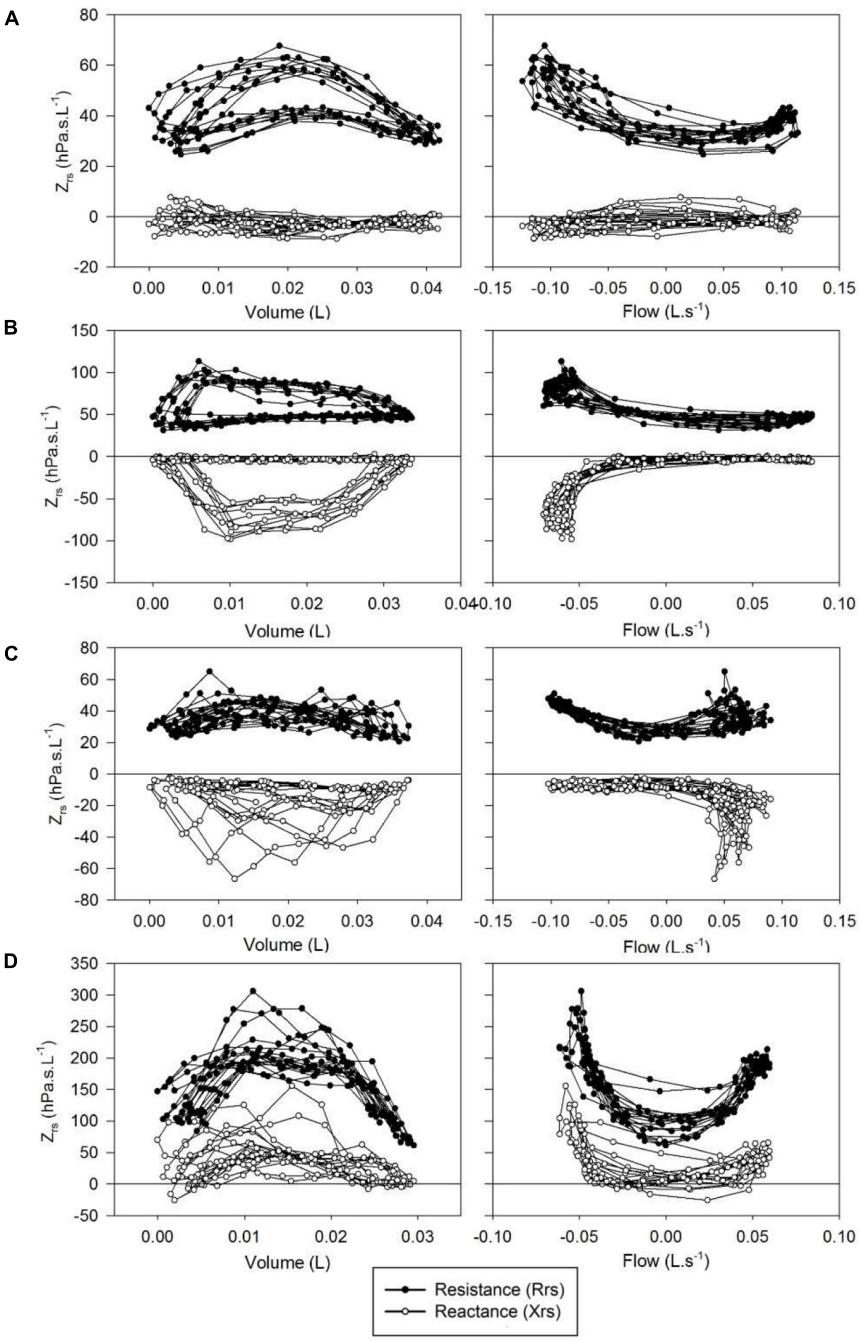

FIGURE 3 | Typical patterns of intrabreath changes in respiratory impedance (Zrs). **(A)** Insignificant changes in reactance (Xrs) and mild flow non-linearity in resistance (Rrs); **(B)** marked fall in Xrs and increase in Rrs during expiration; **(C)** marked fall in Xrs in inspiration; **(D)** increases in Xrs and Rrs with both inspiratory and expiratory flow.

DISCUSSION

The 94% success rate in the present study confirms earlier observations on the feasibility of oscillometry in unsedated newborns (5) and infants (2, 4, 7) although its outstanding value can largely be attributed to the favorable environmental and time allocation circumstances in the neonatal ward. These factors enabled a more detailed assessment of short-term variability of Zrs in healthy term neonates.

Intra-Breath Changes in Rrs

The characteristic effect of V' on Rrs was documented in early studies using single-frequency oscillations in orally breathing adult subjects (15, 16). These biphasic changes in

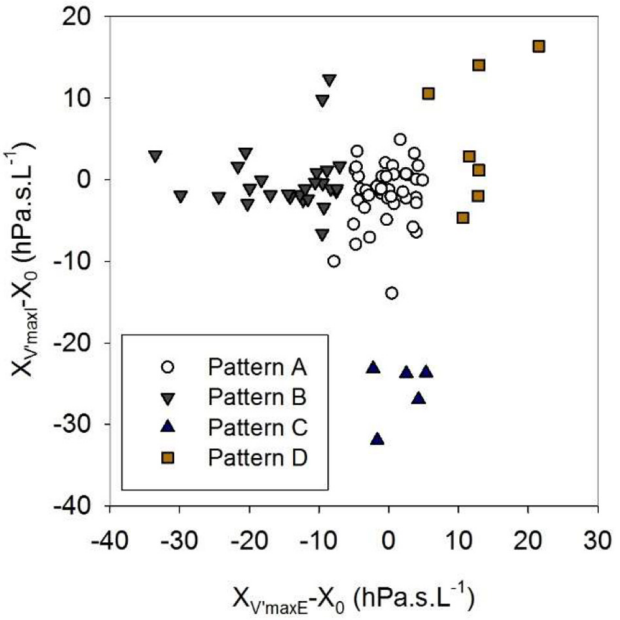

FIGURE 4 | Clusters established in the relationships between inspiratory and expiratory flow dependences of reactance. $X_{V'maxI}$ and $X_{V'maxE}$ are reactance values at peak inspiratory and expiratory flows, X_0 is the average zero-flow value of reactance. For definitions of Patterns A-D, see text or the legend to **Table 1**.

Rrs, characterized by minimum values at zero V' and local maxima at peak inspiratory and expiratory V' (V'$_{maxI}$ and V'$_{maxE}$, respectively) were a marked feature in the neonates of this study, with the non-linearity in expiration usually exceeding that of inspiration. Previous observations suggest that the non-linear, V'-dependent increase in Rrs originates from the upper airways (12, 17, 18), obeying the classical empirical description by Rohrer (19).

An unexpected finding in the present investigation was the fact that R_{eI} was higher than R_{eE} (i.e., ΔR was negative) in almost half of the subjects. This is in contrast to previous intra-breath studies where the typically positive ΔR values were attributed to the tidal dilatation of the pulmonary airways (7, 20, 21). One important specific factor in infancy is the large contribution of the extrathoracic pathways to Rrs, whose transmural pressures are dependent on V' rather than V and are opposite to that of the pulmonary airways; this may lead to narrowing of the upper airways during inspiration and possibly some residual constriction at end inspiration. Another factor, also augmented in nasal breathing is the non-steady flow patterns that develop at fast transitions of V' in the upper airways of irregular geometry. This leads to extra dissipation, which has been shown to depend on the rate of change in V' (i.e., on V") (12, 17, 18), and would add to the true "zero-flow" values of R_{eE} and R_{eI}. In the present study, the asymmetry of respiratory phase change (as characterized by the ratio V"$_{eE}$/V"$_{eI}$) was shown to correlate with ΔR. Since the transition from inspiration to expiration is usually faster than *vice versa*, it can lead to low, or even negative values in ΔR. These factors discussed above suggests that the contributions of the upper airway to ΔR may mask the change in pulmonary airway caliber. Nevertheless, the near-zero mean value of ΔR is at variance with the results of the intra-breath measurements in infants (7) where an average of 4.43 hPa.s.L^{-1} (IQR: 0.65–8.13 hPa.s.L^{-1}) was observed. Since the same custom-made wave-tube device was employed in both studies and the spectral Zrs measures are similar, differences between the 2 populations, such as ethnic (Caucasians vs. Black Africans), age (newborns vs. 6 week old infants), gestational age (term vs. term + late preterm) and other characteristics may explain the different ΔR values.

Intra-Breath Changes in Xrs

While the changes in Rrs within the respiratory cycle are dominated by the "U" shape in V' dependence of different degrees and asymmetry, Xrs exhibited qualitatively more distinct intra-breath patterns. We defined a group with the lowest V'-dependent changes in Xrs (pattern A) and considered it the control group. The rest (45%) of the examined neonates exhibited diverse and strong V' dependences of Xrs. Three additional typical V'-dependent patterns were identified qualitatively and verified by cluster analysis. Inference to the underlying mechanisms of each pattern is burdened by the lack of

TABLE 2 | Comparison of spectral oscillometry data between subject groups of different patterns of flow dependence of respiratory reactance.

	All (n = 86)	Pattern A (n = 47)	Pattern B (n = 27)	Pattern C (n = 5)	Pattern D (n = 7)
R (hPa.s.L^{-1})	48.7 ± 12.9	46.0 ± 12.6	48.7 ± 11.5	59.9 ± 17.4	58.3 ± 9.4*
C (mL.hPa^{-1})	1.08 ± 0.30	1.13 ± 0. 32	1.01 ± 0. 29	1.05 ± 0.28	1.06 ± 0. 15
L (hPa.s^2.L^{-1})	0.068 ± 0.028	0.071 ± 0.027	0.057 ± 0.023*	0.047 ± 0.031	0.102 ± 0.020**
R_8 (hPa.s.L^{-1})	63.2 ± 16.8	59.6 ± 16.3	64.6 ± 16.4	77.3 ± 22.1	72.0 ± 11.2*
X_8 (hPa.s.L^{-1})	−14.9 ± 5.4	−13.9 ± 5.1	−16.7 ± 5.8*	−17.1 ± 5.8	−13.3 ± 4.2
R_{8-32} (hPa.s.L^{-1})	18.6 ± 7.3	16.9 ± 6.4	20.6 ± 8.5	24.7 ± 5.9*	17.6 ± 5.0
f_{res} (Hz)	21.4 ± 5.9	20.1 ± 5.2	23.7 ± 4.7**	29.2 ± 11.9	16.3 ± 1.9**
Ax (hPa.L^{-1})	103.1 ± 59.6	90.7 ± 55.1	124.8 ± 58.5*	157.0 ± 80.3	64.0 ± 20.8*

Mean ± SD values. For definitions of Patterns A-D, see text or the legend to ***Table 1****. R, resistance (model fitting); C, compliance (model fitting); L, inertance (model fitting); R_8, resistance at 8 Hz; X_8, reactance at 8 Hz; R_{8-32}, resistance difference between 8 and 32 Hz; f_{res}, resonance frequency; Ax, reactance area below f_{res}.*
**$p < 0.05$ vs. Pattern A; **$p < 0.01$ vs. Pattern A.*

TABLE 3 | Comparison of intra-breath oscillometry data between subject groups of different patterns of flow dependence of respiratory reactance.

	All (n = 86)	Pattern A (n = 47)	Pattern B (n = 27)	Pattern C (n = 5)	Pattern D (n = 7)
R_{eE} (hPa.s.L^{-1})	41.7 ± 11.3	38.7 ± 10.1	41.9 ± 9.0	53.3 ± 16.0	52.7 ± 13.2*
R_{eI} (hPa.s.L^{-1})	42.1 ± 13.5	38.5 ± 13.4	43.7 ± 11.7	51.3 ± 15.8	53.5 ± 11.2*
X_{eE} (hPa.s.L^{-1})	−1.35 ± 3.98	−1.55 ± 3.55	−1.516 ± 3.14	−6.74 ± 2.84*	4.53 ± 3.86**
X_{eI} (hPa.s.L^{-1})	−3.73 ± 4.21	−3.14 ± 3.54	−5.45 ± 3.69*	−8.05 ± 4.23	1.92 ± 3.92*
ΔR (hPa.s.L^{-1})	−0.40 ± 6.48	0.23 ± 6.30	−1.83 ± 7.48	2.03 ± 2.43	−0.81 ± 5.16
ΔX (hPa.s.L^{-1})	2.39 ± 3.44	1.58 ± 3.30	3.93 ± 3.72**	1.30 ± 1.74	2.62 ± 2.36
$R_{ppE}/\|Z_0\|$	0.91 ± 0.33	0.80 ± 0.26	1.08 ± 0.32**	0.67 ± 0.20	1.25 ± 0.43*
$R_{ppI}/\|Z_0\|$	0.56 ± 0.28	0.52 ± 0.24	0.50 ± 0.22	0.87 ± 0.21*	0.85 ± 0.46
$X_{ppE}/\|Z_0\|$	0.45 ± 0.27	0.32 ± 0.13	0.70 ± 0.31**	0.28 ± 0.08	0.50 ± 0.14**
$X_{ppI}/\|Z_0\|$	0.32 ± 0.19	0.30 ± 0.13	0.28 ± 0.09	0.90 ± 0.28**	0.33 ± 0.14

Mean ± SD values. For definitions of Patterns A–D, see text or the legend to ***Table 1****. R_{eE}, resistance at end expiration; R_{eI}, resistance at end inspiration; X_{eE}, reactance at end expiration; X_{eI}, reactance at end inspiration; ΔR, tidal change in resistance (R_{eE}-R_{eI}); ΔX, tidal change in reactance (X_{eE}-X_{eI}); R_{ppE}, peak-to-peak resistance difference in expiration; R_{ppI}, peak-to-peak resistance difference in inspiration; X_{ppE}, peak-to-peak resistance difference in expiration; X_{ppI}, peak-to-peak resistance difference in inspiration; $|Z_0|$, impedance magnitude at zero flow [1/2($|Z_{eE}|$ + $|Z_{eI}|$)].*
**$p < 0.05$ vs. Pattern A; **$p < 0.01$ vs. Pattern A.*

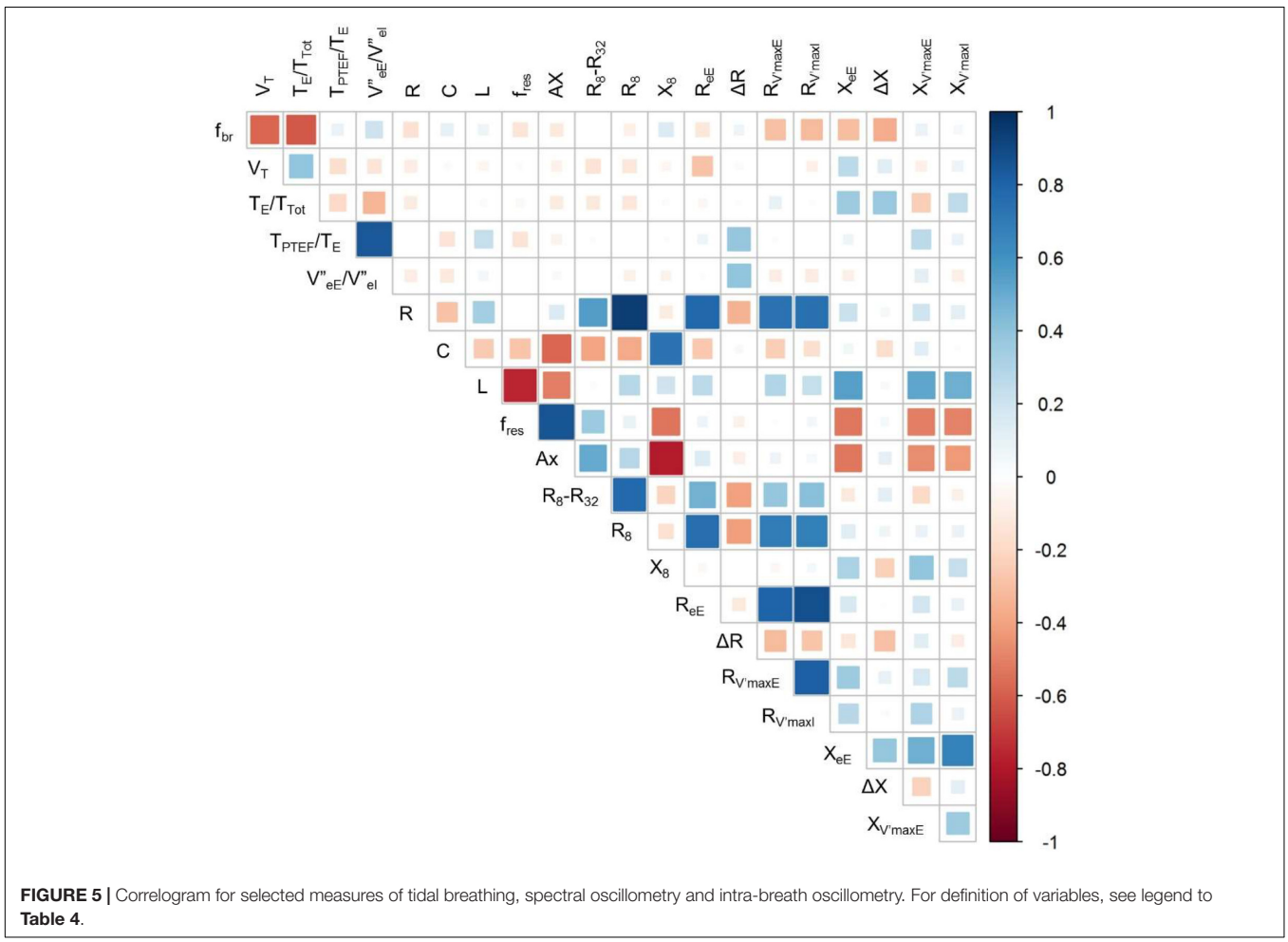

FIGURE 5 | Correlogram for selected measures of tidal breathing, spectral oscillometry and intra-breath oscillometry. For definition of variables, see legend to **Table 4**.

additional signals (e.g., nasopharyngeal pressure) unavailable in the non-invasive setting of the current study. Nevertheless, a decrease in Xrs during expiration (pattern B) is most likely caused by glottic braking that help maintain the end-expiratory lung volume in the early phase of postnatal lung and chest wall development (22). The small but highly significant increase in the T_E/T_{Tot} ratio in this group (**Table 1**) supports the above argument. Intuitively, a similar change in Xrs but in inspiration

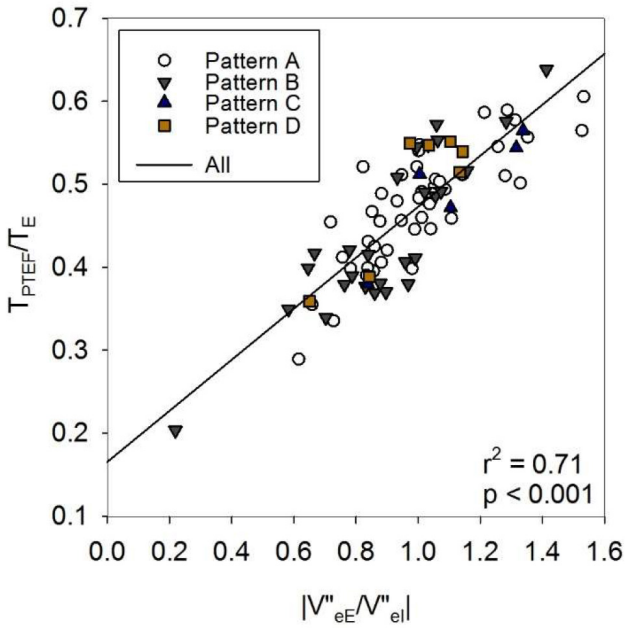

FIGURE 6 | Effect of asymmetry in volume acceleration (V") ratio on T_{PTEF}/T_E. eE: end expiration; eI: end inspiration; T_{PTEF}: time to peak tidal expiratory flow; T_E: expiratory time. For definitions of Patterns A–D, see text or the legend to **Table 1**.

TABLE 4 | Within-session variability presented as coefficient of variation (in%) of tidal breathing, spectral oscillometry and intra-breath oscillometry indices.

f_{br}	14.0 (3.9–38.2)
V_T	21.9 (7.8–42.3)
T_E/T_{tot}	7.9 (3.3–13.8)
T_{PTEF}/T_E	19.6 (11.1–44.4)
R	10.3 (1.9–29.7)
C	20.3 (3.3–88.4)
L	26.6 (3.6–154.0)
$\|Z_8\|$	13.6 (5.3–30.7)
R_{8-32}	26.5 (5.2–64.6)
f_{res}	15.7 (1.9–67.6)
Ax	37.9 (7.5–186.1)
$\|Z_{eE}\|$	19.6 (5.3–117.7)
$\|Z_{eI}\|$	23.1 (4.9–100.6)
$\|Z_{V'maxE}\|$	23.6 (4.3–71.0)
$\|Z_{V'maxI}\|$	22.2 (5.5–58.0)

Mean (range) values. f_{br}, respiratory rate; V_T, tidal volume; V'_{maxE}, peak expiratory flow; T_E, expiratory time; T_{tot}, total respiratory cycle time; T_{PTEF}, time to peak tidal expiratory flow; R, resistance (model fitting); C, compliance (model fitting); L, inertance (model fitting); $|Z_8|$, impedance magnitude at 8 Hz; R_{8-32}, resistance difference between 8 and 32 Hz; f_{res}, resonance frequency; Ax, reactance area below f_{res}.; $|Z_{eE}|$, impedance magnitude at end expiration; $|Z_{eI}|$, impedance magnitude at end inspiration; $|Z_{V'maxE}|$, impedance magnitude at maximum expiratory flow; $|Z_{V'maxI}|$, impedance magnitude at maximum inspiratory flow.

(Pattern C) can be attributed to the negative pressure swings in the glossopharyngeal area, which lead *via* deformation of soft tissues to inspiratory V' limitation and are augmented by the large nasal component of Rrs. This suggests that the nasal impedance is not only a significant additive component in Zrs (8, 11, 23) but it may modulate the transmural pressures in the compliant structures of distal extrathoracic airways more than in the case of oral breathing. Whereas Patterns B and C describe temporary changes in Xrs, pronounced in mid-expiration or mid-inspiration, respectively (**Figure 3**), Pattern D is characterized by marked positive increases in Xrs with both inspiratory and expiratory V'. This is likely to be associated with the increased impedance of the nasal pathway, in terms of both resistance and inertance, as reflected by the higher values of R and L in this group (**Table 2**), also manifested in the significant elevations in zero-V' Xrs (X_{eE} and X_{eI}, **Table 3**). Note that while the relatively low numbers of Pattern C and Pattern D subjects warrant considerations in their statistical assessments, the frequency of these patterns can be regarded as an inherent feature of the studied healthy term infants. Importantly, Xrs patterns suggesting intrapulmonary expiratory flow limitation observed in the South African cohort of 6-week-old infants (7) were not detected in the present study.

The respiratory pattern can undergo gradual or abrupt changes in a relatively short time (**Figure 2**). After examination of individual recordings, it can be concluded that a V'-dependent Xrs pattern is not a permanent characteristic of a newborn, but a temporary feature. Sudden changes in the V'-non-linearities might explain the huge day-to-day variability of spectral oscillometry (5). Therefore, measurements of both intra-breath and spectral oscillometry in the same session are recommended to detect and explain the short term changes in respiratory mechanics.

Within-Session Variability of Oscillometry Measures

The 90-s recordings allowed us to have a closer look into the short-term changes in intra-breath Zrs, which sometimes even disclosed transitions from one pattern of V' dependence into another. The within-session variability of intra-breath Zrs measures was slightly larger than that of the breathing pattern descriptors, which were obtained from the same recordings (**Table 4**). Although this may suggest that fluctuations in the spirogram cause changes in the intra-breath parameters, correlation analysis did not confirm such a relationship; similarly, no direct correlations were found between the tidal breathing pattern and the within-session variability of spectral oscillometry (data not reported).

The fact that the most stable spectral measures were R and $|Z_8|$ is somewhat surprising, as we expected a large variability contributed by the nasal pathway. Explanations based solely on our non-invasive measurement data would be speculative; however, there is indication that the nasal and the distal pulmonary resistances can change in opposite direction to maintain a relatively constant total resistance (23). The highest variability was observed in Ax, which is widely considered as a robust measure of elastic properties of the respiratory system (24). However, as the area of the negative Xrs domain is terminated by f_{res}, changes in the dominant nasal inertance would strongly influence the Ax values.

Indeed, the intra-breath analysis revealing the patterns of V' dependence indicated that Ax was biased by changes in Xrs (**Table 2**), whereas the model fitting of Zrs spectra accounted for the changes in L and resulted in remarkably constant estimates of C for all patterns in spontaneously breathing infants. The model-based approach supported by intra-breath analysis thus makes the values of C less influenced by the strong upper airway compartment and more specific to the elastic properties of the lungs.

Implications in Oscillometry Procedures in Infants

Technical standards and protocols of spectral oscillometry have been developed for cooperating children and adults (25, 26); these include reproducibility criteria based on repeated measurements that are separated by intervals when the subject is detached from the device. This protocol is clearly impractical to adopt in infant studies, primarily because of the removal and replacement of the face mask may alter the breathing pattern and the sleep stage *via* excitation of the facial nerves (27). Additionally, a minimum of 3 measurement epochs whose lowest-frequency Rrs values have a CoV of $\leq$ 10% (adults) or $\leq$ 15% (children) has been suggested as the reproducibility criterion (25). The wide ranges of within-session CoV values of tidal breathing and Zrs parameters observed in the present study (**Table 3**) may reflect a higher degree of natural variability in respiratory mechanics in neonates (28) compared with older subjects. Therefore, more permissive reproducibility criteria combined with the equally important Xrs measures and based on longer recordings should be established for infants. On the other hand, inclusion of the nasal passages in the infant oscillometry requires careful inspection of the patency of this pathway; congestion may lead to extreme values in R and L and associated with the Xrs pattern D, as in the current measurements.

Instrumentation Requirements

The spectral measures of Zrs in the present study, as expressed by the R, C and L parameter values (**Table 2**), are very close to that obtained with the same technique previously (2, 4, 5) and correspond to an impedance magnitude of 40–60 hPa.s.L^{-1}. Far above these values representing *averages* for whole breathing cycles, huge *peak values* in Zrs were identified by the intra-breath tracking to occur at instances of V'_{maxE} and V'_{maxI}. As illustrated in **Figures 2**, **3**, and quantified by the R_{ppI}/Z_0 and R_{ppE}/Z_0 data in **Table 2**, Zrs often exceeded 200 hPa.s.L^{-1} in the healthy term newborns of this study. This highlights the need for accurate measurements at peak values of Zrs and not only in intra-breath analysis, as the average values obtained in the conventional spectral oscillometry would also be distorted if an upper range of Zrs is misestimated. The wave-tube principle (29) employed in the present work is particularly advantageous in the measurements of high Zrs, and it was considered as the gold standard technique in the comparison of commercially available oscillometry devices (30). Device dependence might have been the primary reason for the large differences in the Rrs and Xrs values reported recently (13, 31), compared with that from the present and previous measurements with the wave-tube technique (2, 4, 5, 7).

Implications in Tidal Breathing Analysis

Comparative analysis of tidal breathing and oscillometry indices has revealed generally modest interrelationships (**Figure 5**) but pinpointed a strong connection between T_{PTEF}/T_E and an asymmetry measure of V" ($V"_{eE}/V"_{eI}$). T_{PTEF}/T_E can be obtained in relatively simple measurement settings and it has often been considered as a useful index to detect airway obstruction (32–34), although the assessment of T_{PTEF}/T_E as a surrogate of mechanical tests is controversial in the literature.

In the current study, T_{PTEF}/T_E did not correlate with the intra-breath Rrs or Xrs variables, and was not different between groups of V' dependence of Xrs. However, the mean values of $V"_{eE}/V"_{eI}$ of the subjects and the corresponding T_{PTEF}/T_E data covered wide ranges (**Figure 6**) with a strong linear relationship. This suggests that in healthy term newborns, such as those in the present study, marked differences in the activity of the respiratory control mechanisms rather than airway obstruction exist and determine the values of T_{PTEF}/T_E (35, 36).

Limitations

(i) The spectral and intra-breath oscillometry data were derived from recordings collected separately. In order to minimize systematic errors, the two modalities were alternated and, whenever possible, without the removal/repositioning of the face mask. Although there was good agreement in the mean 16-Hz Zrs data collected from the two modalities, the unchanged status of the respiratory mechanical system could not be guaranteed.

(ii) Although sleep state can be an important factor when interpreting lung function measurements in sleeping infants, addressing the relationship between the sleep state and respiratory mechanics was beyond the scope of the current study. Sleep states such as the active (rapid eye movement – REM) sleep and the quiet (non-REM) sleep typically last for 50–70 min in healthy newborns (37), and while we cannot exclude the possibility that a transition between sleep states took place during the measurements, it was more likely that the same state persisted during our recording sessions of typically 14-min duration. Since the estimated ratio of active and quiet sleep is approximately 2:1 in healthy term newborns (37), we can assume that a non-negligible portion of recordings was collected during active sleep. Regularity of the respiratory pattern is also known to be different during active and quiet sleep (38, 39); from the present data it can only be inferred that the variability of T_{tot} and V_T was independent of the Xrs pattern of V' dependence (**Table 1**).

(iii) The measurement device imposes some impedance against the breathing, which may alter the pattern of tidal breathing without this load. In the present study, the total load including the bacterial filter, the wave-tube, the pneumotachograph and the breathing tube amounted to 6.5 hPa.s.L^{-1}, i.e., roughly 10–15% of Rrs. Even if this additional load does not interact with the breathing pattern significantly, it increases the flow-dependent changes in the glossopharyngeal area and may augment the upper airway non-linearities.

CONCLUSION

The impedance tracking employed in the present study revealed marked intra-breath changes in Rrs and Xrs in healthy term neonates during natural sleep in the first few days of life. These changes were dominated by the increases in Rrs with V' in both inspiration and expiration, whereas Xrs exhibited different patterns of change, such as inspiratory and expiratory flow limitation. It is suggested that these intra-breath non-linearities are of upper airway origin, with fundamental contributions from the nasal pathways. Intra-breath changes exert a biasing effect on the conventional measures of the multi-frequency oscillometry that are intended to characterize pulmonary mechanics. It is recommended that the measurements of Zrs in infants cover longer study intervals than that required from cooperative subjects to account for the variable mechanical status of the developing respiratory system. Use of intra-breath oscillometry is proposed to gain more insight into the mechanisms determining Zrs and to properly interpret the results of conventional spectral oscillometry in infants.

DATA AVAILABILITY STATEMENT

The original contributions presented in the study are included in the article/supplementary material, further inquiries can be directed to the corresponding author.

ETHICS STATEMENT

The studies involving human participants were reviewed and approved by Institutional Clinical Ethics Committee of the University of Szeged (91/2011, renewed in 2017). Written informed consent to participate in this study was provided by the participants' legal guardian/next of kin.

AUTHOR CONTRIBUTIONS

BR, ZGy, and ZH: study design and evaluation of measurements. BR and ZGy: impedance measurements. GM, ZGy, and ZH: design of the infant oscillometry system. BR, GM, ZGy, DC, and ZH: development of the infant intra-breath analysis. BR, DC, and ZH: interpretation of results. BR and ZH: drafting of the manuscript. All authors contributed to the article and approved the submitted version.

FUNDING

This study was supported by Hungarian Scientific Research Fund grants (K 105403, K 128701, and FK 129237), and European Respiratory Society Clinical Research Collaboration award CRC_2013-02_INCIRCLE. DC was supported by János Bolyai Research Scholarship of the Hungarian Academy of Sciences, the ÚNKP-19-4-SE-96 New National Excellence Program of the Ministry of Human Capacities.

REFERENCES

1. Frey U. Forced oscillation technique in infants and young children. *Paediatr Respir Rev.* (2005) 6:246–54. doi: 10.1016/j.prrv.2005.09.010
2. Gray D, Czovek D, Smith E, Willemse L, Alberts A, Gingl Z, et al. Respiratory impedance in healthy unsedated South African infants: effects of maternal smoking. *Respirology.* (2015) 20:467–73. doi: 10.1111/resp.12463
3. Gray D, Willemse L, Visagie A, Czovek D, Nduru P, Vanker A, et al. Determinants of early-life lung function in African infants. *Thorax.* (2017) 72:445–50. doi: 10.1136/thoraxjnl-2015-207401
4. Gray D, Willemse L, Visagie A, Smith E, Czovek D, Sly PD, et al. Lung function and exhaled nitric oxide in healthy unsedated African infants. *Respirology.* (2015) 20:1108–14. doi: 10.1111/resp.12579
5. Hantos Z, Czovek D, Gyurkovits Z, Szabo H, Maar BA, Radics B, et al. Assessment of respiratory mechanics with forced oscillations in healthy newborns. *Pediatr Pulmonol.* (2015) 50:344–52. doi: 10.1002/ppul.23103
6. Hantos Z. Intra-breath oscillometry for assessing respiratory outcomes. *Curr Opin Physiol.* (2021) 22:4.
7. Gray DM, Czovek D, McMillan L, Turkovic L, Stadler JAM, Vanker A, et al. Intra-breath measures of respiratory mechanics in healthy African infants detect risk of respiratory illness in early life. *Eur Respir J.* (2019) 53:1800998. doi: 10.1183/13993003.00998-2018
8. Polgar G, Kong GP. The nasal resistance of newborn infants. *J Pediatr.* (1965) 67:557–67. doi: 10.1016/s0022-3476(65)80425-5
9. Solow B, Peitersen B. Nasal airway resistance in the newborn. *Rhinology.* (1991) 29:27–33.
10. Desager KN, Buhr W, Willemen M, van Bever HP, De Backer W, Vermeire PA, et al. Measurement of total respiratory impedance in infants by the forced oscillation technique. *J Appl Physiol.* (1991) 71:770–6. doi: 10.1152/jappl.1991.71.2.770
11. Hall GL, Hantos Z, Wildhaber JH, Sly PD. Contribution of nasal pathways to low frequency respiratory impedance in infants. *Thorax.* (2002) 57:396–9. doi: 10.1136/thorax.57.5.396
12. Radics BL, Makan G, Coppens T, Andre N, Page C, Degrugilliers L, et al. Effect of nasal airway nonlinearities on oscillometric resistance measurements in infants. *J Appl Physiol.* (1985) 2020:591–8. doi: 10.1152/japplphysiol.00128.2020
13. Klinger AP, Travers CP, Martin A, Kuo HC, Alishlash AS, Harris WT, et al. Non-invasive forced oscillometry to quantify respiratory mechanics in term neonates. *Pediatr Res.* (2020) 88:293–9. doi: 10.1038/s41390-020-0751-7
14. Miller TK, Pimmel RL. Forced noise mechanical parameters during inspiration and expiration. *J Appl Physiol.* (1982) 52:1530–4. doi: 10.1152/jappl.1982.52.6.1530
15. Davidson RN, Greig CA, Hussain A, Saunders KB. Within-breath changes of airway caliber in patients with air-flow obstruction by continuous measurement of respiratory impedance. *Brit J Dis Chest.* (1986) 80:335–52. doi: 10.1016/0007-0971(86)90087-2
16. Peslin R, Hixon T, Mead J. [Variations of thoraco-pulmonary resistance during the respiratory cycle studied by the oscillation method]. *Bull Physio Pathol Respir.* (1971) 7:173–88.
17. Isabey D, Chang HK. Steady and unsteady pressure-flow relationships in central airways. *J Appl Physiol Respir Environ Exerc Physiol.* (1981) 51:1338–48. doi: 10.1152/jappl.1981.51.5.1338
18. Isabey D, Chang HK, Delpuech C, Harf A, Hatzfeld C. Dependence of central airway resistance on frequency and tidal volume: a model study. *J Appl Physiol.* (1985) 61:113–26. doi: 10.1152/jappl.1986.61.1.113
19. Rohrer F. Der Strömungswiderstand in den menschlichen Atemwegen und der Einfluss der unregelmässigen Verzweigung des Bronchialsystems auf den Atmungsverlauf in verschiedenen Lungenbezirken. *Pflüger's Archiv Gesamte Physiol Menschen Tiere.* (1915) 162:225–99. doi: 10.1007/bf01681259

20. Chiabai J, Friedrich FO, Fernandes MTC, Serpa FS, Antunes MOB, Neto FB, et al. Intrabreath oscillometry is a sensitive test for assessing disease control in adults with severe asthma. *Ann Allergy Asthma Immunol.* (2021) 127:372–7. doi: 10.1016/j.anai.2021.06.005
21. Lorx A, Czovek D, Gingl Z, Makan G, Radics B, Bartusek D, et al. Airway dynamics in COPD patients by within-breath impedance tracking: effects of continuous positive airway pressure. *Eur Respir J.* (2017) 49:1601270. doi: 10.1183/13993003.01270-2016
22. Kosch PC, Hutchison AA, Wozniak JA, Carlo WA, Stark AR. Posterior cricoarytenoid and diaphragm activities during tidal breathing in neonates. *J Appl Physiol.* (1988) 64:1968–78. doi: 10.1152/jappl.1988.64.5.1968
23. Lacourt G, Polgar G. Interaction between nasal and pulmonary resistance in newborn infants. *J Appl Physiol.* (1971) 30:870–3. doi: 10.1152/jappl.1971.30.6.870
24. Goldman MD. Clinical application of forced oscillation. *Pulm Pharmacol Ther.* (2001) 14:341–50. doi: 10.1006/pupt.2001.0310
25. King GG, Bates J, Berger KI, Calverley P, de Melo PL, Dellacà RL, et al. Technical standards for respiratory oscillometry. *Eur Respir J.* (2020) 55:1900753. doi: 10.1183/13993003.00753-2019
26. Oostveen E, MacLeod D, Lorino H, Farre R, Hantos Z, Desager K, et al. The forced oscillation technique in clinical practice: methodology, recommendations and future developments. *Eur Respir J.* (2003) 22:1026–41. doi: 10.1183/09031936.03.00089403
27. Kuypers K, Martherus T, Lamberska T, Dekker J, Hooper SB, te Pas AB. Reflexes that impact spontaneous breathing of preterm infants at birth: a narrative review. *Arch Dis Childh Fetal Neonat Edn.* (2020) 105:F675–9. doi: 10.1136/archdischild-2020-318915
28. Beydon N, Davis SD, Lombardi E, Allen JL, Arets HGM, Aurora P, et al. An official American thoracic society/European respiratory society statement: pulmonary function testing in preschool children. *Am J Resp Crit Care.* (2007) 175:1304–45. doi: 10.1164/rccm.200605-642ST
29. Van de Woestijne KP, Franken H, Cauberghs M, Làndsér FJ, Clément J. A modification of the forced oscillation technique. In: Hutás I, Debreczeni L editors. *Proceedings of the 28th International Congress of Physiological Sciences*. Budapest: Akadémiai Kiadó (1981). p. 655–60. doi: 10.1016/b978-0-08-026823-1.50083-1
30. Dandurand RJ, Lavoie JP, Lands LC, Hantos Z. Comparison of oscillometry devices using active mechanical test loads. *ERJ Open Res.* (2019) 5:0160–2019. doi: 10.1183/23120541.00160-2019
31. Travers CP, Klinger AP, Aban I, Hoover W, Carlo WA, Ambalavanan N. Noninvasive oscillometry to measure pulmonary mechanics in preterm infants. *Am J Resp Crit Care.* (2021) 204:485–8. doi: 10.1164/rccm.202101-0226LE
32. Baldwin DN, Pillow JJ, Stocks J, Frey U. Lung-function tests in neonates and infants with chronic lung disease: tidal breathing and respiratory control. *Pediatr Pulm.* (2006) 41:391–419. doi: 10.1002/ppul.20400
33. Banovcin P, Seidenberg J, Von der Hardt H. Assessment of tidal breathing patterns for monitoring of bronchial obstruction in infants. *Pediatr Res.* (1995) 38:218–20. doi: 10.1203/00006450-199508000-00014
34. Celik E, Uysal P. Pulmonary function testing with tidal breath analyze technique is useful in predicting persistant small airway damage in infants with acute bronchiolitis. *Pediatr Allergy Immunol.* (2021) 32:60–6. doi: 10.1111/pai.13318
35. Hutten GJ, van Eykern LA, Latzin P, Kyburz M, van Aalderen WM, Frey U. Relative impact of respiratory muscle activity on tidal flow and end expiratory volume in healthy neonates. *Pediatr Pulmonol.* (2008) 43:882–91. doi: 10.1002/ppul.20874
36. van der Ent CK, van der Grinten CP, Meessen NE, Luijendijk SC, Mulder PG, Bogaard JM. Time to peak tidal expiratory flow and the neuromuscular control of expiration. *Eur Respir J.* (1998) 12:646–52. doi: 10.1183/09031936.98.12030646
37. Curzi-Dascalova L, Peirano P, Morel-Kahn F. Development of sleep states in normal premature and full-term newborns. *Dev Psychobiol.* (1988) 21:431–44. doi: 10.1002/dev.420210503
38. Curzi-Dascalova L, Lebrun F, Korn G. Respiratory frequency according to sleep states and age in normal premature infants: a comparison with full term infants. *Pediatr Res.* (1983) 17:152–6. doi: 10.1203/00006450-198302000-00014
39. Hoppenbrouwers T, Harper RM, Hodgman JE, Sterman MB, McGinty DJ. Polygraphic studies on normal infants during the first six months of life. II. Respiratory rate and variability as a function of state. *Pediatr Res.* (1978) 12:120–5. doi: 10.1203/00006450-197802000-00011

Conflict of Interest: The authors declare that the research was conducted in the absence of any commercial or financial relationships that could be construed as a potential conflict of interest.

Publisher's Note: All claims expressed in this article are solely those of the authors and do not necessarily represent those of their affiliated organizations, or those of the publisher, the editors and the reviewers. Any product that may be evaluated in this article, or claim that may be made by its manufacturer, is not guaranteed or endorsed by the publisher.